McMASTER

TO DETERMINE THE INFLUENCE OF FRICTION ON THE PREDICTION OF FORMABILITY AND PRESS SHOP PERFORMANCE FOR GALVANIZED LOW AND HIGH STRENGTH STEEL

prepared for the

Department of Energy, Mines and Resources - CANMET

under

DSS File No. 22ST. 23440-4-9047.

138pp.

Engineering

87-02220/

FACULTY OF ENGINEERING
McMaster University, Hamilton, Canada L8S 4L7
Telephone: (416) 525-9140 *Extension:* 4288 *Telex:* 061 8347

Final Report Submitted to the Department of Energy, Mines and Resources

Title: To Determine the Influence of Friction on the Prediction of Formability and Press Shop Performance for Galvanized Low and High Strength Steel

DSS File No. 22 ST. 23440-4-9047, Serial OST 84-00187

Principal Investigators:

J.L. Duncan (Mechanical Engineering Department)
J.D. Embury (Metallurgy and Materials Science)
R. Sowerby (Mechanical Engineering Department)

McMaster University

Scientific Authority:

Dr. A.F. Crawley,

Canada Centre for Mineral and Energy Technology,
Physical Metallurgy Research Laboratories,
Department of Energy, Mines and Resources.

Report Prepared: September 1986.

138pp

MICROMEDIA

Executive Summary

Chapters 1 to 3 of this report provide an account of the work conducted during Phase I of the contract.

Mechanical and metallurgical tests were performed on four hot-dipped galvanized steel sheets, with a drawing quality steel substrate. For comparison, two uncoated steel sheets, of essentially the same composition, were subjected to the same series of tests. These four galvanized coatings were classified as, Regular Spangle, Minimum Spangle, Spangle Free (Ultra-coat) and Alloyed; all the steels were supplied by Dofasco Incorporated.

The mechanical tests are described in Chapter 1. Data were obtained from uniaxial tests, hydraulic bulge tests and limiting dome height (LDH) tests; a forming limit diagram (FLD) was also obtained for each material. The formability of the materials, both coated and uncoated, in each of the tests was very similar.

Chapter 2 deals with the determination of the plastic strain ratio (the r-value) for the materials. All the sheets exhibited planar anisotropy, and showed extensive earing in the Swift cupping test. The uncoated steels showed a much higher value of normal anistropy than the coated materials, and the alloy coated steel had a particularly low r-value.

The metallurgical tests were performed on the materials before and after hydraulic bulging, and the results are given in Chapter 3. Although the deformation characteristics of the individual coatings were distinct, there was no evidence to suggest that this affected the deformation of the substrate in any signficant way.

In Phase II of the programme additional mechanical and metallurgical tests were performed on the four hot-dipped galvanized steel sheets, described in Phase I, and also on one hot-dipped galvanized, high strength steel.

The mechanical tests carried out on the high strength galvanized sheet included, uniaxial tensile, hydraulic bulging, punch stretching and strip friction tests. A forming limit curve (F.L.C.) was also constructed for the material. The yield strength of the material was 379 MPa (the yield stress of the four low strength steels ranged from 210 to 290 MPa) and it showed comparable ductility to the four lower strength sheets. In the strip fricton test it was not possible to stretch the material in the horizontal portion of the strip without a lubricant applied to the pins and test piece. This suggests that problems may be encountered in certain stamping operations, particularly in the forming of shallow panels if the lubricant is squeezed out from between the tools and the workpiece.

The tests on the four low strength galvanized sheets were devoted mainly to assessing the behaviour of the zinc coatings during punch stretch and strip friction tests. Grain boundary cracking was a common occurence in each of the four coatings at low plastic strain. Cleavage cracks and unsightly deformation twins were also characteristic of the materials.

The ease at which the coatings cracked raises questions about the corrosion resistance of the materials. The irregular surface of the coatings after straining and the presence of unsightly deformation markings may necessitate extra paint applications to cover the surface.

Unlike the high strength galvanized sheet, the four lower strength materials could be deformed in the strip friction test without a lubricant. Furthermore, in the presence of a lubricant the calculated coefficients of friction were less than the values computed for the high strength material. This implies that the lower strength grades will be easier to form in actual stamping operations.

The plastic strain ratio (the r-value) was determined for the four low strength materials in the as-received condition and with the zinc coating removed. With two of the sheets (the Regular Spangle and Minimum Spangle) the

measured r-value increased quite significantly when the coating was removed. However, the strain hardening behaviour in uniaxial tension did not appear to be affected. The Regular Spangle material was subjected to a number of x-ray diffraction tests to ascertain whether residual stresses were the cause of the variation in the r-value. However, the tests were inconclusive.

The nature of the Regular Spangle coating was also examined using an energy dispersive x-ray spectrometer. The variation in Fe, Zn and Al was examined in the coating and adjacent substrate; an intermetallic layer of about 1μm was identified, although its composition was not revealed. It is difficult to imagine that such a layer could exert a very strong influence on the r-value.

PHASE I

1. FORMABILITY CHARACTERISTICS OF GALVANIZED STEEL SHEET*

1. INTRODUCTION

Galvanized steel is widely used in the automotive industry for autobody panels. The use of various grades of zinc-coated steel is increasing rapidly to extend a vehicle's useful lifetime and improve its appearance. Galvanized steel is now produced by many major steel companies using various methods and diverse equipment and technology.

Depending on the coating requirements for the vehicle parts, galvanized steel will exhibit different coating characteristics. It is necessary to deal with the formability characteristics of galvanized steel to provide a guide for stamping in production. The formability of galvanized steel may be affected by the steel substrate, the coating thickness, the method of coating (i.e. hot dip or electrogalvanized), etc.

The Limiting Dome Height test and the Forming Limit Diagram are two methods to rank the formability of sheet metal. They both simulate failure strain in a stamping but the Limiting Dome Height (LDH) is a more convenient measure of formability in comparison to the determination of a Forming Limit Diagram (FLD).

This report describes the formability characteristics of some zinc-coated steels and some cold rolled steel sheets manufactured by Dofasco Inc. In order to compare the results, both the FLD and the LDH data were determined for all materials tested.

2. EXPERIMENT

2.1 Apparatus and Process

The punch testing apparatus is a press with a 100 mm diameter, hemispherical punch (shown in figure 1). Sheet metal specimens are securely clamped at the periphery and then stretched to failure over the punch.

The clamp force is sufficient to allow no slippage within the lock bead of the specimen. In order to determine the clamping force, the tests have been carried out using different pressure levels for specimen size 200 mm by 200 mm. The LDH value decreases with increased clamp pressure (shown in Figure 2). Beyond a certain value of clamping pressure,

* This chapter is available as a McMaster Metal Forming Research Report No. 85-008.

the LDH value remains unchanged for any further increase in pressure. The clamp pressure should be equal to or greater than this pressure. Clamping pressure is dependent on the width of the specimen (see Figure 3).

The NADDRG recommended practice [1] for LHD testing was followed. The LDH values are recorded by an X-Y plotter, which is calibrated daily. Figure 4 illustrates a typical LDH plot where the LDH value and the load may be read directly from the plot.

The specimens are 200 mm long with widths ranging from 25 to 200 mm. The short edges of the specimens are parallel to the rolling direction. After shearing, the shear burr was removed and circle grids of 5 mm diameter were imprinted onto the sheet surface by electro-chemical etching. Before testing, the specimen surfaces were cleaned with mineral oil and wiped dry. The punch and clamping areas were cleaned, first with 600 grit paper, then with mineral oil and dried.

The major and minor strains for the FLD were measured with a toolmaker's microscope. Three types of ellipses were observed according to the Hecker designation [2]:

type 1: fractured

type 2: necked or fracture affected

type 3: acceptable (where the ellipses fall outside the area affected by necking or fractures).

LDH values were measured from the recorded curve. Figures 5 and 6 show typical LDH and FLD curves.

2.2 Repeatability of LDH and FLD

There are two methods to clean the punch. It can be cleaned with 600 grit paper, either (1) before a group (8 specimens) testing, or (2) between each specimen. The punch is then wiped clean with mineral oil and dried with clean paper.

Figure 7 illustrates the LDH results using each method. The range of LDH values when the punch is cleaned before a group of specimens is about $\pm 2\%$ of the average value. For the other cleaning method, the range is $\pm 1\%$ of the average value. Figure 8 illustrates

the results of the FLD for both methods. The range for the first method is ±3.5% and for the second method is ±1.6%. Cleaning the punch between each sample gives a lower range of LDH values on repeat tests.

2.3 Materials

Six materials were provided by Dofasco Inc. Four of them were galvanized steels:

a) Regular Spangle,

b) Minimized Spangle,

c) Alloyed Coating, and

d) Spangle Free or "Ultracoat"*

Two uncoated steels, one with a rough surface and one with a smooth surface, were also tested. For each material, the mechanical properties, the average roughness and the thickness of the coating layer were measured. Table 1 in Appendix I and Tables 1 and 2 summarize these measured values for the different materials. Further information regarding the mechanical properties of these materials may be found in reference [3].

3. RESULTS

The formability behaviour of the different materials are shown in Figs. 9 and 10 and described briefly as follows:

1. The FLDs of the galvanized steels are higher than those of the uncoated steels (as shown in Figure 9). The LDH curves for all materials are very close to each other (Figure 10). Results for materials of similar thickness are plotted together.
2. In comparing the galvanized steels with the uncoated steels, the galvanized steels show a higher yield stress, lower n-values and maximum uniform strains. Also, the galvanized steels show lower tensile/yield strength ratios. This may be due to the

---

* Registered trade name with Dofasco Inc.

different thermo-mechanical processes used for galvanizing. The roughness of the materials ranges widely from 0.4 to 2.84 μm, see Table 1 in the Apendix.

3. From the data obtained from steels of similar thickness, the greater the n-value, the higher the LDH. The higher LDH value of the uncoated steel with the rough surface as compared to the steel with the smooth surface may be attributed to its higher n-value rather than its higher average roughness.

Note that the relationship between n-value and FLD is not as obvious as the relationship between n-value and LDH.

4. CONCLUSIONS

1) The formability of the galvanized sheet does not vary significantly from the uncoated sheet in the LDH test, while the FLDs of the galvanized steels are slightly higher than those of the uncoated steels.

2) The coated sheet generally shows a higher yield stress, lower n-value and a lower maximum uniform strain than the uncoated cold rolled sheet.

3) LDH data is typically less scattered than the comparable FLD. To rank the formability of materials, either the LDH or the FLD may be used where testing conditions will not greatly influence the results, but the LDH test is more suitable to use in the plant.

5. ACKNOWLEDGEMENTS

The authors gratefully acknowledge the funding provided by CANMET-PMRL for this research. The guidance provided by Drs. Duncan, Sowerby, and Embury at McMaster University has been invaluable and is accepted with thanks.

REFERENCES

1. NADDRG LDH Committee: Recommended Practice for the Limiting Dome Height (LDH) Test, Oct. 1984.

2. Siegfried S. Hecker: Simple Techniques for Determining Forming Limiting Curves. Sheet Metal Industry, November 1975.

3. Ru Zheng; D. Overby; J.L. Duncan and R. Sowerby: Normal Plastic Anisotropy in Galvanized and Uncoated Drawing Quality Sheet Steel, 1985, Metal Forming Research Report 85-003.

TABLE 1

UNIAXIAL TENSILE TEST RESULTS

MATERIAL	ORIENTATION W.R.T ROLLING DIRECTION	YIELD STRENGTH (MPa)	U.T.S. (MPa)	ε_u	$\sigma = K\varepsilon^n$ (MPa) n	K	r
REGULAR SPANGLE	0	284	331	.22	.24	582	1.57
	45	297	335	.19	.24	600	1.24
	90	288	330	.21	.26	611	1.44
MINIMIZED SPANGLE	0	288	323	.25	.25	584	1.14
	45	290	333	.20	.24	595	.73
	90	278	321	.20	.26	594	1.44
SPANGLE FREE	0	220	336	.20	.19	544	1.29
	45	231	344	.19	.19	555	1.09
	90	220	338	.18	.19	555	1.50
ALLOYED COATING	0	275	342	.22	.22	575	1.03
	45	293	344	.21	.23	607	0.88
	90	302	345	.19	.22	598	1.11
UNCOATED (ROUGH)	0	194	300	.22	.27	547	1.74
	45	219	320	.18	.26	611	1.41
	90	212	302	.20	.26	566	2.45
UNCOATED (SMOOTH)	0	202	315	.21	.25	597	2.40
	45	230	340	.20	.24	617	1.33
	90	231	325	.20	.23	575	2.19

Table 2: The Values of FLD_0† and LDH_0†

Materials	t (mm)	FLD_0	LDH_0 (mm)	n_T*	n_B*
Regular spangle	0.890	0.33	31.24	0.237	0.227
Minimized spangle	0.787	0.32	32.77	0.247	0.223
Spangle free	0.787	0.35	31.50	0.189	0.225
Alloyed coating	1.295	0.38	31.50	0.220	0.235
Uncoated (rough)	1.219	0.31	33.27	0.269	0.239
Uncoated (smooth)	1.168	0.31	30.99	0.248	0.231

† subscript indicates plane strain value.

* n_T and n_B represent the n-values from Tensile Test and Bulge Test respectively.

APPENDIX I

Table 1: Roughness[1] and Coating Layer Thickness[2]

Material	Test Direction[3] (deg)	Thickness (mm)	Ra (μm)	Coating Layer Thickness (μm)	Unit Weight of Coating L (gm/m^2)	One or Both Sides
1. Galvanized Steels						
Regular Spangle	0	0.890	0.41	27		
	45	0.890			137	one
	90	0.890				
Alloyed	0	1.295	2.84	45		
Minimum Spangle	0	0.787	1.60	34	200/100	both/one
Ultracoat	0	0.787	0.71	27	200	both
2 Uncoated Steels						
Rough Surface	0	1.219	1.42	–		
Smooth Surface	0	1.168	0.89	–		

1 Roughness measured by Talysurf. 10

2 Coating Thickness Layer measured by scanning electron microscope

3 Test direction is with respect to rolling direction.

FIGURE 1
LIMITING DOME HEIGHT
TEST EQUIPMENT

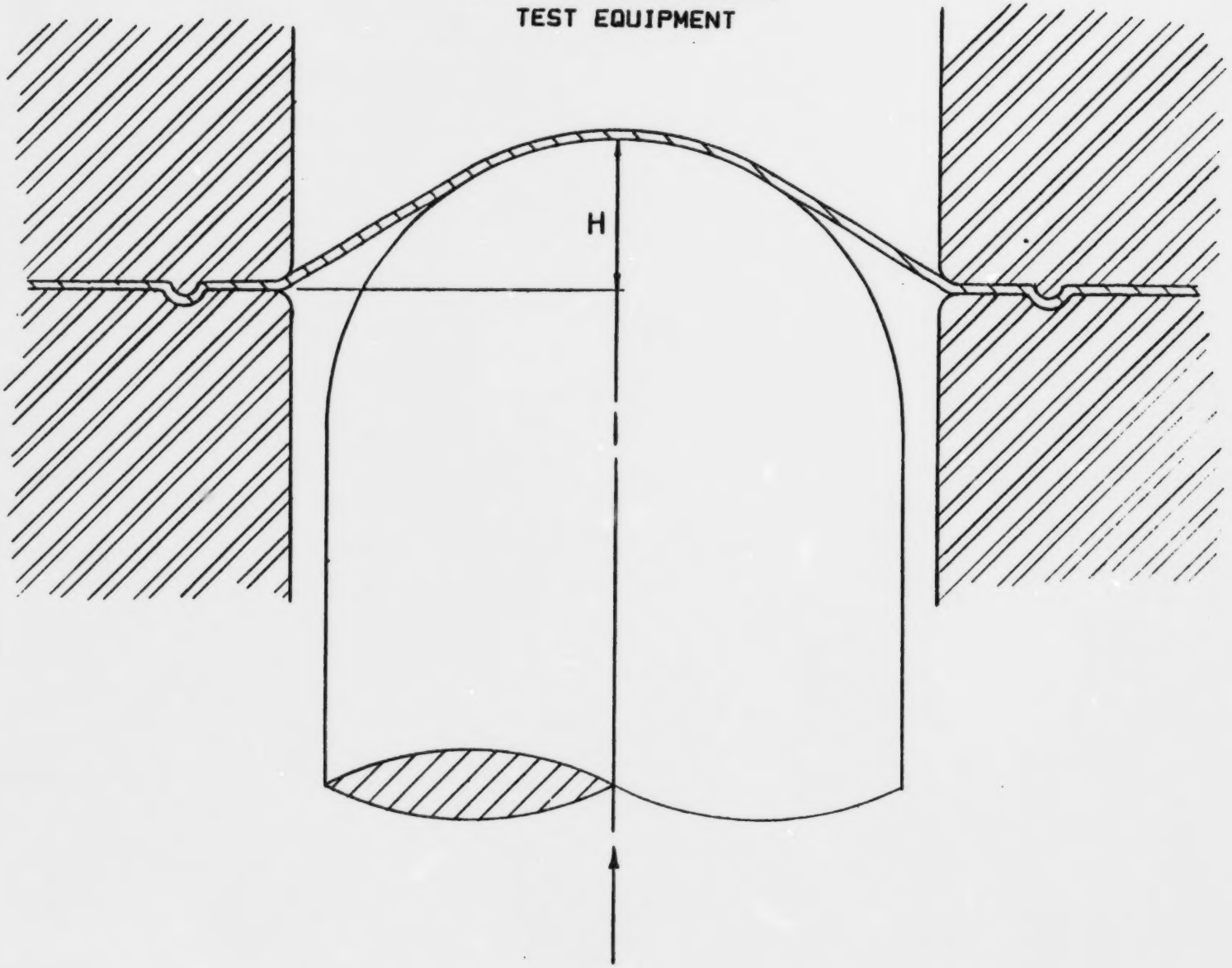

FIGURE 2
LDH VS. CLAMPING PRESSURE

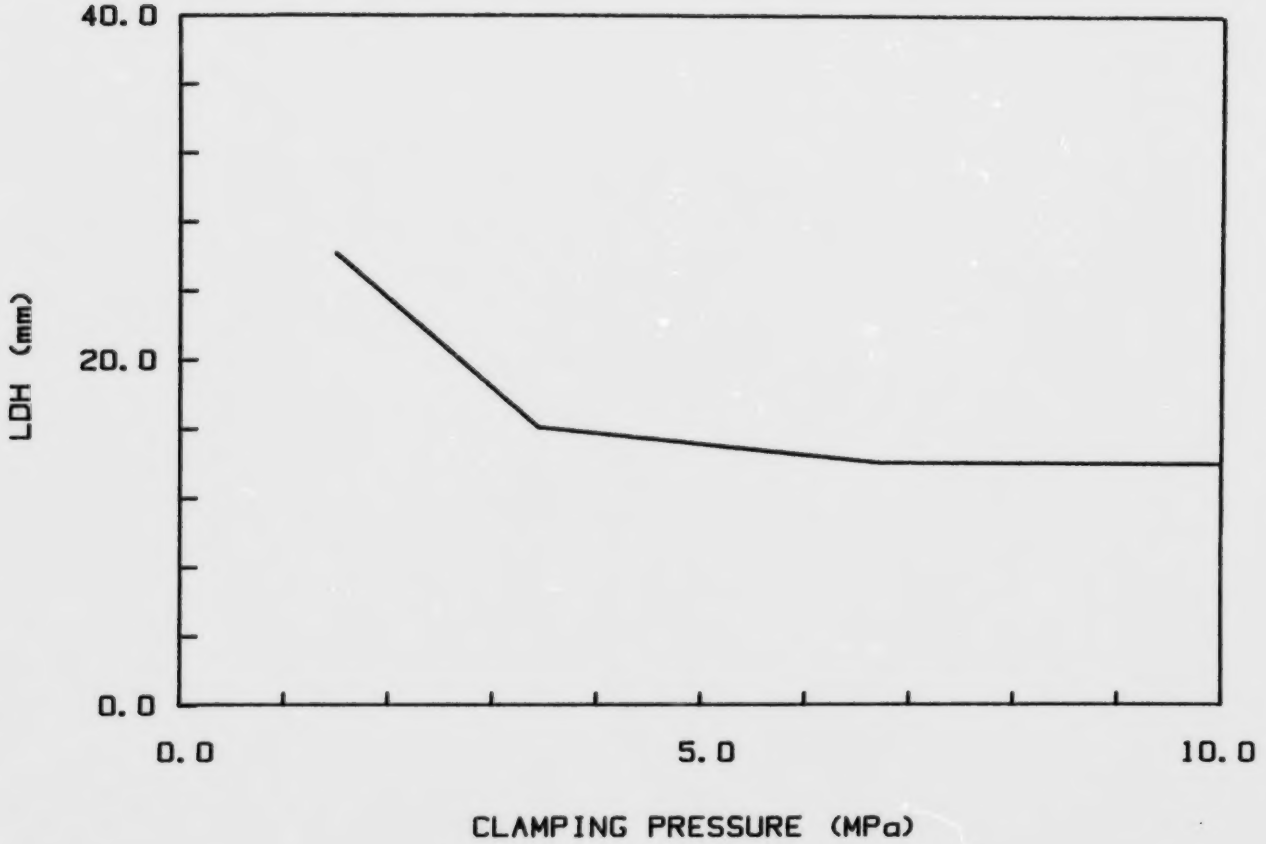

FIGURE 3

CLAMPING PRESSURE FOR THE LDH TEST

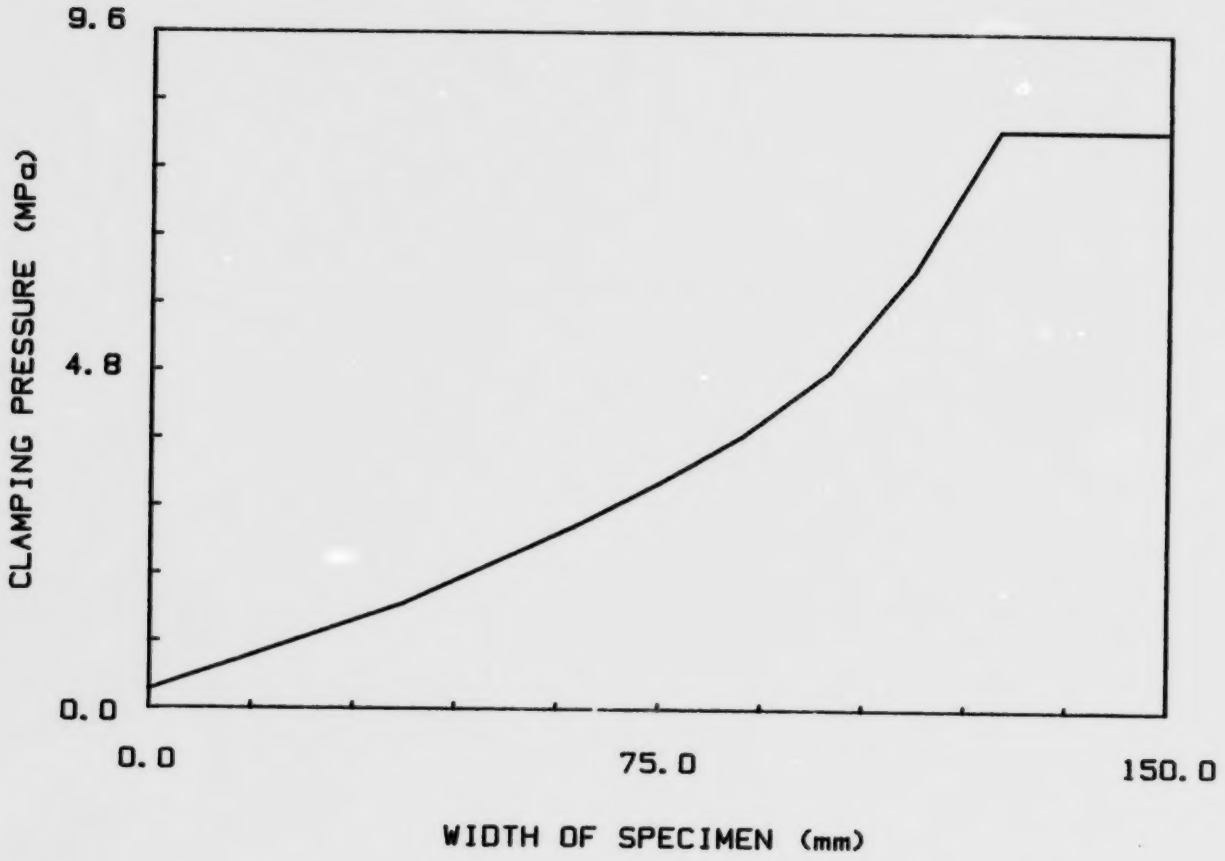

FIGURE 4
TYPICAL DOME HEIGHT PLOT

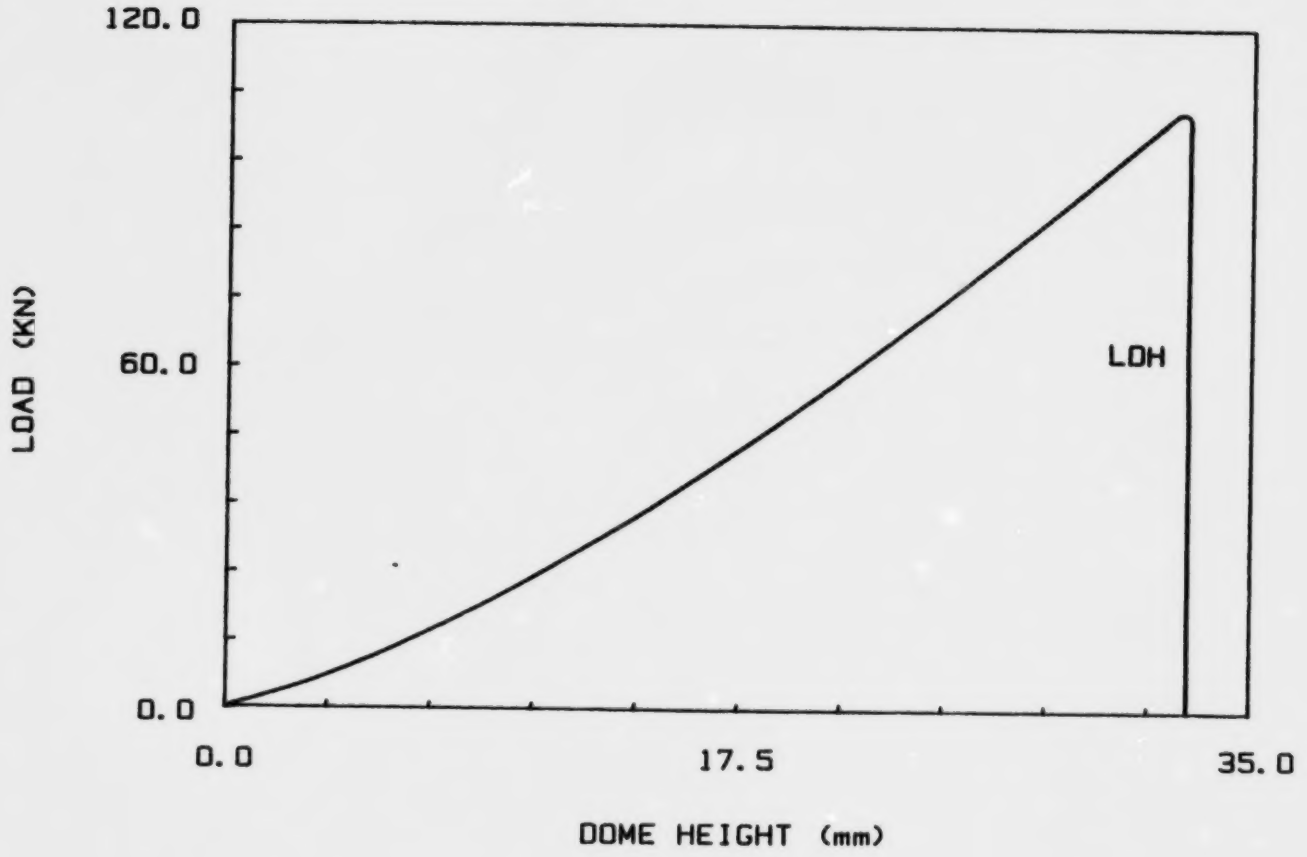

FIGURE 5

TYPICAL LDH CURVE

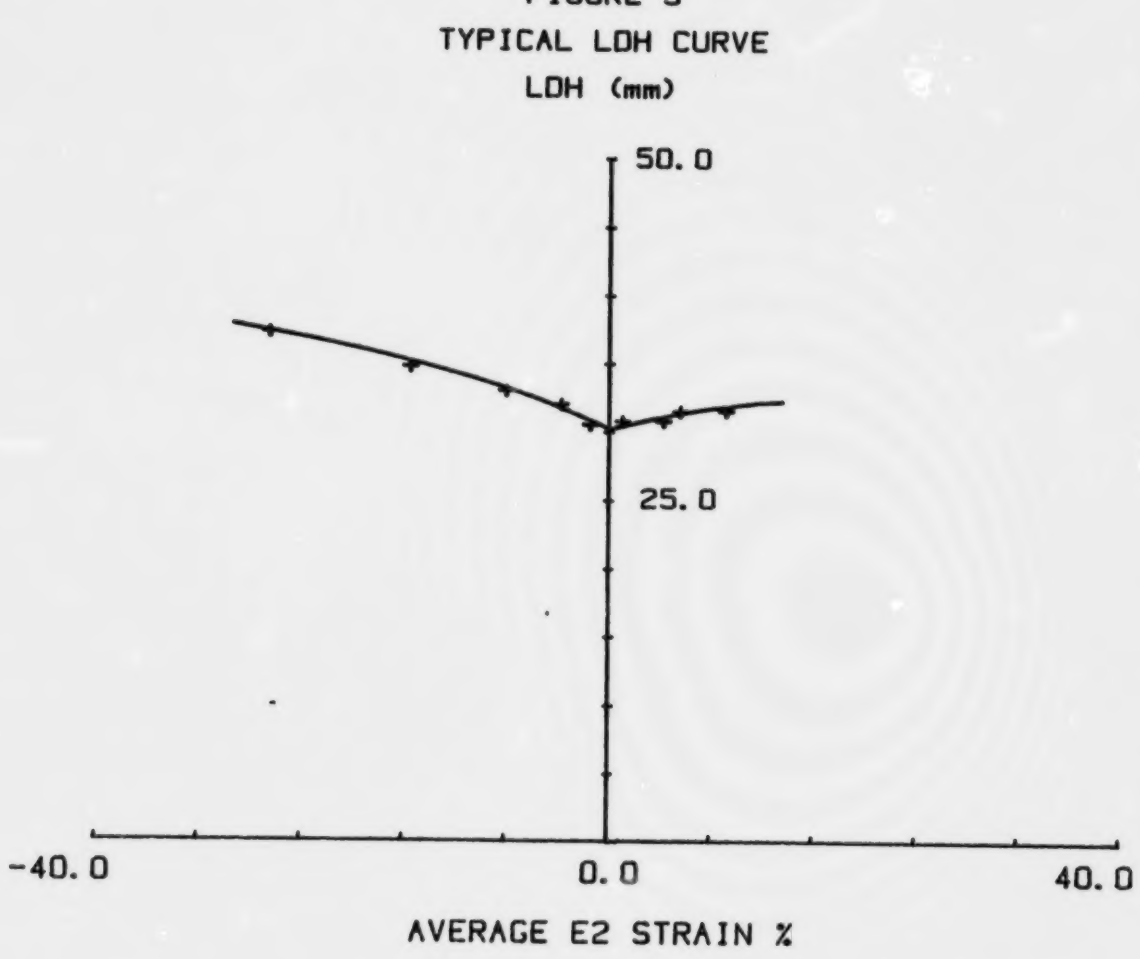

FIGURE 6
TYPICAL FORMING LIMIT DIAGRAM

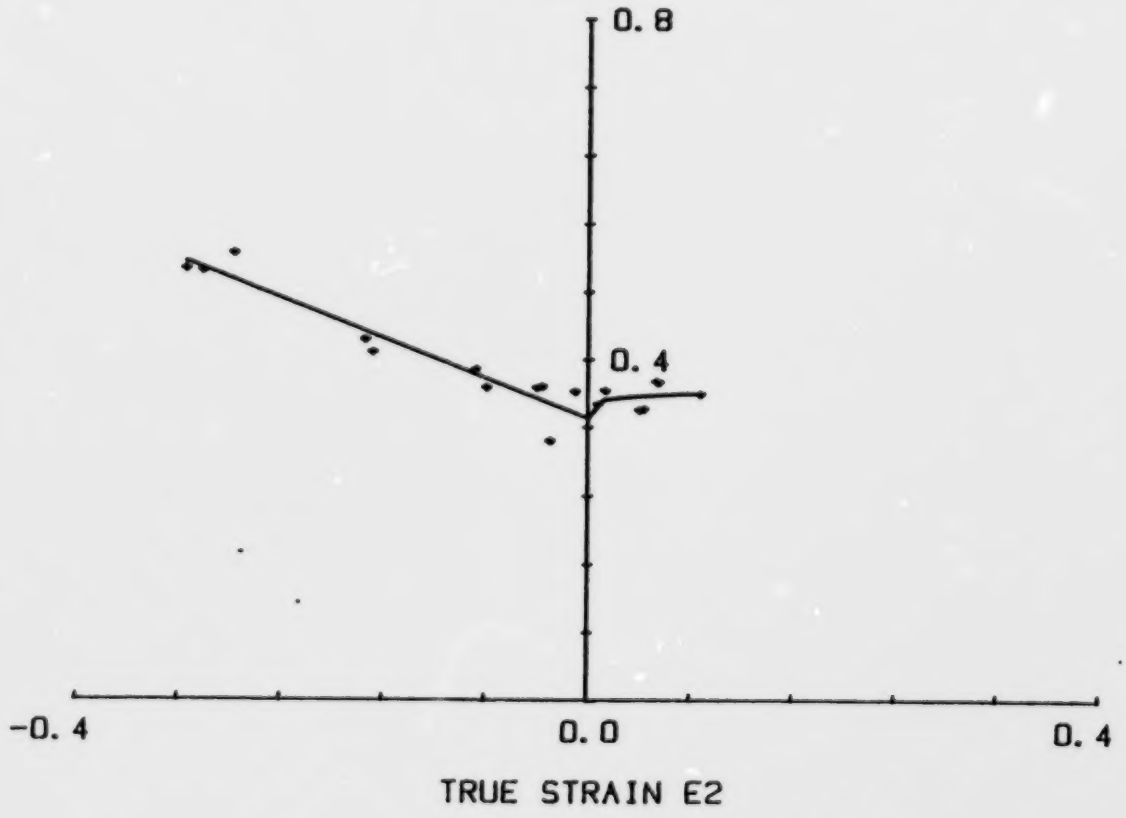

FIGURE 7

REPEATABILITY OF THE LDH VALUE
* : CLEANING PUNCH WITH 600 GRIT BEFORE EACH GROUP
+ : CLEANING PUNCH WITH 600 GRIT BETWEEN EACH TEST

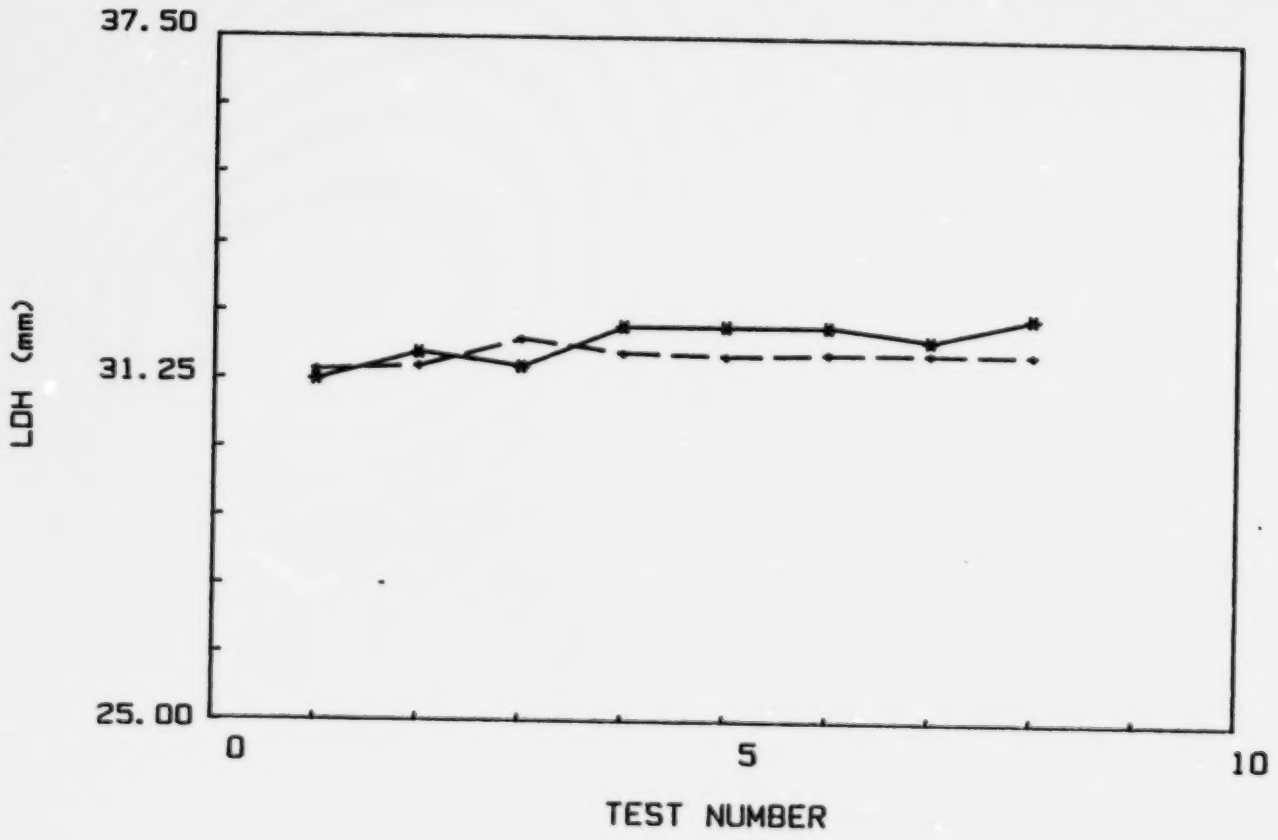

FIGURE 8

REPEATABILITY OF THE FLD

* : CLEANING PUNCH WITH 600 GRIT BEFORE EACH GROUP

+ : CLEANING PUNCH WITH 600 GRIT BETWEEN EACH TEST

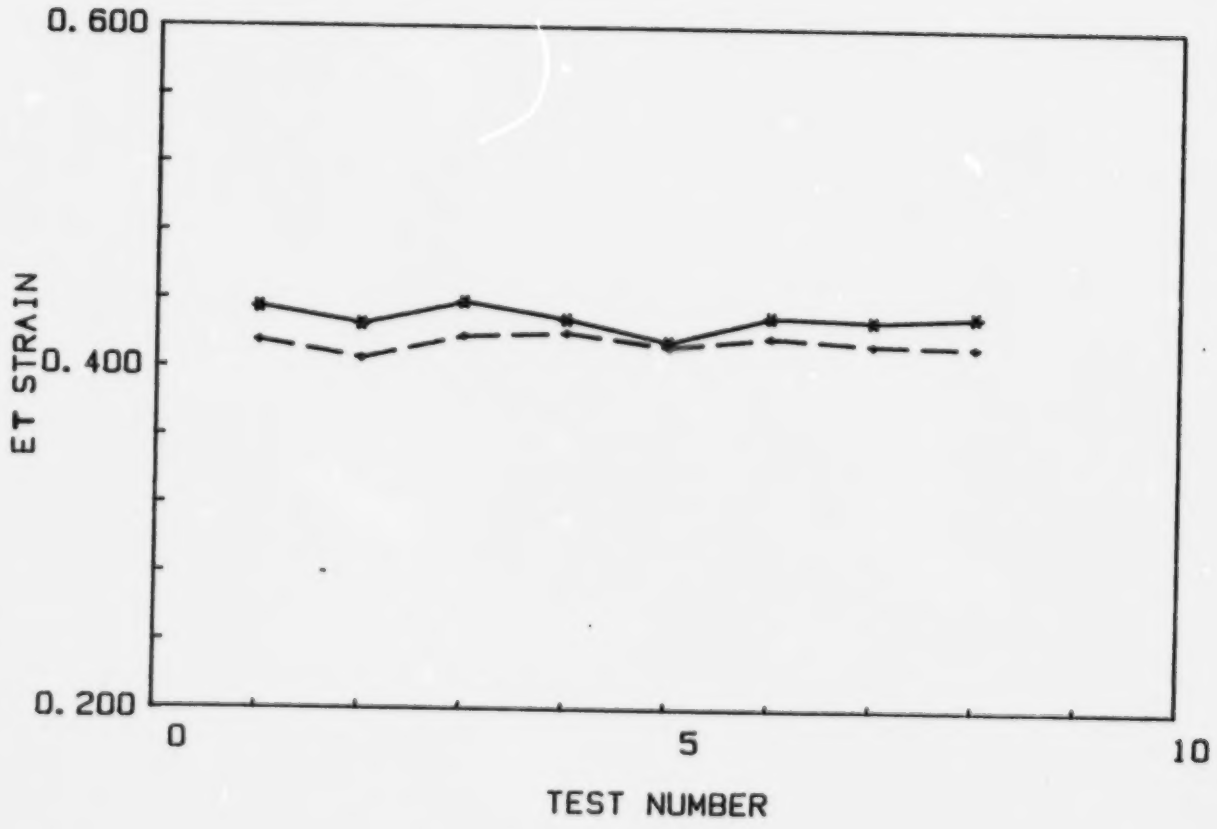

FIGURE 9.1

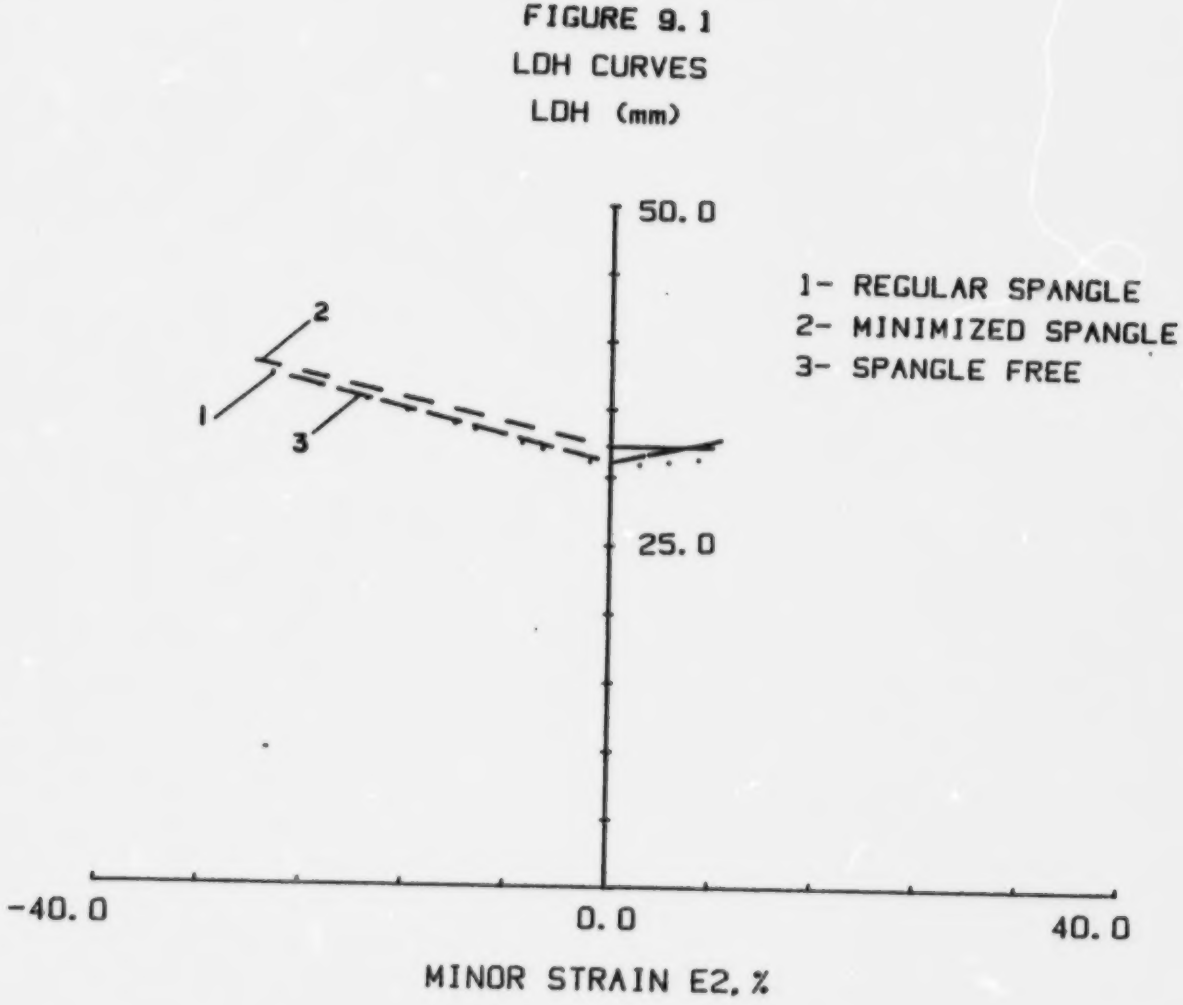
LDH CURVES
LDH (mm)
50.0
25.0
-40.0
0.0
40.0
1
2
3
1- REGULAR SPANGLE
2- MINIMIZED SPANGLE
3- SPANGLE FREE
MINOR STRAIN E2, %

FIGURE 9.2
LDH CURVES
LDH (mm)

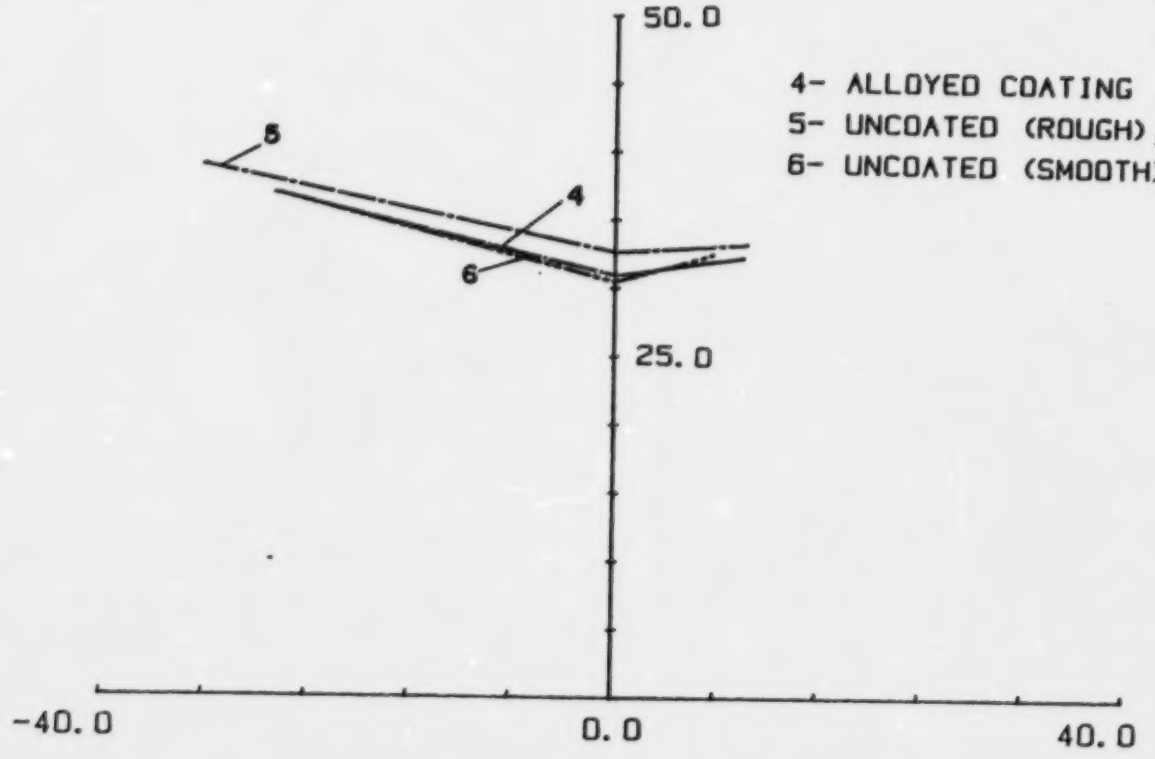

FIGURE 10.1
FLD CURVES

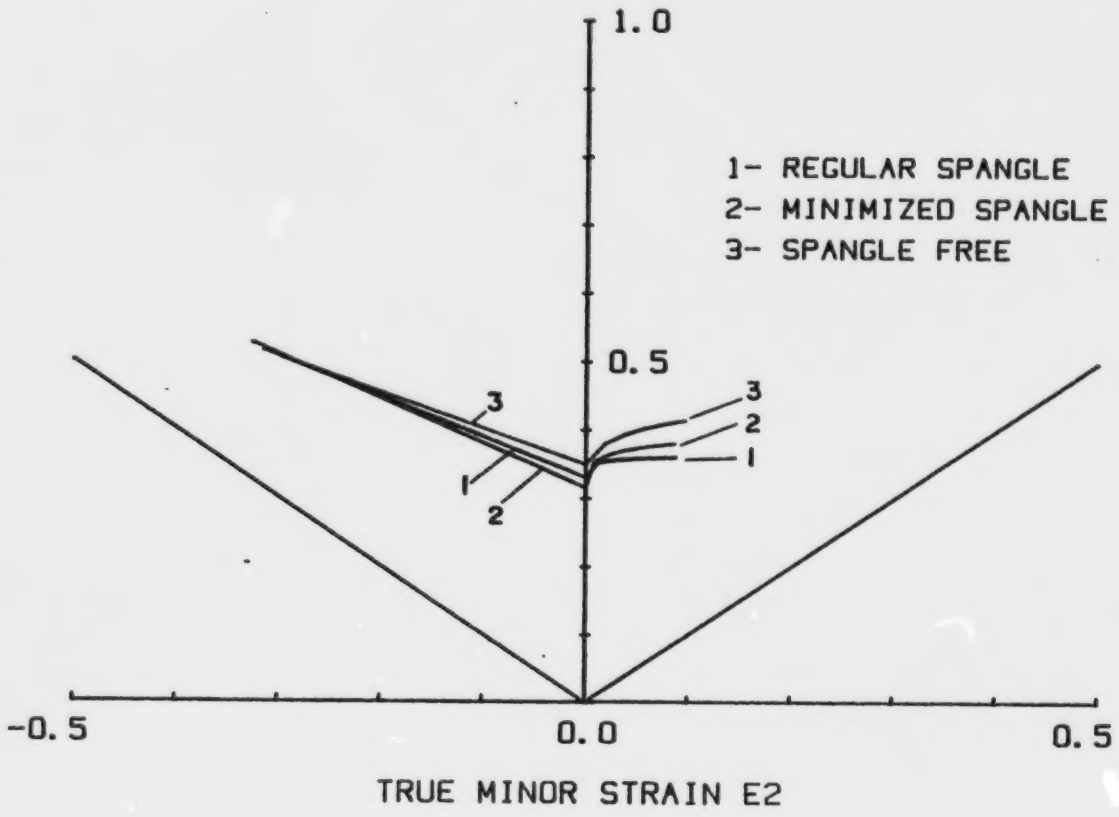

FIGURE 10.2
FLD CURVES

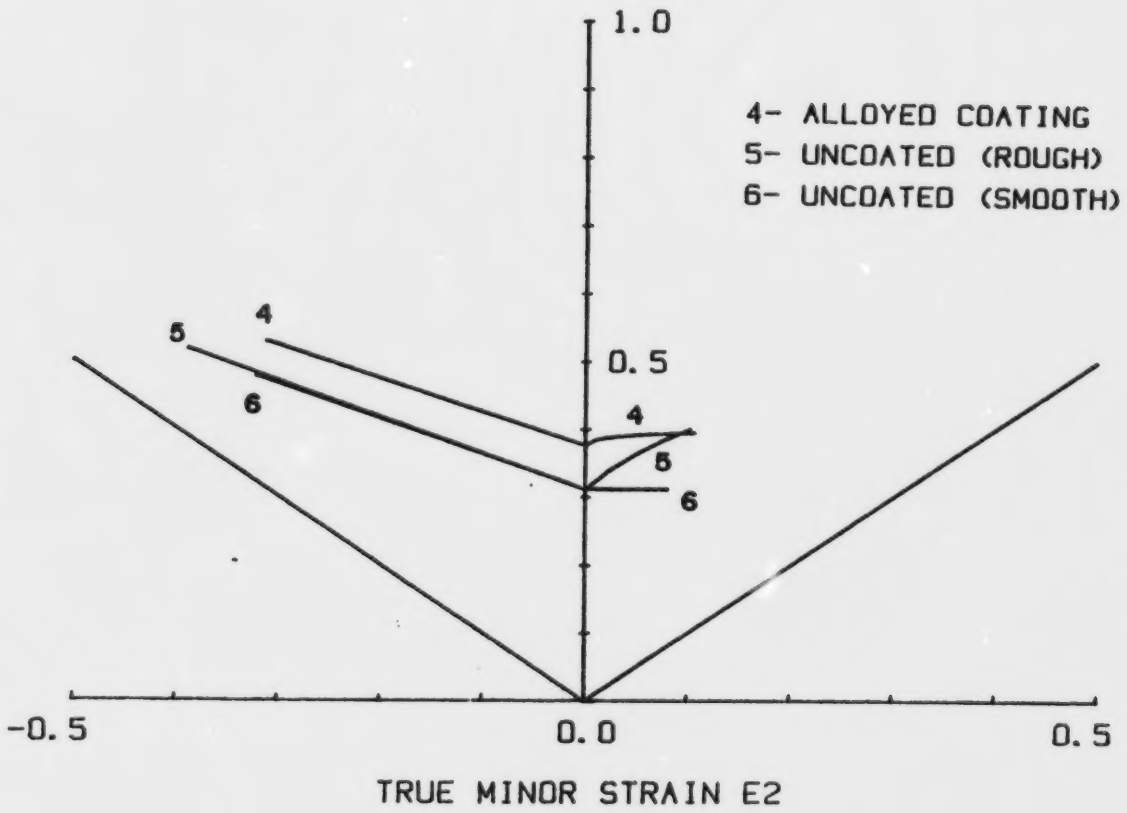

2. STRUCTURAL CHARACTERISTICS OF GALVANIZED COATINGS*

* This Chapter is available as a McMaster Metal Forming Research Report No. 85-005.

1. INTRODUCTION

The general objective of the investigation is to characterize galvanized sheet produced by various processes and to identify modes of failure of the coating and substrate during different sheet forming processes. This is an interim report covering work performed from September, 1984 to March, 1985.

Various samples of uncoated and hot-dip sheet have been obtained and the results of metallographic examination are given in Section 2. These materials represent the range of sheet likely to be used in formable applications.

2. STRUCTURAL CHARACTERISTICS OF GALVANIZED COATINGS

In order to characterize the behaviour of the various forms of galvanized coatings in formability tests, a series of detailed S.E.M. observations have been initiated. To date, the materials have been compared in the as-received condition and after hydraulic bulge testing. In the future, observations will be made of the materials after friction testing in order to determine their behaviour in relation to large surface deformations.

Let us consider first the scale of the coatings and their microstructural features relative to the steel substrate. This is illustrated schematically in Figure 1 which compares the grain size of the steel with the scale of the spangle for a conventional hot-dip galvanized product. The grain size of the steel substrate was of the order of 30 μm in all the materials considered in this study. This basic data concerning both the mechanical behaviour in the uniaxial tensile test and the thickness and surface roughness of the galvanized coating is summarized in Table I.

2.1 Structural Features in the Materials in the As-Received Condition

In characterizing the materials in the "as-received" condition, it is germane to note that some materials were subject to temper rolling and others were subject to post galvanizing

thermal cycles. These treatments can make significant differences both to the surface topography of the coating and the extent of pre-existing surface cracking. The basic coating history of the various materials is summarized in Table II.

Let us now consider the essential features of each material in the as- received condition.

a) Regular Spangle

The regular spangle material is characterized by a large scale dendritic structure (Figure 2). This was the only material in which significant quantities of extraneous surface contaminant were observed (Figure 3).

b) Minimized Spangle

This material had a much smaller scale dendritic structure (Figures 4 and 5).

c) Alloyed Coating

This material had a dendritic structure similar in scale to that of the minimized spangle (Figure 6). However the material also showed evidence of boundary cracking and changes in topography due to the surface tension of the galvanized layer (Figure 7). These changes are consistent with exposure of the material to an elevated temperature thermal cycle after galvanizing.

d) Ultracoat

This material had a fine grain structure which showed evidence of surface deformation consistent with its passage through a temper rolling or roller levelling operation (Figures 8 and 9).

e) Electrogalvanized Material

This showed a fine scale granular deposit with no evidence of dendrites but with copious evidence of layered growth defects in the granules (Figure 10). In the electrogalvanized material tested in the strip friction tester, there was evidence for deformation of the granular structure by shear (Figure 11).

2.2 Structural Features After Bulge Testing

Materials were tested in the hydraulic bulge test and samples were obtained from low strain and high strain regions as shown in Figure 12.

For clarity, examples are given for each material from the low strain and high strain regions. The high strain regions are from the centre of the bulge where equal biaxial stretching (thinning) occurs. The low strain regions are from the edge where the circumferential strain is zero and the radial is usually about half the membrane strain at the pole; this illustrates coating behaviour during plane strain deformation at low strain levels.

a) Regular Spangle

At low strain this material forms microcracks on well defined crystallographic planes (Figure 13). At large strains the microcracks increase in number (Figure 14) and in addition there is clear evidence of plastic deformation in the zinc from the observation of regular slip lines (Figure 15).

b) Minimized Spangle

The material exhibits, at small strains, much smaller microcracks consistent with the smaller scale of the spangle structure (Figure 16). As the strain increases, the surface topography characteristic of the dendritic structure becomes less pronounced. In the region adjacent to fracture in the bulge test, it is clear (Figure 17) that the coating fails by ductile rupture due to the large local strains in the steel substrate.

c) Alloyed Coating

An important characteristic of this material was that the sheet failed perpendicular to the rolling direction in the bulge test. This may reflect the heterogeneity of the underlying substrate and is being studied further. At low strains the material exhibited microcracks and enlargement of the interdendritic cracks observed in the as-received structure (Figure 18). At high strains, slip lines were observed indicating plastic deformation of the zinc together with an increase in the density of interdendritic cracks (Figure 19).

d) Ultracoat

At low strains this material does not exhibit crystallographic microcracks but shows abundant evidence of intergranular cracks as shown in Figure 20. Close to the fracture region it is clear that the steel substrate has failed by shear causing ductile tearing in the coating and delamination from the steel in the immediate vicinity of the fracture (Figure 21).

CONCLUSIONS

To date, only the behaviour in the bulge test has been examined. However, there is no structural evidence to suggest that failure occurs due to the propagation of cracks from the coating to the substrate. The scale and orientation of the grains in the coating clearly influences the processes of deformation and microcracking. The structural studies will be extended to consider cross sections of failed material, the behaviour of the electrogalvanized material and the deformation and fracture processes associated with friction on the galvanized layer.

TABLE I

Mechanical Properties of Materials Tested

Material	Yield (MPa)	UTS (MPa)	n	K	ε_u	ε_{tot} (%)	r	R_{ave} (μm)	Coating Thickness (μm)
Regular Spangle	284	325	.24	582	.22	39.7	1.37	0.41	27
Minimized Spangle	288	324	.25	584	.25	65.9	1.01	1.60	34
Alloyed Coating	271	342	.22	575	.22	53.2	0.84	2.84	45
"Ultracoat"	220	336	.19	544	.20	43.0	1.24	0.71	27
Electro-galvanized	198	312	.20	512	.20	47.5	2.06	1.73	30

TABLE II

Coating History of Materials Tested

1.	Regular spangle	–	Z275 coating (approx. 138 g/m^2 each side)
		–	AK-DDQ substrate
2.	Minimized spangle	–	Z200 coating (approx. 100 g/m^2 each side)
		–	zinc grain size reduced with an air quench
		–	AK-DDQ substrate.
3.	Alloyed coating	–	minimized spangle coating heat treated to produce a coating consisting entirely of Fe-Zn intermetallic.
4.	Ultracoat	–	Z200 coating
		–	zinc dust blown onto suface to produce a very fine grain size.
		–	rimmed - Al killed substrate.
5.	Electrogalvanized	–	electroplated to a thickness resembling Z90 one side (90 g/m^2)
		–	characterized by the orientation of the grains' basal planes parallel to the sheet surface.

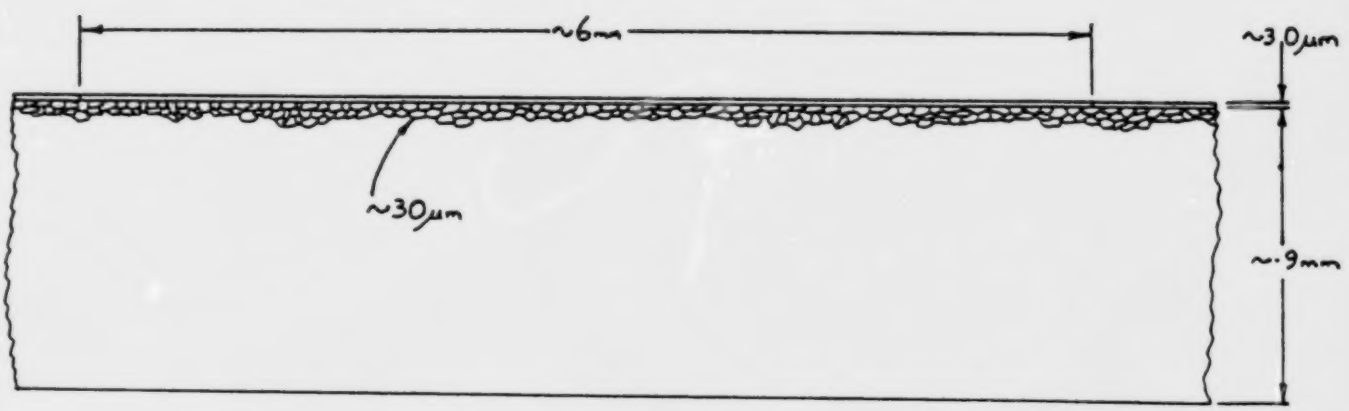

Fig. 1 Comparison of Zinc grain size for regular spangle with steel grain size.

Fig. 2 Large scale dendritic structure of regular spangle coating as received (Etched in CrO_3, Na_2SO_4 solution to show grain size).

Fig. 3 Surface contaminant on regular spangle sheet.

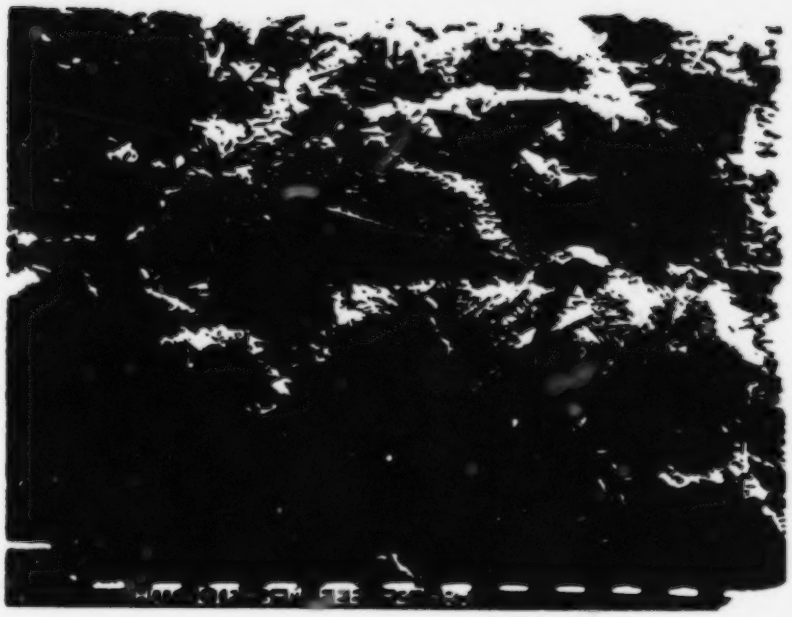

100 μm

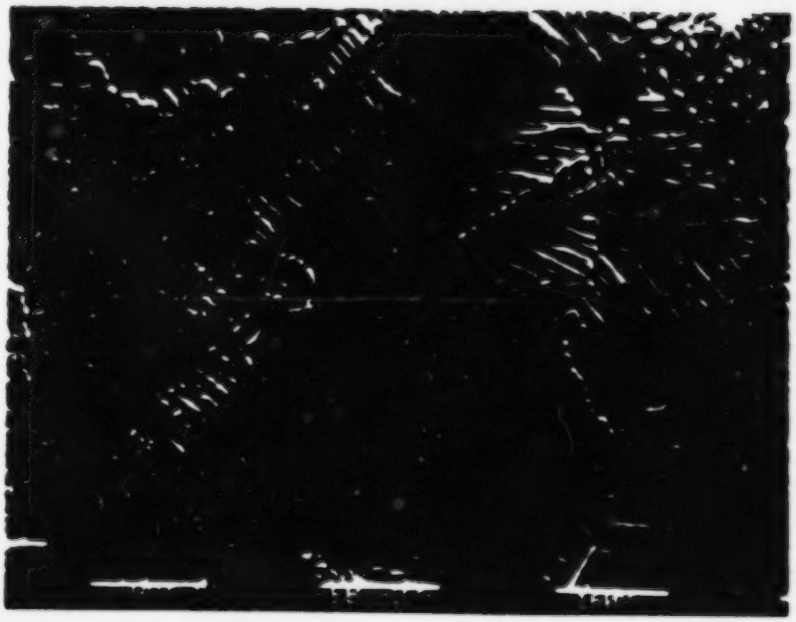

100 μm

Fig. 4 & 5 Minimized spangle surface structure as received.

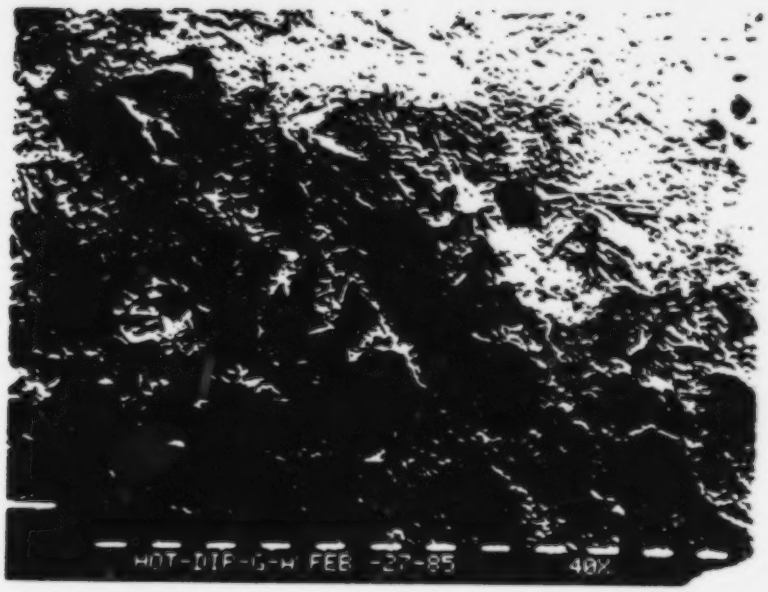

100 μm

Fig. 6 Alloyed coating surface structure as received.

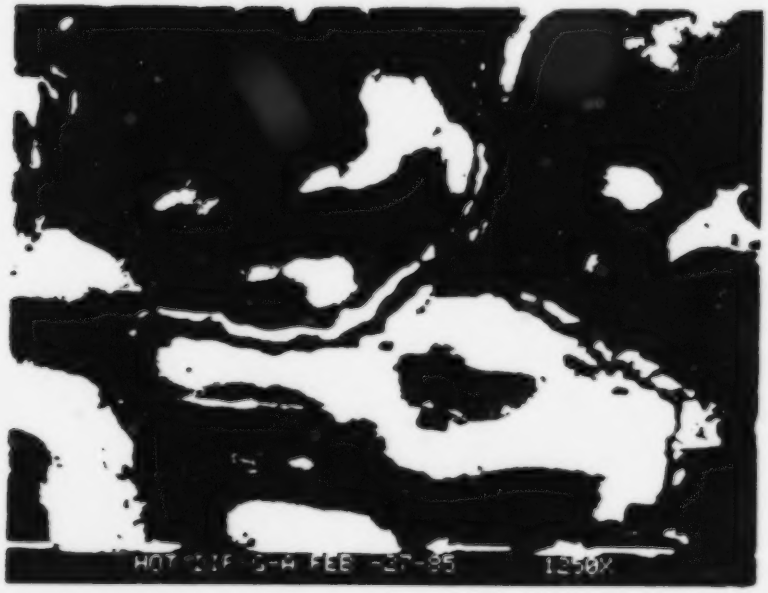

10 μm

Fig. 7 Alloyed coating as received. Note the boundary cracking.

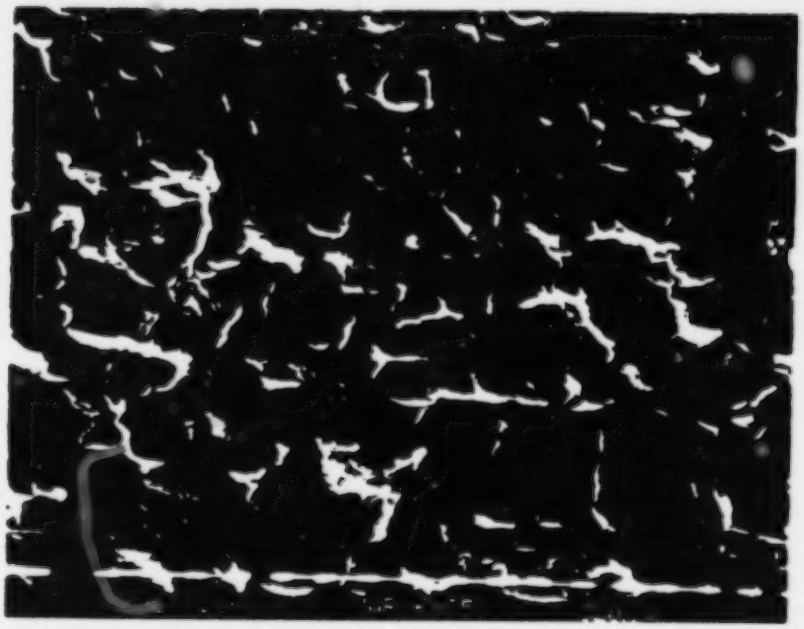

20 μm

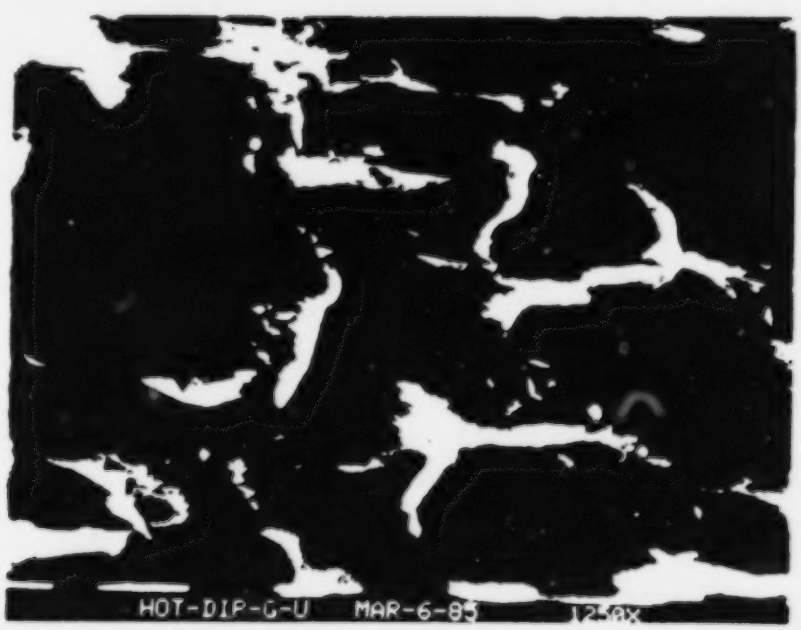

10 μm

Fig. 8 & 9 "Ultracoat" as received. Note the lack of dendrites and the evidence of temper rolling.

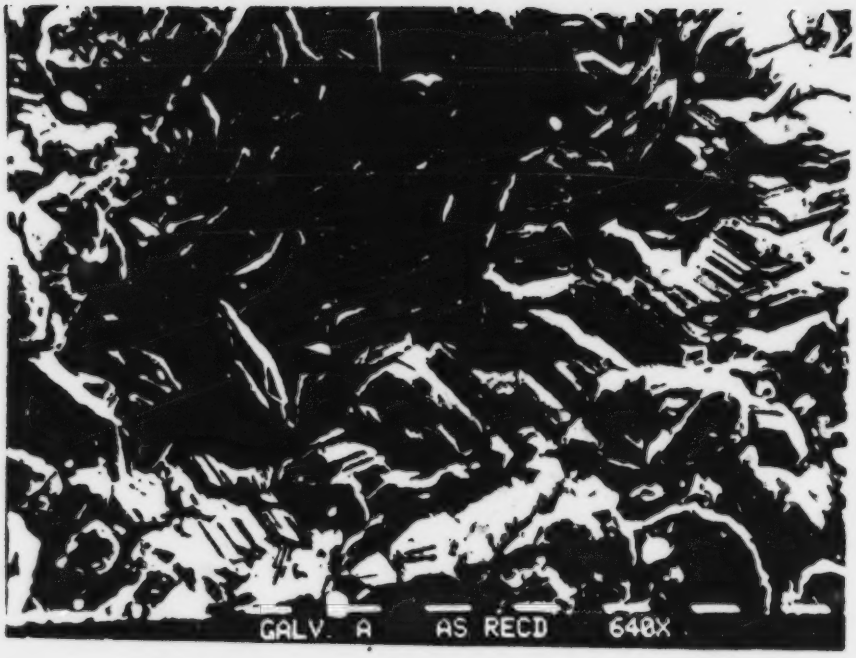

10 μm

Fig. 10 Electrogalvanized material as received.

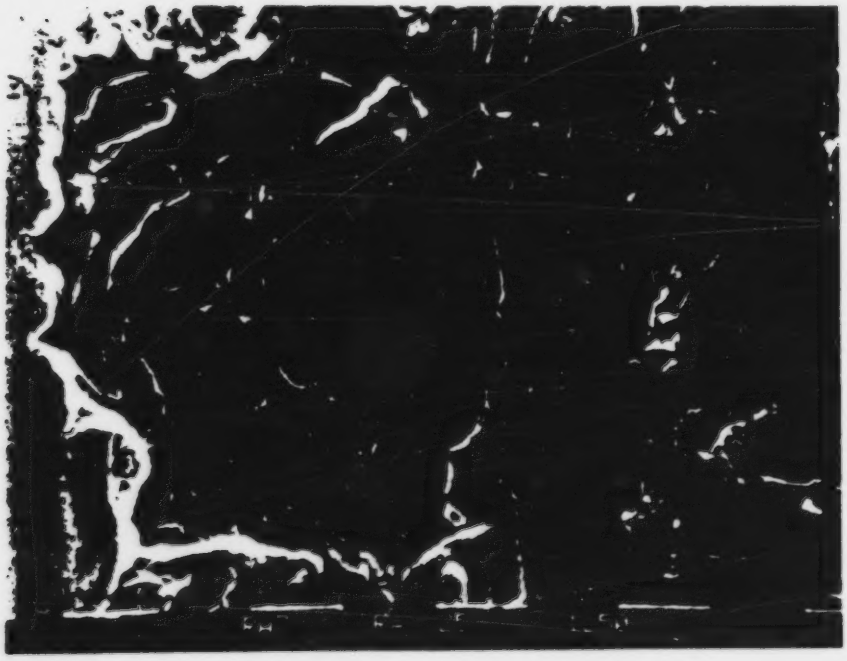

10 μm

Fig. 11 Electrogalvanized surface after deformation in strip friction test.

Bulge Test Observations

Fig. 12 Regions observed in fractured hydraulic bulge test samples.

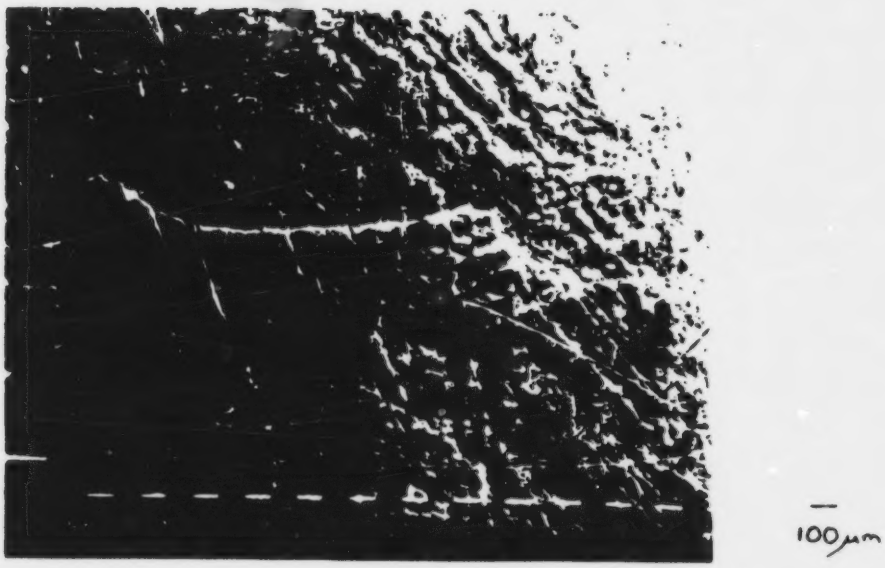

Fig. 13 Microcracks observed at low strain in regular spangle coating.

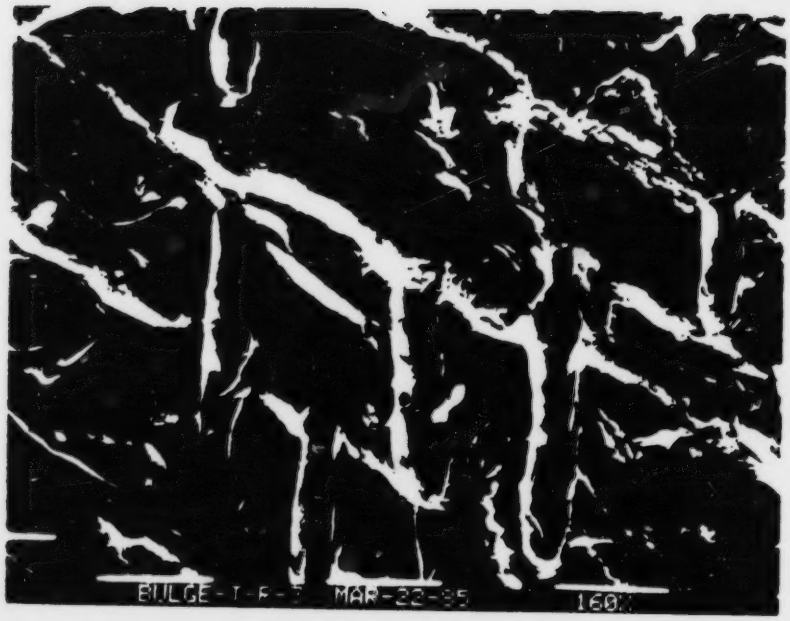

100 μm

Fig. 14 Increased density of microcracks at large strain.

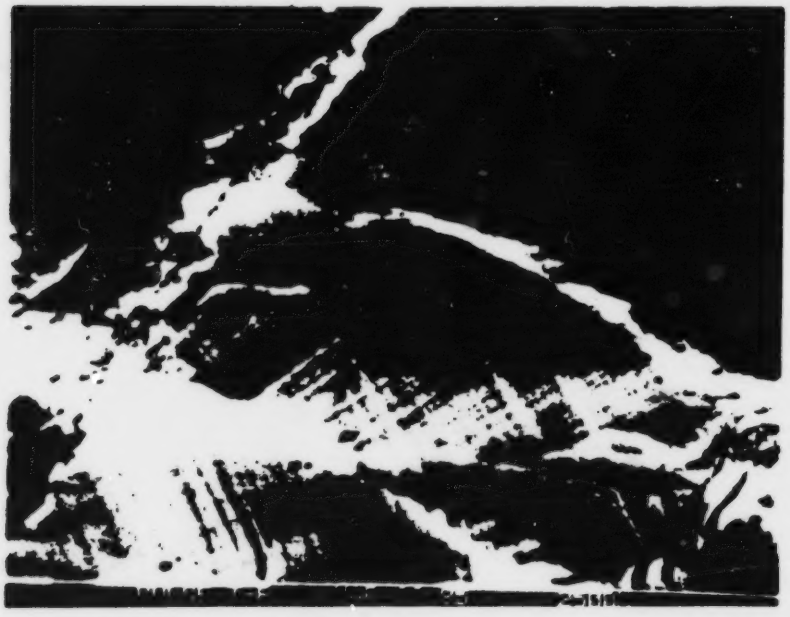

10 μm

Fig. 15 Slip lines on regular spangle grains at large strain.

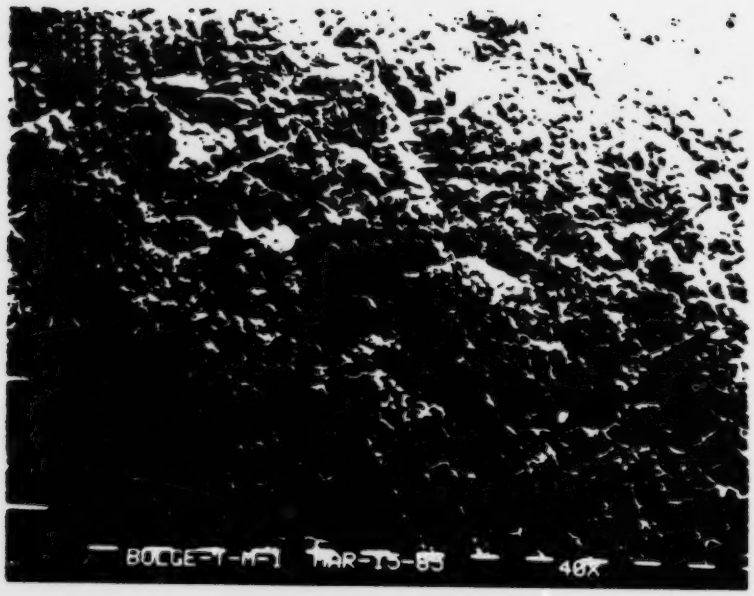

100 μm

Fig. 16 Minimized spangle - microcracks at low strain.

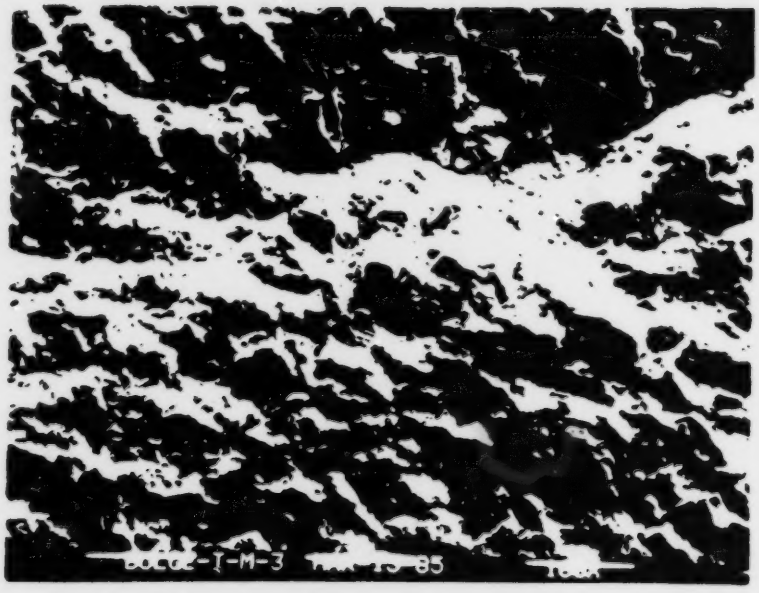

100 μm

Fig. 17 Rupture of the minimized spangle coating in the vicinity of the fracture.

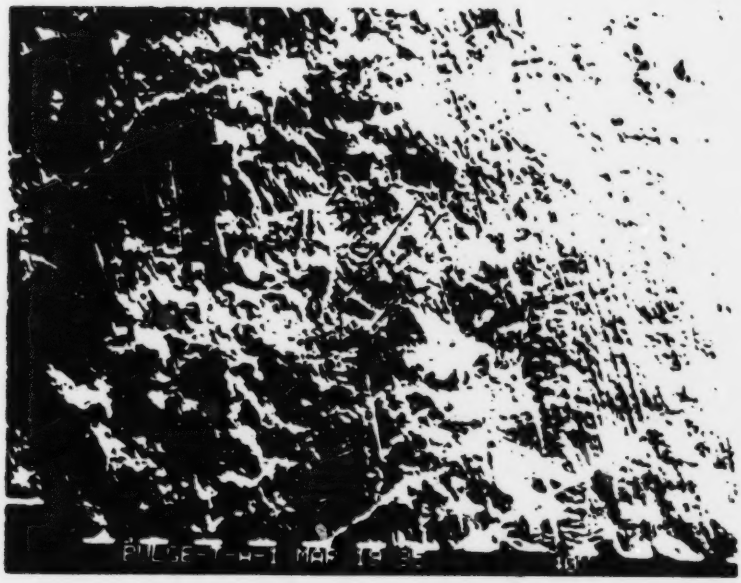

100 μm

Fig. 18 Alloyed coating - microcracks at low strain.

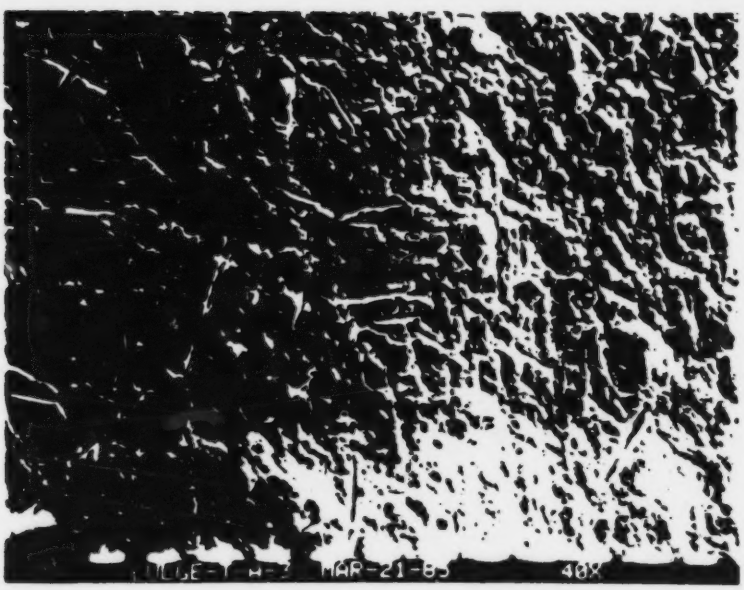

100 μm

Fig. 19 Alloyed coating - increased density of microcracks at large strain.

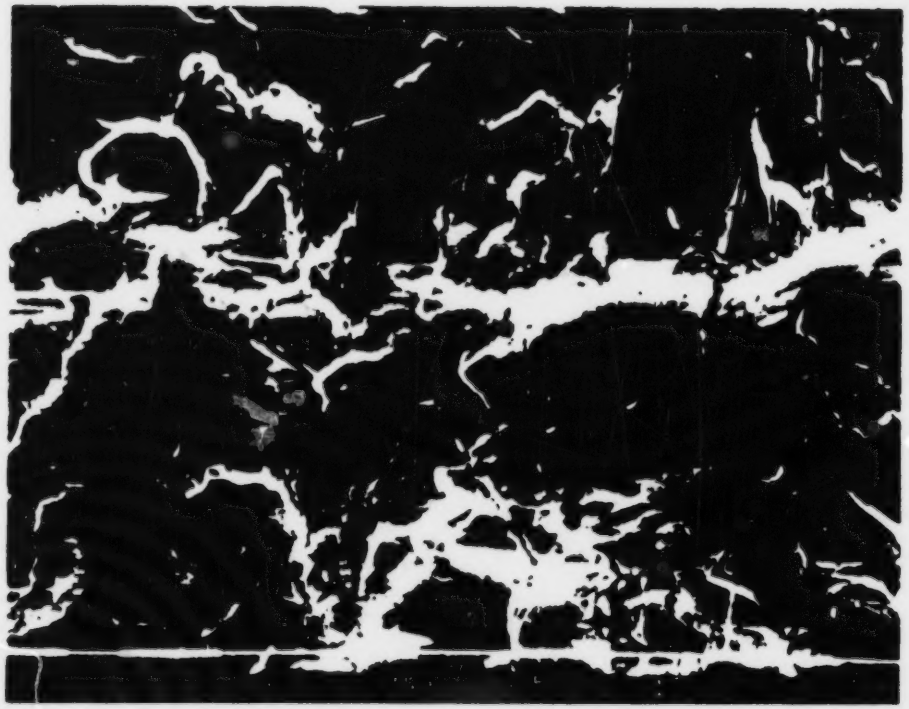

Fig. 20 Intergranular cracking at low strains in Ultracoat.

Fig. 21 Ductile tearing of coating and delamination from the substrate near the fracture in Ultracoat.

3. NORMAL PLASTIC ANISOTROPY IN GALVANIZED AND UNCOATED DRAWING QUALITY STEEL*

INTRODUCTION

The tensile r-value is considered an important formability factor in low carbon steel sheet [1,2]. It is the ratio of width to thickness strain in a uniformly deforming tensile strip and is one measure of anisotropy in the sheet. It is important to note that while the r-value will indicate the presence of anisotropy in a sheet, it does not in itself define an anisotropic yield function.

One of the simplest anisotropic yield criteria is due to Hill [3], which reduces to the von Mises yield condition for an isotropic material. For a planar isotropic material, the plane stress yield locus according to Hill's criterion is an ellipse, as is the locus for the von Mises criterion. However, the ellipse for the anisotropic yield function, vis à vis the von Mises ellipse, is either elongated or contracted in the first and third quadrants depending upon whether the r-value is greater or less than unity, respectively.

From the Hill model, r-values greater than unity imply that in a sheet forming process, the deformation takes place more easily within the plane of the sheet than in the through thickness direction, see for example Ref. [4].

For a planar isotropic material, obeying the Hill criterion, it can be shown [1] that increasing the r-value increases the limiting drawing ratio when drawing cylindrical cups from circular discs. Wilson [5] has demonstrated this experimentally using a variety of materials, including materials of hexagonal structure such as zinc and titanium. In spite of the experimental evidence, it is unlikely that all the materials tested by Wilson obeyed Hill's anisotropic yield criterion. Many years earlier, Lankford et al. [6] had equated an increase in deep drawability with an increase in r-value from tests on a number of sheet steels when forming actual components.

Galvanized sheet has been used traditionally for parts of simple shape, but more recently there has been considerable interest in forming complex shapes from galvanized material, particularly for automotive stampings [7,8]. It is important, therefore, to investi-

* This Chapter is available as a McMaster Metal Forming Research Report No. 85-003.

gate the effect of galvanizing on anisotropy [9], and also to consider how this should be measured.

The anisotropy of the galvanized sheet will undoubtedly differ from that of the uncoated material. This follows becauses the texture of the deposited zinc will be different from that of the steel. The zinc coating will impose a constraint on the steel and vice-versa. The response of the galvanized sheet is unlikely to be predicted on the basis of any simple law of mixtures.

The present report deals with the measurement of r-values for uncoated and galvanized sheet, and a comparison of the behaviour of these same materials in uniaxial tension and balanced biaxial tension. It is assumed that the uncoated and coated materials obey Hill's anisotropic yield criterion, although it is anticipated that this is unlikely to be true for the galvanized sheet.

Hill's anisotropic yield criterion has been discussed in many scientific papers, however, the principal features are presented below.

HILL'S ANISOTROPIC YIELD MODEL

For a planar isotropic material, Hill's model for the case of plane stress reduces to

$$\sigma_1^2 - \left(\frac{2r}{r+1}\right)\sigma_1\sigma_2 + \sigma_2^2 = Y^2 \qquad (1)$$

which plots as an ellipse in principal stress space, see Fig. 1. In the above equation, σ_1 and σ_2 are the in-plane principal stresses, Y the yield stress in uniaxial tension and r is of course the r-value. Many investigators have used eqn. (1), even though the material has not been planar isotropic. In such cases, an average r-value has been employed.

As already mentioned when $r > 1$, the ellipse is elongated in the first and third quadrants, see Fig. 1. This results in an increase in strength in biaxial tension* (where $\sigma_1 = \sigma_2$)

---

* It is well known that an increase in biaxial yield strength implies an increase in the through thickness strength

and a decrease in strength in the drawing mode ($\sigma_1 = -\sigma_2$), vis à vis the von Mises ellipse. The reverse is true when $r < 1$.

Normal anisotropy is often defined by the empirical expression

$$r = \frac{r_0 + r_{90} + 2r_{45}}{4} \tag{2}$$

or some variant on this theme. In eqn. (2), the r_0, etc., refers to experimentally determined r-values from tensile specimens, cut at 0, 45 and 90 degrees, respectively to the rolling direction. For a planar isotropic material $r_0 = r_{45} = r_{90}$ 1.

From eqn. (1), the r-value can also be determined by comparing the bulge and tensile test data. If σ_b is the biaxial yield strength, i.e. $\sigma_b = \sigma_1 = \sigma_2$, then, from (1), the ratio between the biaxial and uniaxial yield strength, Y, is

$$\sigma_b/Y = \sqrt{\frac{r+1}{2}}, \tag{3}$$

the ratio is greater or less than unity, depending upon whether r is greater or less than one. The above expression is valid, providing the material obeys the anisotropic yield function (1).

However, it is generally not appreciated that σ_b and Y should not be determined at the same percentage strain from the bulge and tensile tests i.e. the raw data should be adjusted before a comparison of the stresses is made. Woodthorpe and Pearce [10] have found conflicting experimental evidence to the trend predicted by eqn. (3), for a number of materials where $r < 1$, i.e. the stress-strain curve for the bulge test was found to lie above the tensile stress-strain curve. Hence, these materials did not obey the quadratic function given in eqn (1). Alternative yield functions which can explain the experimental results found by Woodthorpe and Pearce have been proposed in Refs. [11-13]. These latter criteria will not be discussed further in this report.

MATERIALS

Four hot-dipped galvanized and two uncoated drawing quality sheet steels were tested. Further details of material production and the structure of the coating may be found in Ref. [14], but the mechanical properties are given here.

The hot-dipped galvanized materials were:

regular spangle (RS),

minimized spangle (MS),

spangle free (SF),

alloyed coating (AC).

The uncoated materials were:

cold rolled steel – rough surface (VR), R_a = 1.42 μm,

cold rolled steel – smooth surface (US), R_a = 0.89 μm.

The chemical composition of the substrate was provided by DOFASCO, for all the materials, other than the alloyed coated. The chemistry was essentially the same for all the steels and typical of a drawing quality grade with aluminium additions. The carbon content of the ultracoat was 0.07%, and somewhat higher than that of the other steels which ranged from 0.04 - 0.05%.

The substrate of the coated sheets had experienced a different processing history than the uncoated steels. The former had been continuously annealed followed by a batch anneal overage, while the latter had been batch annealed only (30 hours at 1300°F). In addition both uncoated steels and the ultracoat material had been temper rolled, while the remaining coated sheets had not. One further distinction was the material gauge, all the coated sheets were nominally 0.030 in. (0.75 mm) thick while the uncoated steels were 0.045 in. ($\simeq$1.00 mm).

EXPERIMENTAL METHODS

Uniaxial tensile tests were performed on samples oriented at 0°, 45° and 90° to the rolling direction. Width strain measurements at 15% elongation were made for the r-value calculations.

Biaxial tension tests were carried out on an automated hydraulic bulge tester [15].

RESULTS AND DISCUSSION

Figures 2-7 show the true stress-strain curves for the materials tested. The results are summarized in Tables 1 and 2. For each material, the stress-strain curve from the bulge test is higher than the uniaxial tensile curve. This is consistent with an r-value greater than unity, as given by eqn. (3)†.

Duncan [15] has suggested an alternative relation that enables an average r-value to be calculated using uniaxial tensile and hydraulic bulge test data, namely

$$r_2 = 2\left[\frac{\sigma_b}{\frac{1}{4}\left(\sigma_0 + 2\sigma_{45} + \sigma_{90}\right)}\right]^{\left(\frac{2}{n+1}\right)} - 1 \qquad (4)$$

The above equation has been derived on the basis of equal work done in the tensile and bulge test. It is assumed that the true stress-true strain curve for each test can be fitted by a power hardening law of the form

$$\bar{\sigma} = K\,\bar{\varepsilon}^{n},$$

and that the strain hardening index, n, is the same for each test. This latter assumption is not unreasonable, as the n-values given in Tables 1 and 2 will testify.

Figure 8 and Table 3 show average r-values calculated using both eqns. (3) and (4), along with the measured values in the uniaxial tensile test. The calculated values, using (3) or (4), are quite close to the average measured r-values. One interpretation of this result is that, to a first approximation, all the materials obey Hill's anisotropic yield function given by eqn. (1).

Bramley and Mellor [17] have demonstrated that a number of stabilized steel sheets fit the criterion (1) reasonably well. However, the same authors [18] have demonstrated that zinc sheet does not. Texture data and the mode of deformation were analyzed in a companion paper [19]. As discussed in Ref. [19], zinc sheet, where the basal planes lie in the plane of the

---

† It is assumed that the materials obey eqn. (1).

sheet, experiences twinning when deformed in uniaxial tension; and this results in rather low r-values, i.e., $r << 1$.

The preceding statement is consistent with the present data, where the measured r-values for the coated materials are much lower than the r-values for the uncoated steel. However it is unlikely that the zinc coating alone is responsible for the diminution in the r-value. As mentioned previously, the processing of the coated and uncoated steels was different and this is likely to be the main reason for the difference in r-value. It is intended to strip the zinc deposit from one of the hot dipped sheets and repeat the r-value measurements on the substrate. This will provide a more positive account of the influence of the zinc coating.

All the materials exhibited planar anisotropy, with the lowest r-value occurring in the 45° direction. Although the r-values were lower for the hot-dipped sheets (see Table 2) the degree of earing, as measured in some preliminary cuping tests, was about the same for all the materials. The percentage earing was evaluated from

$$\left(\frac{\text{Ear Height} - \text{Trough Height}}{\text{Average Cup Height}}\right) \times 100\,,$$

and a value of about 11% was determined.

The data from the tensile and bulge tests suggest that neither the strength nor ductility of the galvanized sheets is significantly different from the uncoated steels. However, as discussed above, the normal anisotropy of the hot dipped materials is less than that of the uncoated steels on the basis of eqn. (2). What influence this might have on press shop performance has not been established. Some experimental work [20], conducted in tandem with the present study, indicates that the limiting dome height (L.D.H.) of the galvanized and uncoated steels is very similar. It must be pointed out that the uncoated sheet is about 50% thicker than the galvanized steels, and this could have some effect on the L.D.H. results.

REFERENCES

1. R.L. Whiteley, Trans. Am. Soc. Metals, Vol. 52, p. 154, 1960.
2. D.J. Blickwede, "New Knowledge about Sheet Steel", ASM, Metals Park, Ohio, 1970.
3. R. Hill, Proc. Roy. Soc., Vol. 198A, p. 281, 1948.
4. W.F. Hosford and R.M. Caddell, Metal Forming: Mechanics and Metallurgy, Prentice-Hall, 1983.
5. D.V. Wilson, J. Inst. Metals, Vol. 94, p. 84, 1966.
6. W.T. Lankford, S.C. Snyder and J.A. Bauscher, Trans. Am. Soc. Metals, Vol. 42, p. 1197, 1950.
7. A.S.M., Proceedings, Conference on the Technological Impact of Surfaces, ASM, Metals, Park, Ohio, 1982.
8. D.J. Meuleman, S.G. Denner and F.L. Cheng, SAE Tech. Paper No. 840370, 1984.
9. I. Aoki, T. Horita and T. Herai, in Proceedings, Conference on Technological Impact of Surfaces, ASM, Metals Park, Ohio, 1982.
10. J. Woodthorpe and R. Pearce, Int. J. Mech. Sci., Vol. 12, p. 341, 1970.
11. R. Hill, Math. Proc. Comb., Phil. Soc., Vol. 85, p. 179, 1979.
12. W.F. Hosford, Proc. 7th North Am. Metalworking Res. Conf., p. 191, SME, 1979.
13. J.L. Bassini, Int. J. Mech. Sci., Vol. 19, p. 651, 1977.
14. Metal Forming Research Report No.85-005, McMaster University, September 1985.
15. J.L. Duncan, J. Kolodziejski and G. Glover, Proc. 9th Biennial Congres of I.D.D.R.G., p. 131, 1976.
16. J.L. Duncan, Int. J. Mech. Sci., Vol. 9, p. 157, 1967.
17. A.N. Bramley and P.B. Mellor, Int. J. Mech. Sci., Vol. 8, p. 101, 1966.
18. A.N. Bramley and P.B. Mellor, Int. J. Mech. Sci., Vol. 10, p. 211, 1968.
19. D.H. Rogers and W.T. Roberts, Int. J. Mech. Sci., Vol. 10, p. 221, 1968.
20. D. Overby and Ru Zheng, Metalforming Research Report 85-004, McMaster University, December 1985.

TABLE 1

UNIAXIAL TENSILE TEST RESULTS

MATERIAL	ORIENTATION W.R.T ROLLING DIRECTION	YIELD STRENGTH (MPa)	U.T.S. (MPa)	ε_u	$\sigma = K\varepsilon^n$ (MPa) n	K	r
REGULAR SPANGLE	0	284	331	.22	.24	582	1.57
	45	297	335	.19	.24	600	1.24
	90	288	330	.21	.26	611	1.44
MINIMIZED SPANGLE	0	288	323	.25	.25	584	1.14
	45	290	333	.20	.24	595	.73
	90	278	321	.20	.26	594	1.44
SPANGLE FREE	0	220	336	.20	.19	544	1.29
	45	231	344	.19	.19	555	1.09
	90	220	338	.18	.19	555	1.50
ALLOYED COATING	0	275	342	.22	.22	575	1.03
	45	293	344	.21	.23	607	0.88
	90	302	345	.19	.22	598	1.11
UNCOATED (ROUGH)	0	194	300	.22	.27	547	1.74
	45	219	320	.18	.26	611	1.41
	90	212	302	.20	.26	566	2.45
UNCOATED (SMOOTH)	0	202	315	.21	.25	597	2.40
	45	230	340	.20	.24	617	1.33
	90	231	325	.20	.23	575	2.19

TABLE 2

HYDRAULIC BULGE TEST RESULTS

MATERIAL	t_o (mm)	YIELD STRENGTH (ksi)	$\sigma = K \varepsilon^n$ (MPa) K	n
REGULAR SPANGLE	0.890	289	658	.22
MINIMIZED SPANGLE	0.787	262	603	.22
SPANGLE FREE	0.787	207	638	.23
ALLOYED COATING	1.295	276	609	.21
UNCOATED (ROUGH)	1.219	207	653	.24
UNCOATED (SMOOTH)	1.168	234	692	.23

TABLE 3

MEASURED AND CALCULATED r-VALUES

MATERIAL	ORIENTATION W.R.T. ROLLING DIRECTION	σ_{true} at 15% (MPa)	Measured r	r_{ave}	n	n_{ave}	σ_{Bulge} at 15% El (MPa)	r_1	r_2
REGULAR	0	363	1.57		.24				
SPANGLE	45	374	1.24	1.37	.24	.24	400	1.32	1.26
	90	366	1.44		.26				
MINIMIZED	0	357	1.14		.25				
SPANGLE	45	371	0.73	1.01	.24	.25	393	1.33	1.25
	90	356	1.44		.26				
SPANGLE	0	374	1.29		.19				
FREE	45	383	1.09	1.24	.19	.19	407	1.28	1.22
	90	381	1.50		.19				
ALLOYED	0	373	1.03		.22				
COATING	45	386	0.69	0.88	.23	.22	365	.96	.97
	90	388	1.11		.22				
UNCOATED	0	322	1.74		.27				
(ROUGH)	45	366	1.41	1.75	.26	.26	407	1.73	1.57
	90	339	2.45		.26				
UNCOATED	0	365	2.40		.25				
(BARE)	45	384	1.33	1.81	.24	.24	441	1.76	1.60
	90	366	2.19		.23				

$$r_1 = 2\left(\frac{\sigma_B}{Y}\right)^2 - 1$$

$$r_2 = 2\left\{\frac{\sigma_B}{\frac{1}{4}\left(\sigma_0 + 2\sigma_{45} + \sigma_{90}\right)}\right\}^{\left(\frac{2}{n+1}\right)} - 1$$

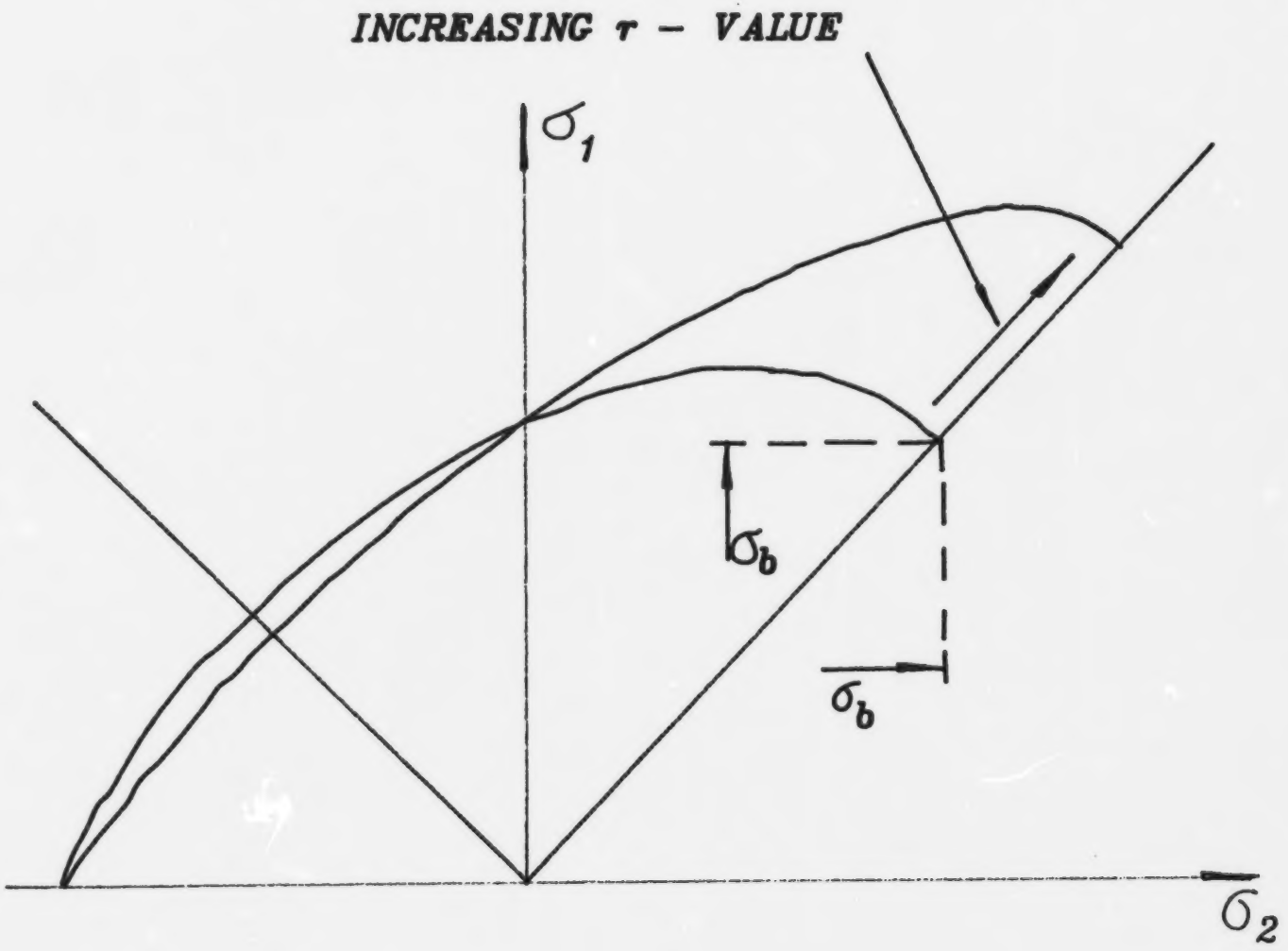

Fig. 1 The Effect of the r-value on the Yield Surface

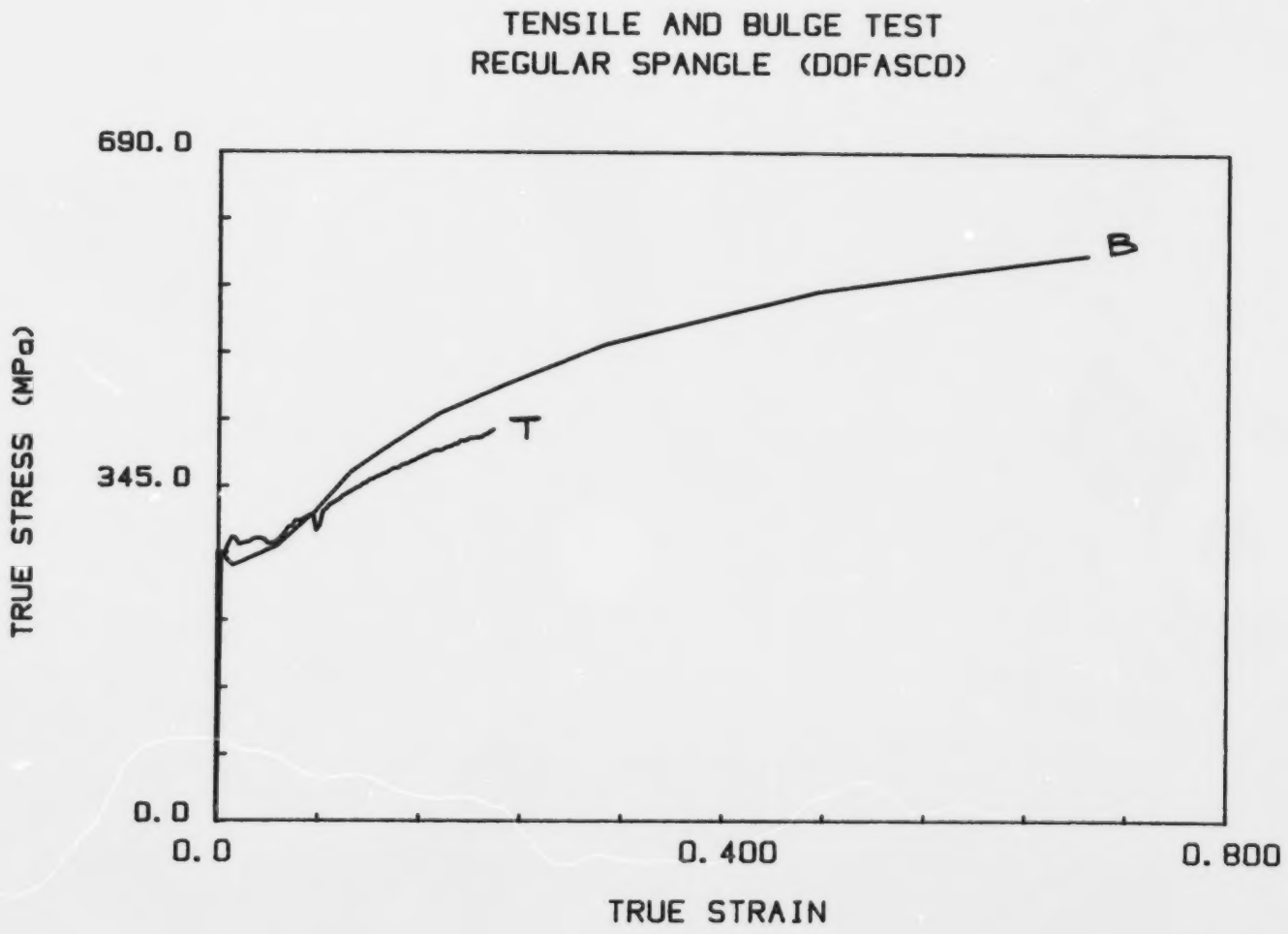

Figure 2: Comparison of the bulge and tensile test's true stress-strain data for the regular spangle material.

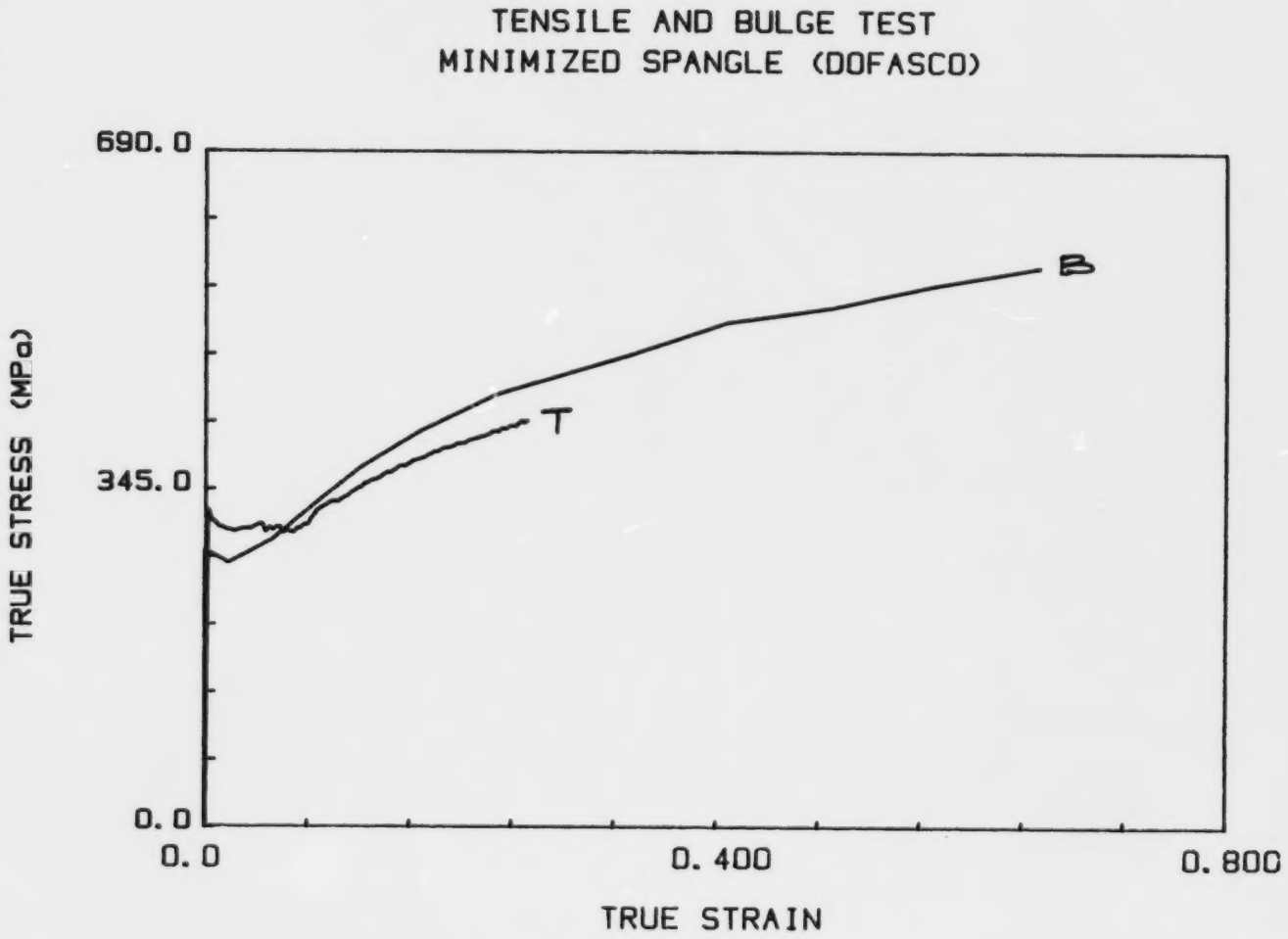

Figure 3: Comparison of the bulge and tensile test's true stress-strain data for the minimum spangle material.

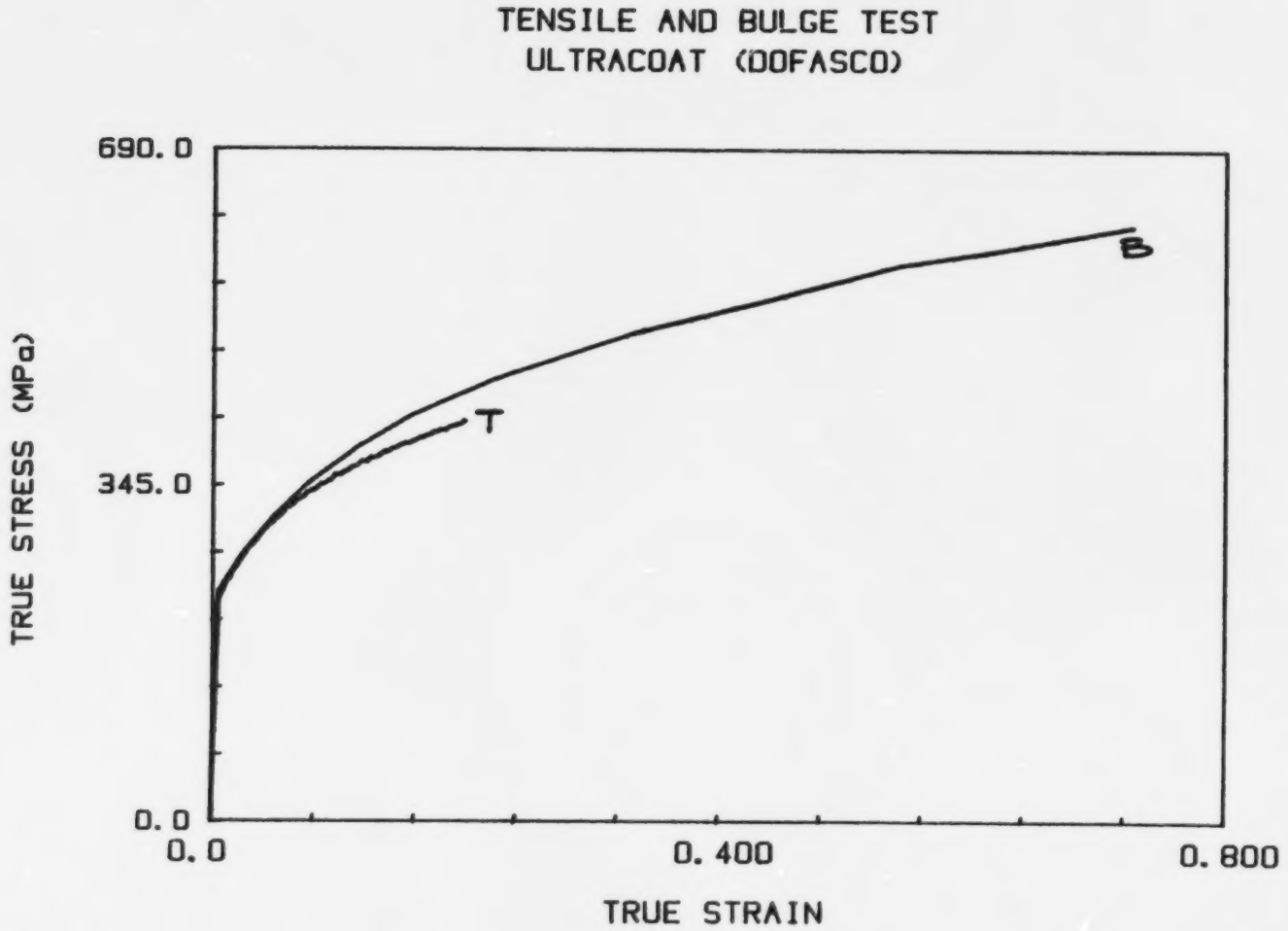

Figure 4: Comparison of the bulge and tensile test's true stress-strain data for the spangle free material.

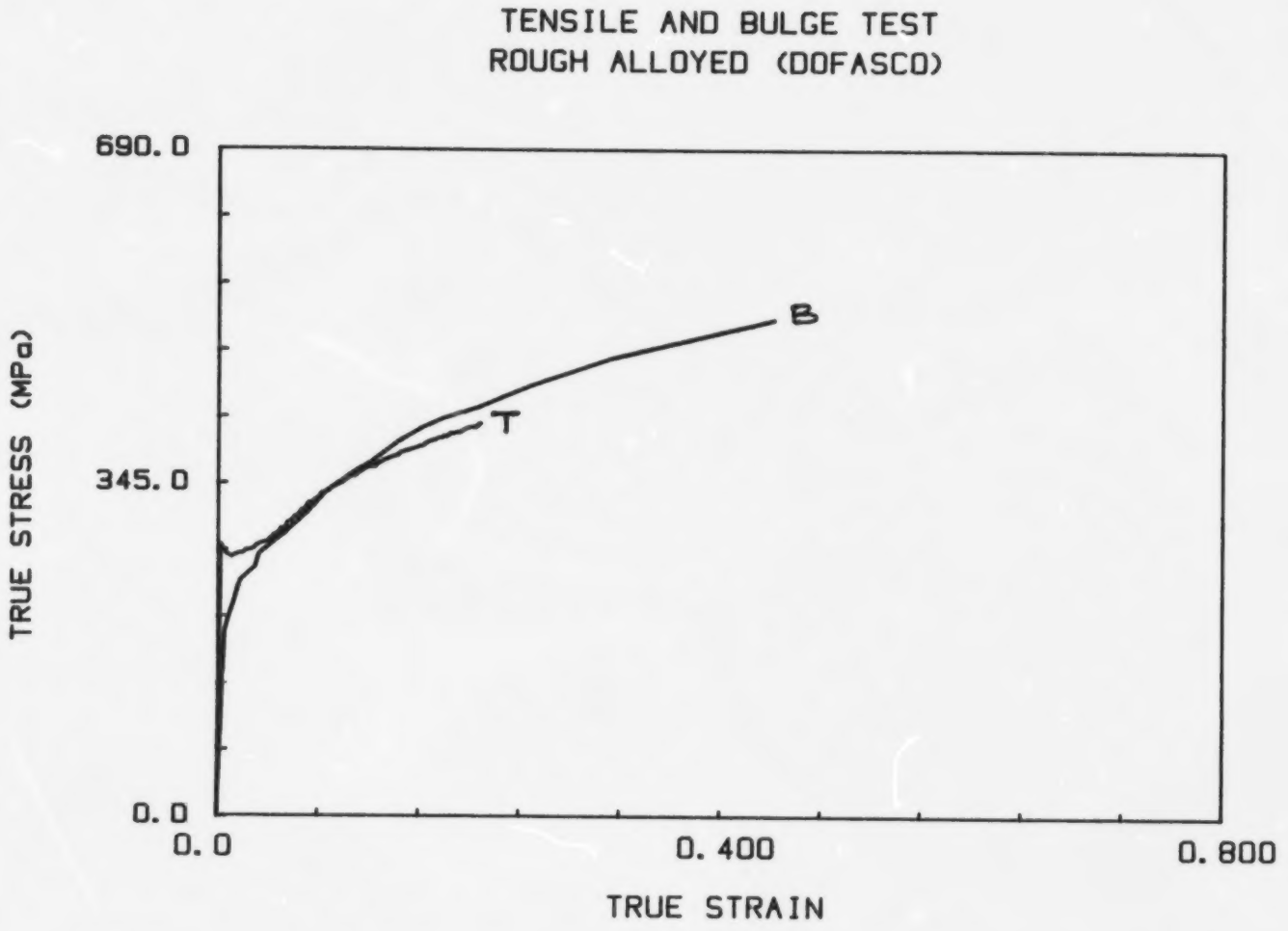

Figure 5: Comparison of the bulge and tensile test's true stress-strain data for the alloyed coating material.

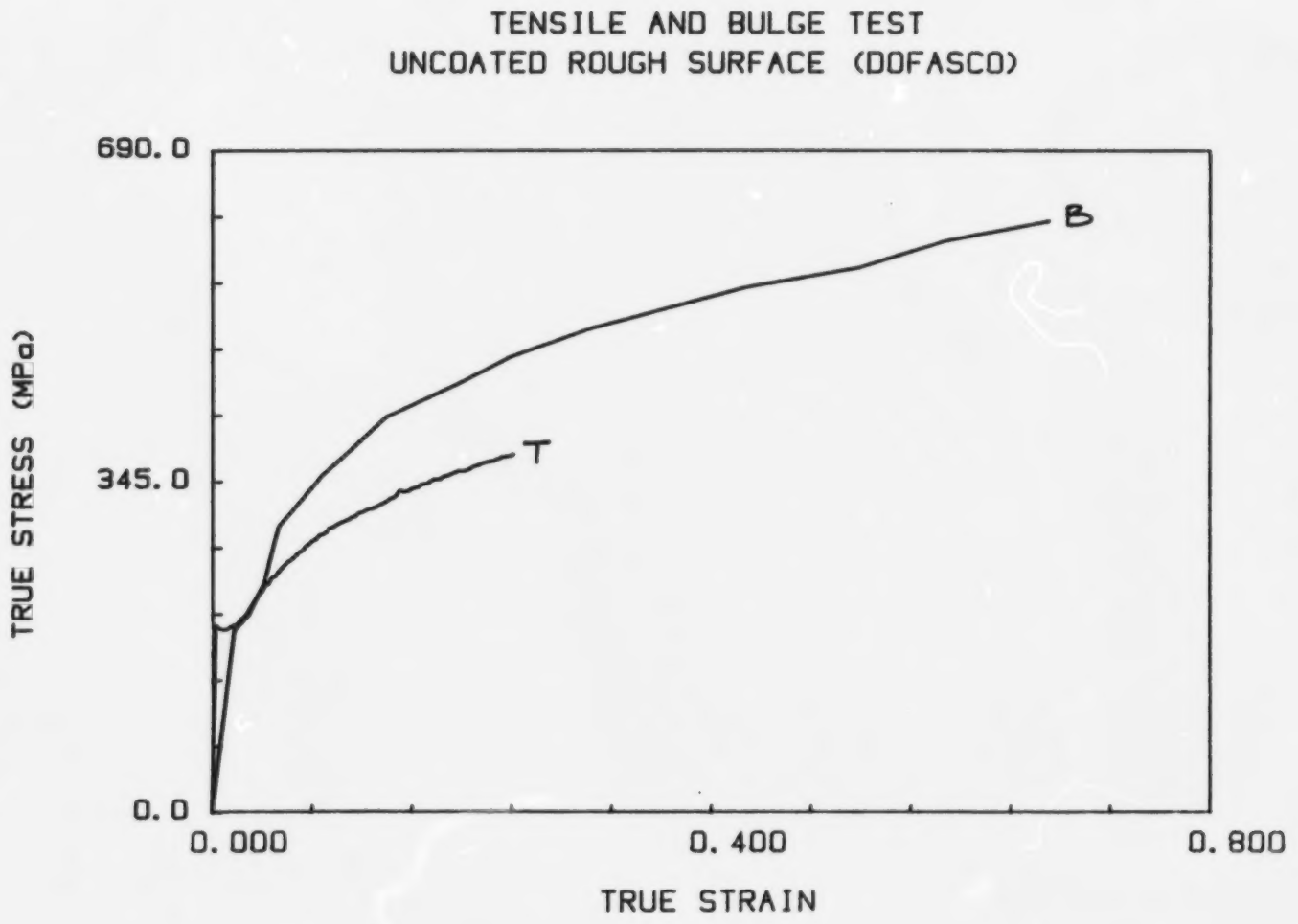

Figure 6: Comparison of the bulge and tensile test's true stress-strain data for the bare steel with the rough surface.

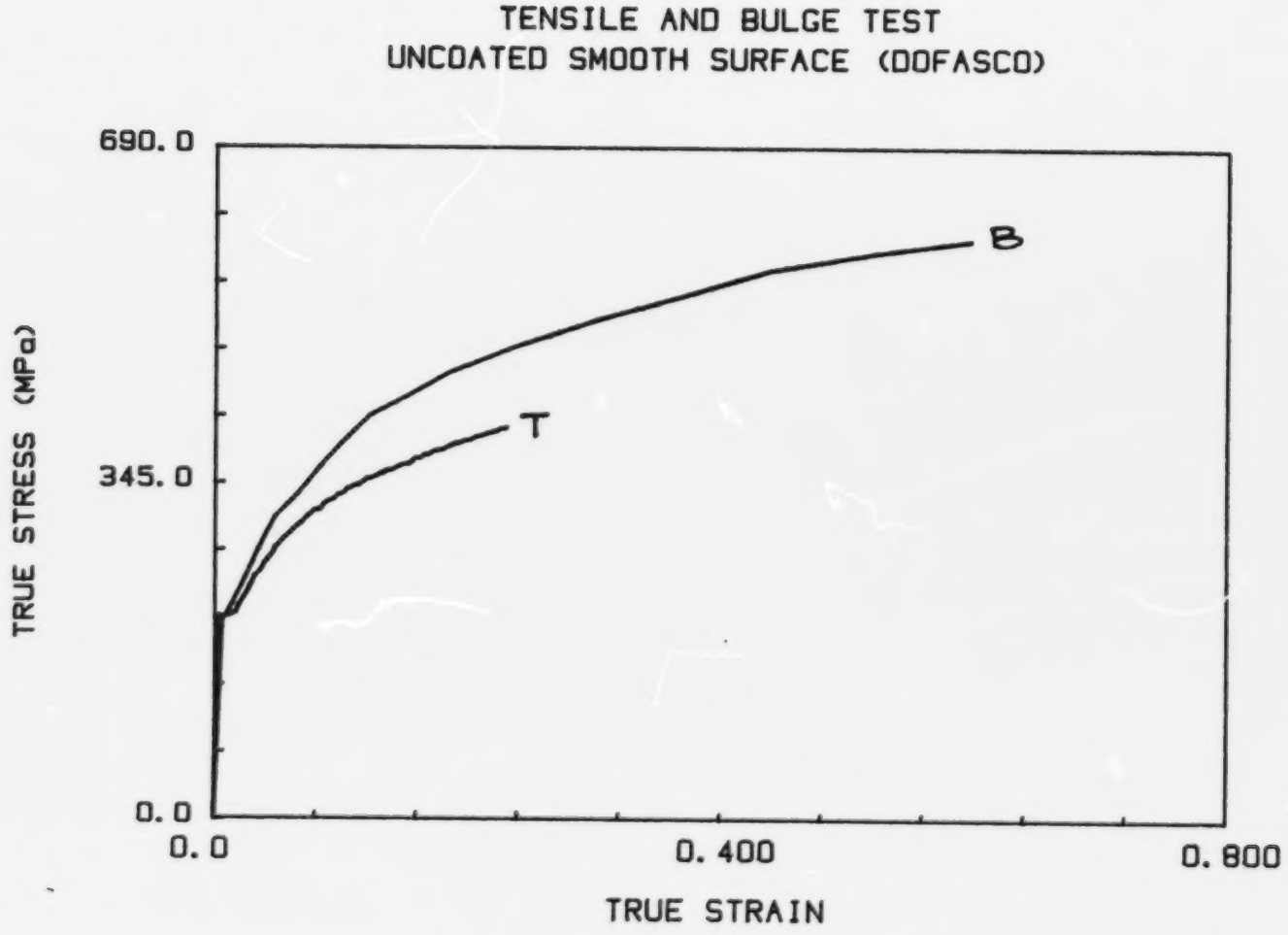

Figure 7: Comparison of the bulge and tensile test's true stress-strain data for the bare steel with the smooth surface.

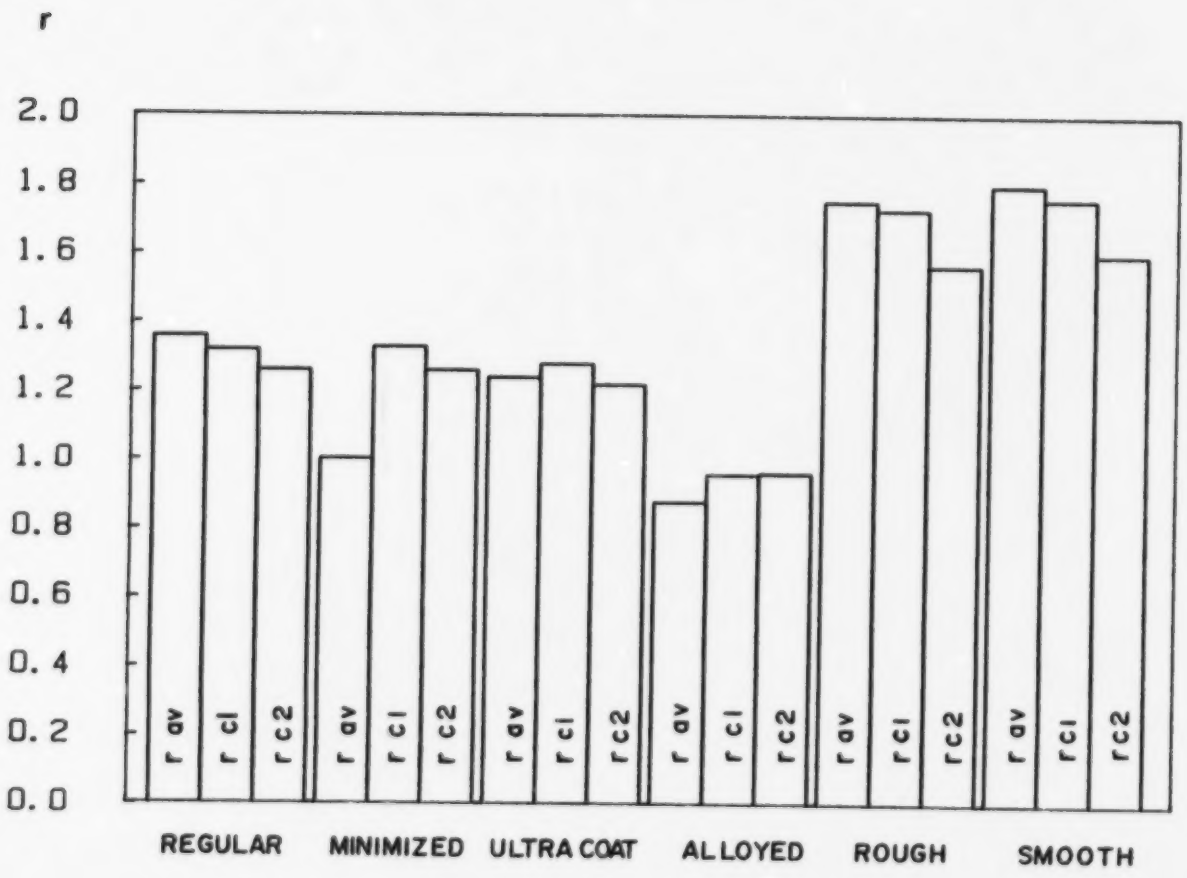

Fig.8 Comparison of Measured and Calculated r-Values.

PHASE I

1. STRIP FRICTION TESTS ON HOT-DIPPED GALVANIZED STEEL SHEET

1.1 Introduction

The strip friction test is described in Refs. [1,2], the latter reference is a report of work undertaken at McMaster University and submitted to CANMET at an earlier phase of the present contract. The work of Ref. [2] was performed on an electro-galvanized steel supplied by the U.S. Steel Company. The present study was undertaken on four hot-dipped galvanized steels supplied by DOFASCO, and designated Regular Spangle (RS), Alloy Coat (AC), Minimum Spangle (MS) and Ultra Coat (UC). Mechanical property data for these steels are provided in Ref. [3].

The coefficient of friction for each of these materials was determined under dry and lubricated conditions. Some of the specimens tested under the lubricated condition were subjected to a metallographic examination. The objective was to examine the nature of the zinc coating following the friction test. Various locations on the surface of the test pieces were examined under a scanning electron microscope (SEM). The regions of inspection included locations well removed from the pins in the strip friction tester as well as domains in the sheet in contact with the pins.

1.2 Experimental Procedure

1.2.1 Strip Friction Tests

The experiments were performed in a MTS testing machine, using the equipment described in Refs. [1,2]. Figure 1 is a diagram of the experimental arrangement, each test was performed at a constant cross-head speed of 100 in/min (2.54 m/min). The diameter of the pins was held constant at 1 in (25.4 mm).

All the test pieces were cropped from the as-received sheets and machined to a width of 0.5 in (12.7 mm). The UC material had been temper rolled, while the RS and MS materials had not. Consequently the latter two steels exhibited a Lüders strain (discontinuous

yielding). To remove this behaviour, test pieces were roller-levelled using a small leveller built at McMaster, see Fig. 2. Some of the specimens were then pulled in uniaxial tension to verify that discontinuous yielding had been eliminated. Figure 3 shows the effect of roller-levelling on the load extension behaviour of the RS sheet, results for the MS material were similar. It can be seen that after about 25 passes the Lüders strain phenomenon had been eliminated.

Prior to performing the friction experiments, the test pieces and pins were cleaned with acetone. This procedure was adopted for all the experiments. The unlubricated (or dry) experiments were conducted immediately after the cleaning operation. For the lubricated tests, an oil (SP-7000) was brushed onto the pins and specimens prior to conducting the test.

The output from the experiment is the load on the strip, P_1, and the extensometer readings, E_1 and E_2. From this information the coefficient of friction, μ, can be calculated in terms of the sliding distance, S, i.e. the distance moved by the strip over each pin. The method of calculating μ is given in Refs. [1,2].

1.2.2 Examination of the Zinc Coating

Following the lubricated strip friction tests, a number of the specimens were retained for metallographic examination. The surfaces of the test pieces were inspected at various locations, using a scanning electron microscope (SEM 515). The regions of inspection are indicated on Fig. 4. Position 1 is in the horizontal portion of the strip and never encounters the pins; similarly position 5 is in the vertical leg of the specimen and is well removed from the pins. In contrast, positions 2-4 are at different locations around the periphery of the pins. It is assumed that this region of sliding contact simulated the conditions which occur in certain regions of an industrial stamping. In particular, those domains where the workpiece moves relative to the tooling, such as bending and stretching of material over a die or punch radius.

1.3 Results and Discussion

1.3.1 Strip Friction Tests

Figure 5 shows a typical output from the strip friction tester; the results are for a RS specimen tested under dry conditions. The load, P_1, in the vertical leg of the strip is plotted against the vertical extension E_1. At the same time the variation in the horizontal extension of the specimen, E_2, with E_1 is recorded. The stretching of the horizontal portion of the strip is delayed until the load in the vertical leg increases to overcome friction around the pins. Lubrication decreases the load to overcome friction.

Figure 6 shows a typical result for the variation in the calculated coefficient of friction, μ, with sliding distance, S. The plot is for a RS test piece under dry conditions.

Table 1 lists the calculated values of μ for all the tests conducted, average quantities are quoted based on at least two tests for each operating condition. It would appear that the zinc coating is having little effect on the value of μ when the tests are performed dry. The presence of lubrication produces a dramatic reduction in the calculated value of the coefficient of friction.

Table 1 Calculated Values of μ

MATERIAL	LUBRICATION CONDITION	AVERAGE CALCULATED VALUE OF μ
RS	DRY	0.102
MS	DRY	0.099
UC	DRY	0.103
AC	DRY	0.105
RS	LUBRICATED	0.020
MS	LUBRICATED	0.047
UC	LUBRICATED	0.039
AC	LUBRICATED	0.042

The regular spangle material does show the lowest value for μ under lubricated conditions. Surface roughness tests performed on a TALYSURF 10 instrument and reported in Ref. [4] showed that the RS material had the smoothest surface followed by UC and then MS.

The calculated values of the coefficient of friction under lubricated conditions are rather low. In the work performed in Ref. [2] on electrogalvanized materials, the presence of a lubricant had less of an effect on the value of μ, compared to the unlubricated tests. However, a different lubricant was used in that particular investigation. At deformation speeds of 2.54m/min., under dry conditions, the calculated values for μ given in Ref. [2] fell within the range $0.1 < \mu < 0.15$ for all the materials tested. These values are comparable with those given here in Table 1, under dry conditions.

Perhaps of more significance is that the present tests have revealed that the hot-dipped materials can move around the pins when no lubrication is employed. The ability of materials to continue to slide over tools and dies in the absence of a lubricant would be of practical importance in stamping operations.

1.3.2 Examination of the Zinc Coatings

The surface of the as-received coatings of each of the four materials has been examined in Ref. [4]. Before discussing the features of the various coatings following the strip friction test, it is worthwhile recapitulating certain features of the test using Fig. 4 as a reference. In locations 1 and 5 the material does not contact the pins, and the deformation mode is one of uniaxial tension. The deformation is less in the horizontal portion of the test piece, position 1, because of friction around the pins. In positons 2-4 the material is being bent under tension, the surface in contact with the pins experiences both normal and tangential (frictional) stresses. The observations following the deformation of the materials are given below.

a) Regular Spangle

All the metallography was performed on this material in location 3. Grain boundary cracking occurred as can be seen from Figs. 7-9. Galling or scoring of the surface is evident particularly in Figs. 8 and 9, in the latter photograph pitting of the surface is also revealed. The as-received coating had a large scale dendritic structure, it also exhibited a significant amount of extraneous surface contaminant. There is some evidence of this extraneous material being smeared out in Fig. 9.

b) Alloyed Coating

Photographs of the deformed surface, again taken on location 3, are shown in Figs. 10 and 11. Boundary cracking can again be observed along with numerous score marks. The as-received coating had a fine dendritic structure and there is some evidence of this in Fig. 11, which shows that some flattening of the peaks has occurred. Fine slip lines within the grains can also be seen in the same figure.

c) Minimum Spangle

The as-received coating also had a fine scale dendritic structure and this is revealed in Figs. 12 and 13 taken at location 2. When the material is first contacting the pins. Grain boundary cracking is displayed, along with the compression of the peaks of the dendrites. Microcracking is also evident in each of the figures.

Photographs taken at location 3, show both grain boundary cracks and microcracks, see Fig. 14. Score or scratch marks can be observed at the peaks of the dendritic structure.

Figure 15 was taken in the vertical leg of the specimen, at location 5. Slip lines within a grain, microcracks and grain boundary cracks are all in evidence. A rather unusual observation was made at location 1, and is shown in Fig. 16. The presence of a particle embedded in the coating has resulted in a number of intergranular cracks radiating outwards from the particle.

d) Ultra Coat

The as-received material had been temper rolled and the deformation of the surface consistent with such a process is evident from Fig. 17. This photograph was taken at location 1, and shows numerous cracks, many of which are intergranular. The density of the cracks increases with increasing strain, as is clear from Fig. 18 taken at location 5.

A myriad of cracks and score marks (arising through sliding contact) are exhibited in Fig. 19, taken at location 3. Pitting of the surface can also be seen in this figure.

From the present series of tests it can be concluded that grain boundary cracking occurs at all locations i.e. 1-5, with each material. The ultracoat was the only material to exhibit extensive intergranular cracks, while fine scale slip lines (within individual grains) was generally observed with the other materials. Score marks or galling was present in regions when sliding occurred (positions 2-4) with all the materials.

Some microcracking took place at the various locations with each material. However, many more micro cracks were observed when the same materials were subjected to bi-axial tension [4]. The ease at which the present materials exhibit grain boundary cracking may be of some concern when considering the effectiveness of the zinc coating in resisting corrosion following plastic defomation.

References

1. X.J. Wang, J.L. Duncan and M.L. Devenpeck, "Punch Friction Tests for Sheet Metal Forming", Jnl. Applied Metalworking, 1983, Vol. 3, p. 3.

2. Ru Zheng and D. Overby, "Strip Friction Tests for Electrogalvanized Steel Sheet", Metal Forming Research Report No. 85-002, McMaster University, Sept., 1985.

3. Ru Zheng et al., "Normal Plastic Anisotropy in Galvanized and Uncoated Drawing Quality Steel", Metal Forming Research Report No. 85-003, McMaster University, Sept., 1985.

4. J.D. Embury et al., "Structural Characteristics of Galvanized Coatings", Metal Forming Research Report No. 85-005, McMaster University, August, 1985.

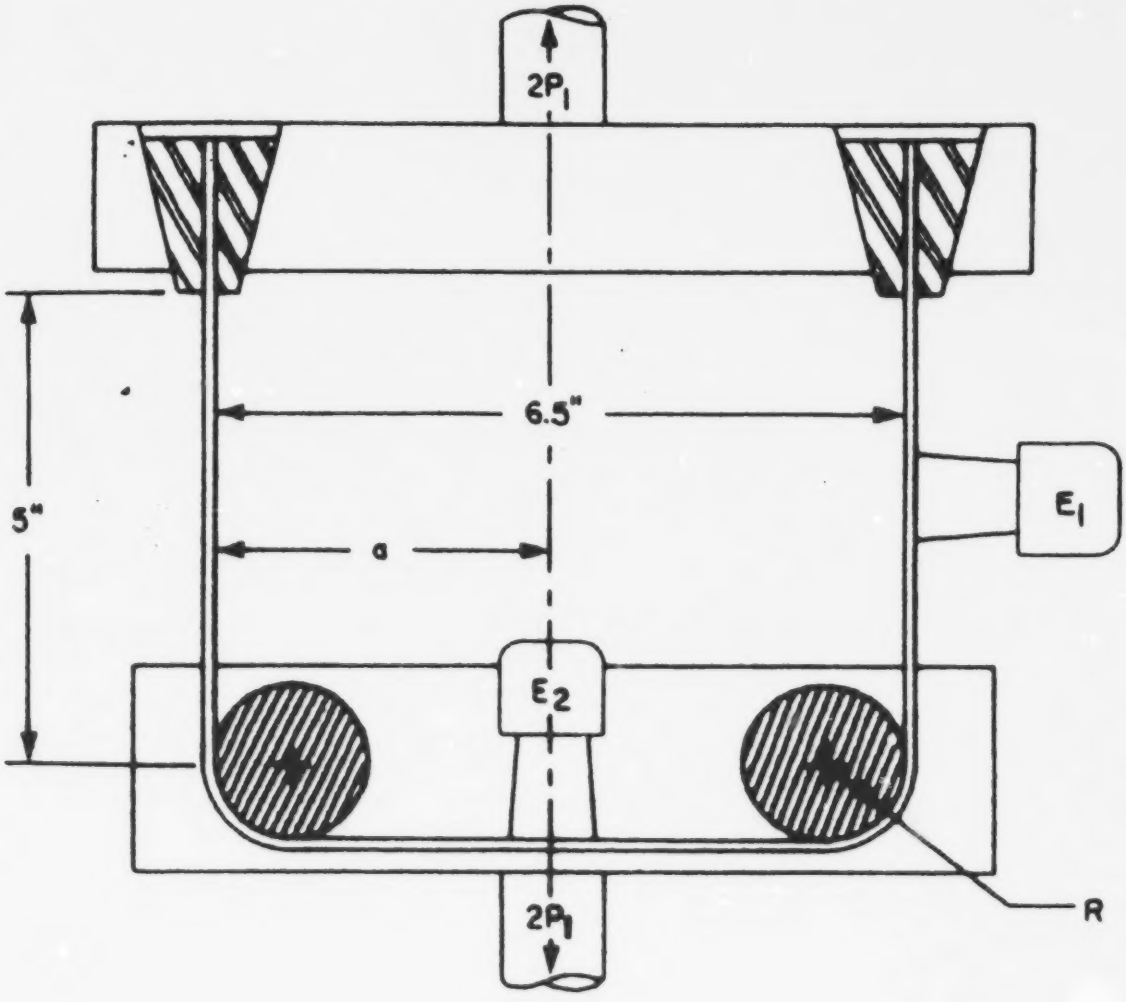

Fig. 1. Strip Friction Test.

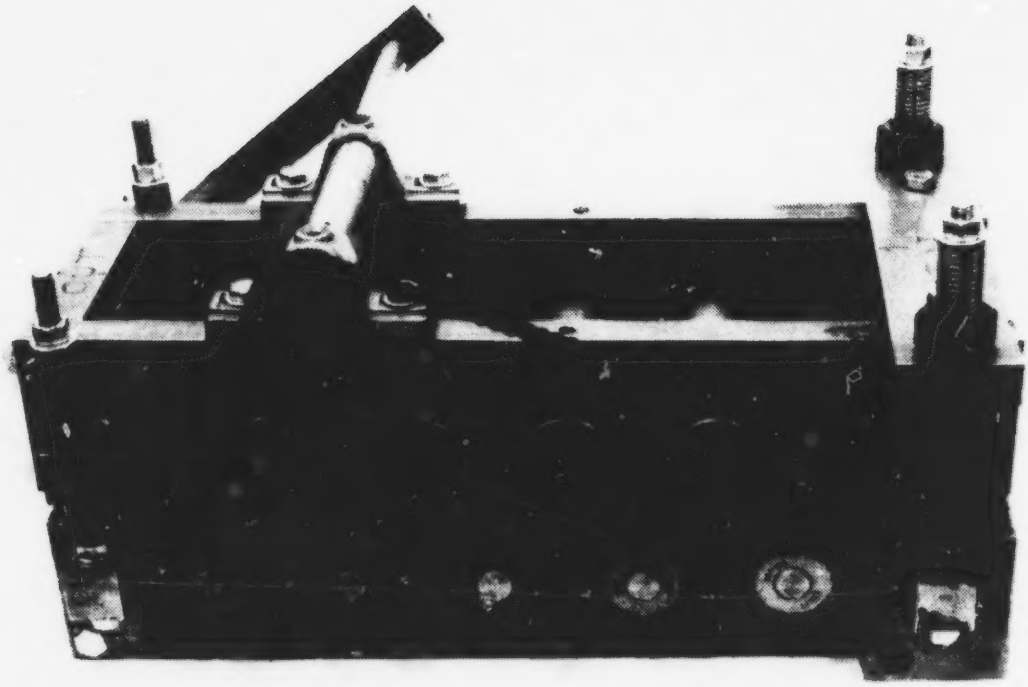

Fig. 2. Roller Levelling Machine.

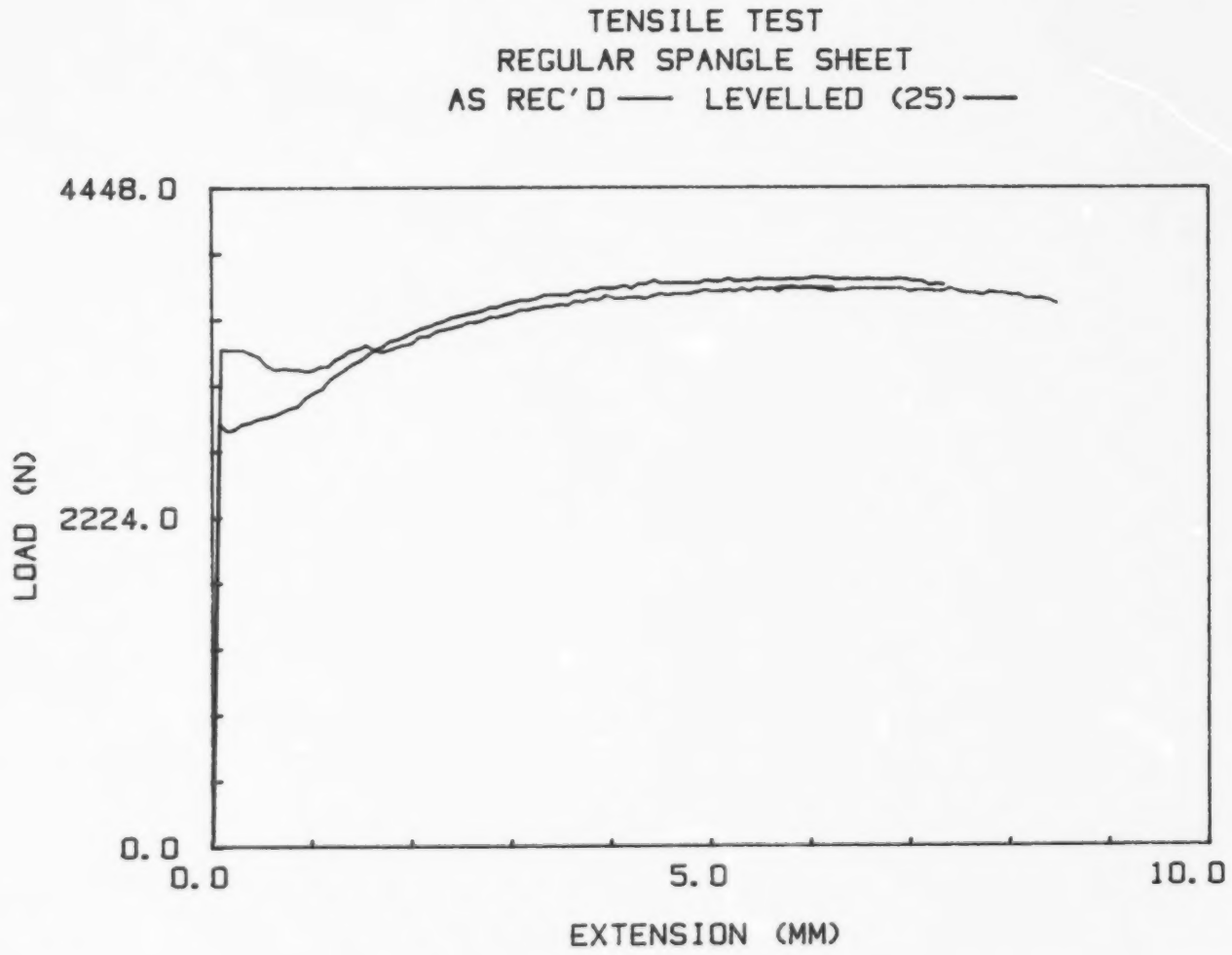

Fig 3: The Effect of Roller Levelling on the Load-Extension Curve in a Tensile Test at 0 deg. Orientation.

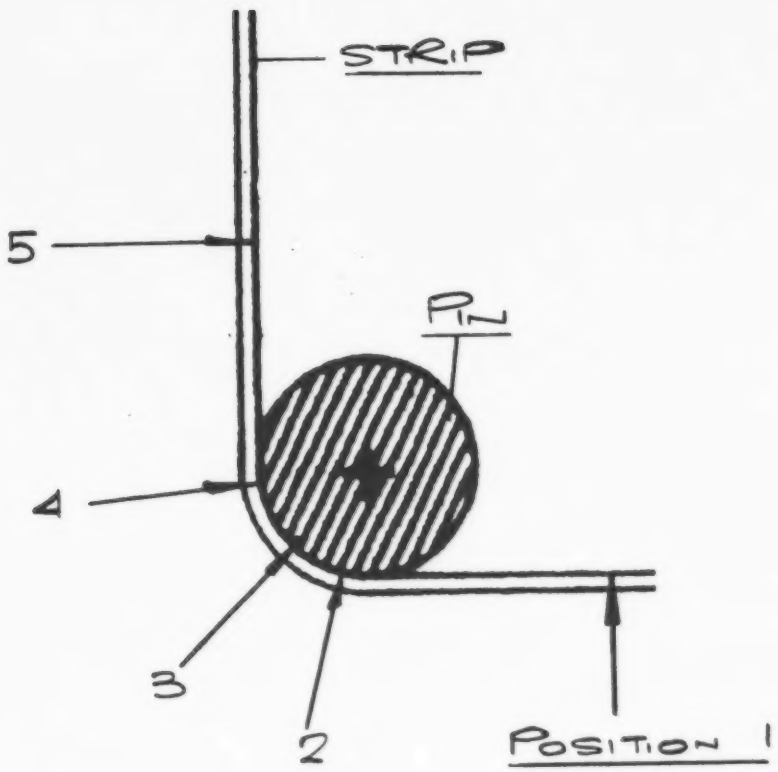

Fig. 4. Locations on the Strip Where the Surface was Examined.

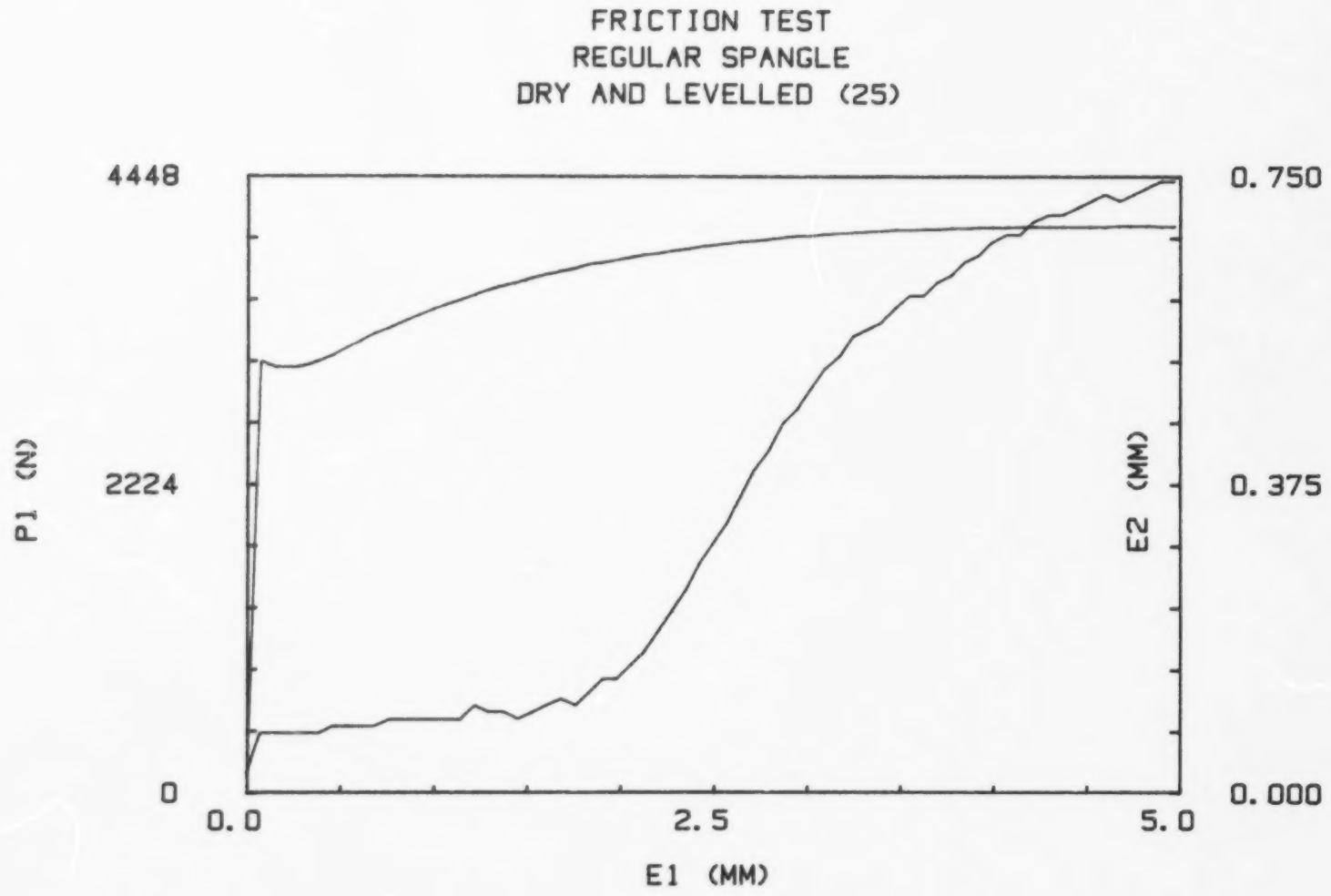

Fig 5: Typical Output from the Strip Friction Tester for the RS Material which had been Roller Levelled.

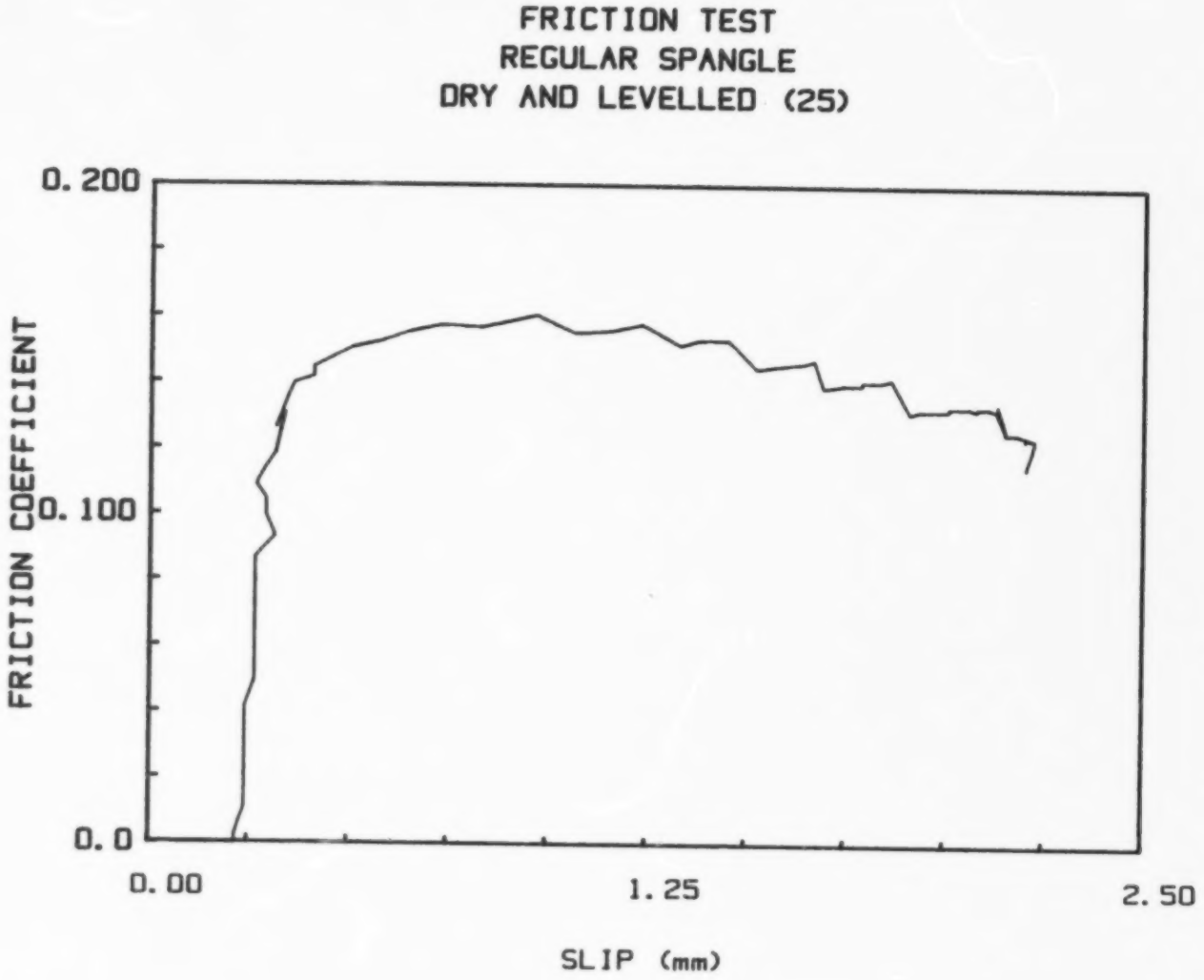

Fig. 6: Calculated Coefficient of Friction against Sliding Distance for the Data given in Figure 5.

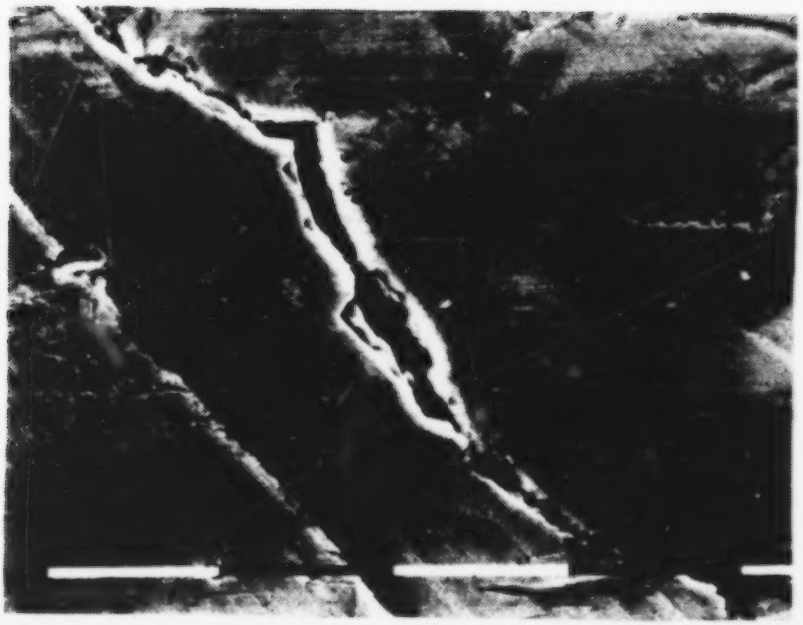

Fig. 7. RS Material at Location 3. Magnification 2400, Micron Marker = 10 μ.

Fig. 8. RS Material at Location 3. Magnification 1200, Micron Marker = 10 μ.

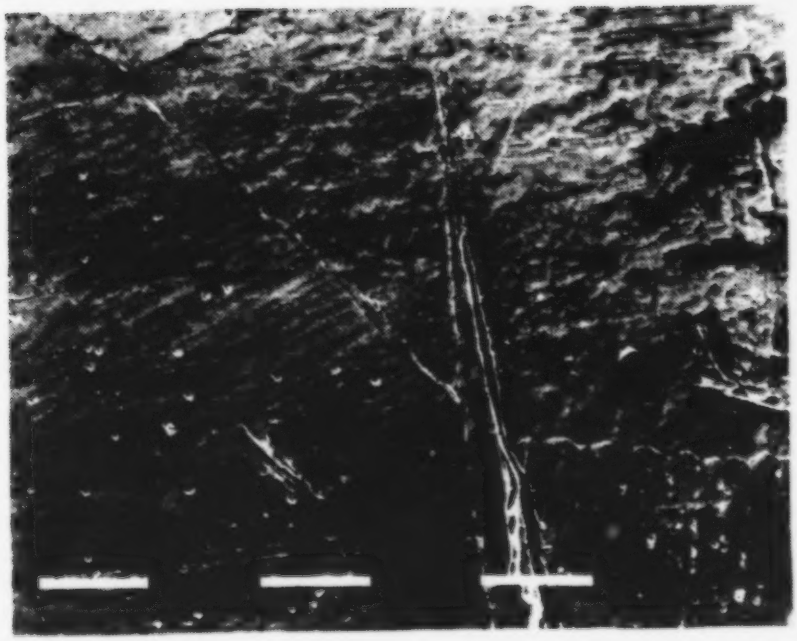

Fig. 9. RS Material at Location 3. Magnification 150, Micron Marker = 100 μ.

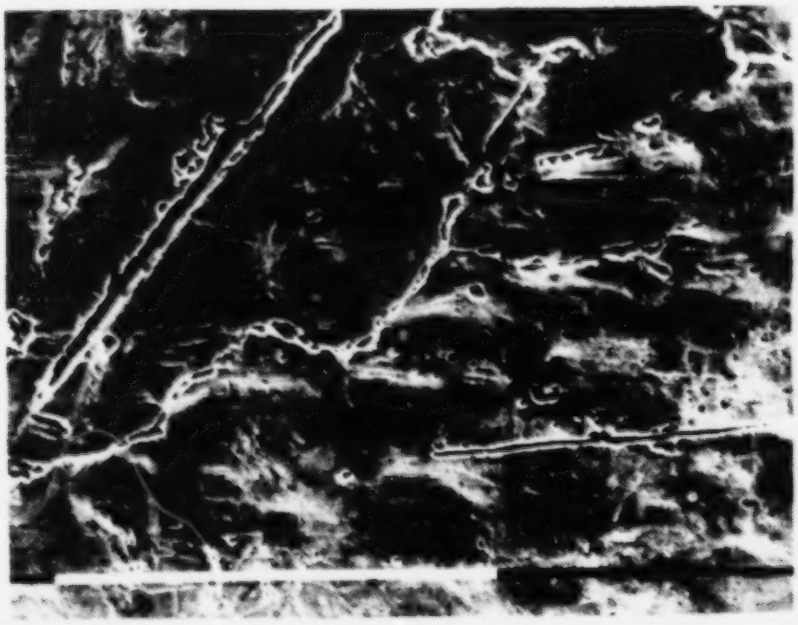

Fig. 10. AC Material at Location 3.
Magnification 625, Micron Marker = 100 μ.

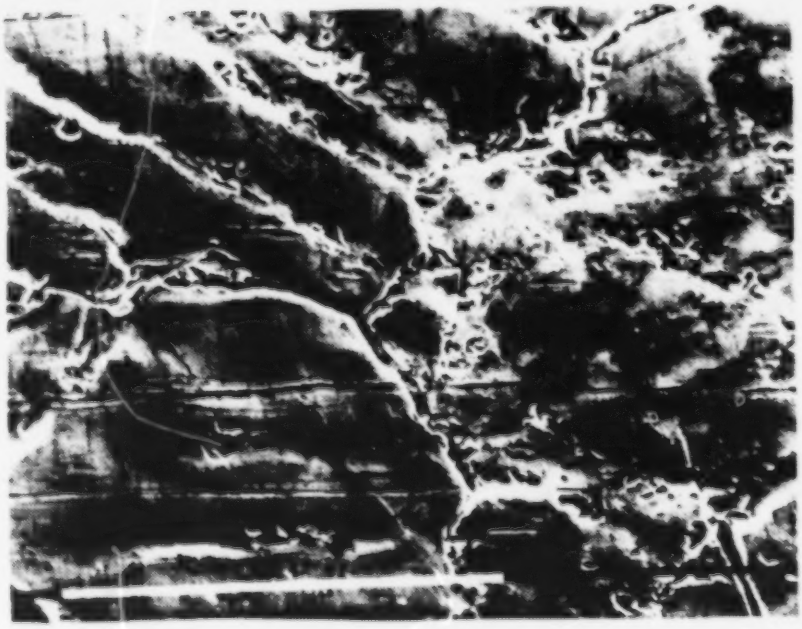

Fig. 11. AC Material at Location 3.
Magnification 625, Micron Marker = 100 μ.

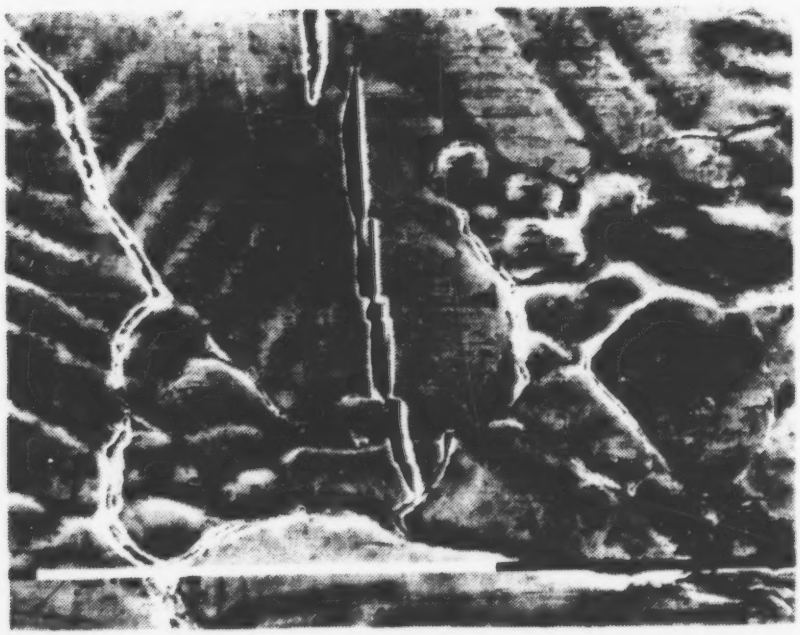

Fig. 12. MS Material at Location 2.
Magnification 625, Micron Marker = 100 μ.

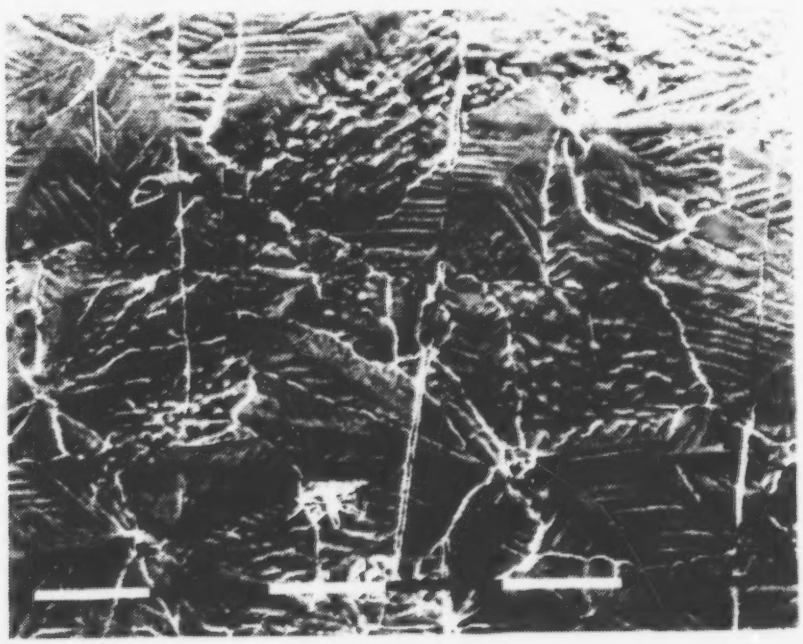

Fig. 13. MS Material at Location 3.
Magnification 156, Micron Marker = 100 μ.

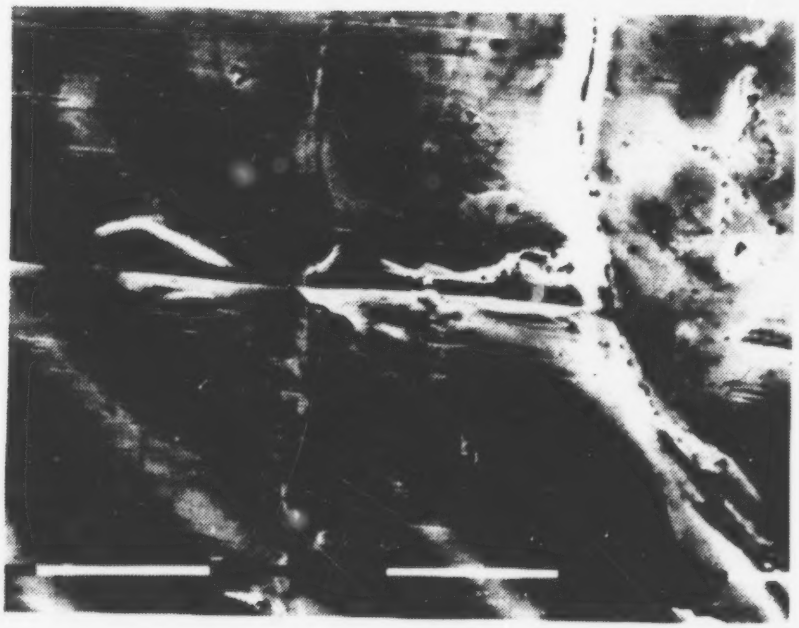

Fig. 14. MS Material at Location 3.
Magnification 2400, Micron Marker = 10 μ.

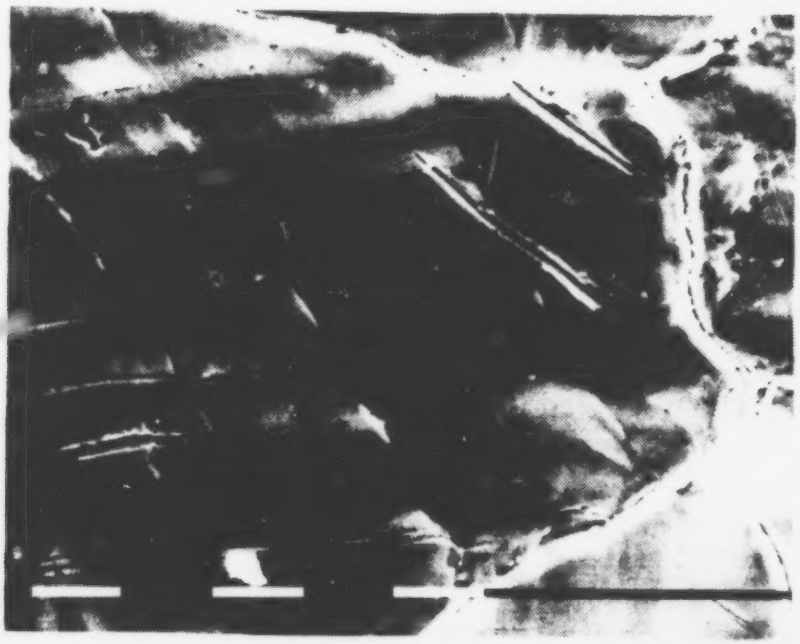

Fig. 15. MS Material at Location 5.
Magnification 1200, Micron Marker = 10 μ.

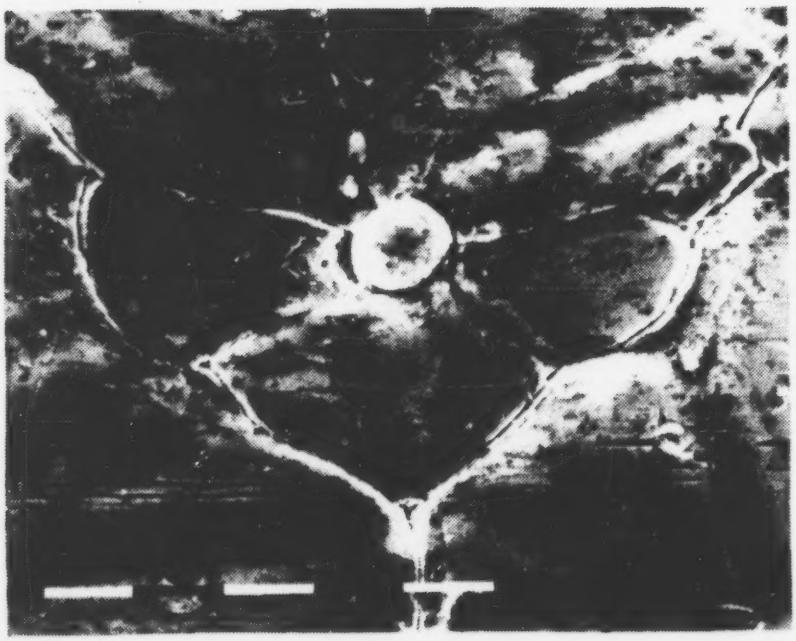

Fig. 16. MS Material at Location 1, showing Embedded Particle. Magnification 1200, Micron Marker = 10 μ.

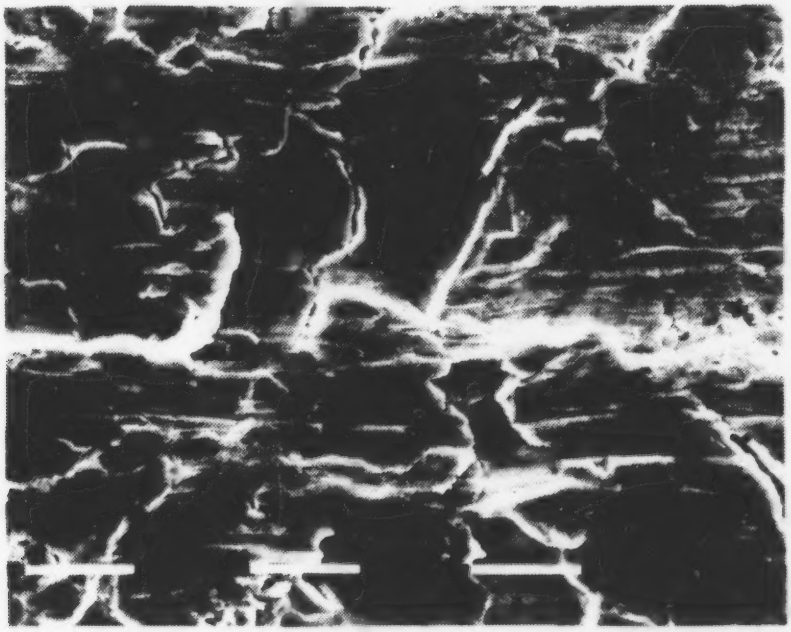

Fig. 17. UC Material at Location 1.
Magnification 1490, Micron Marker = 10 μ.

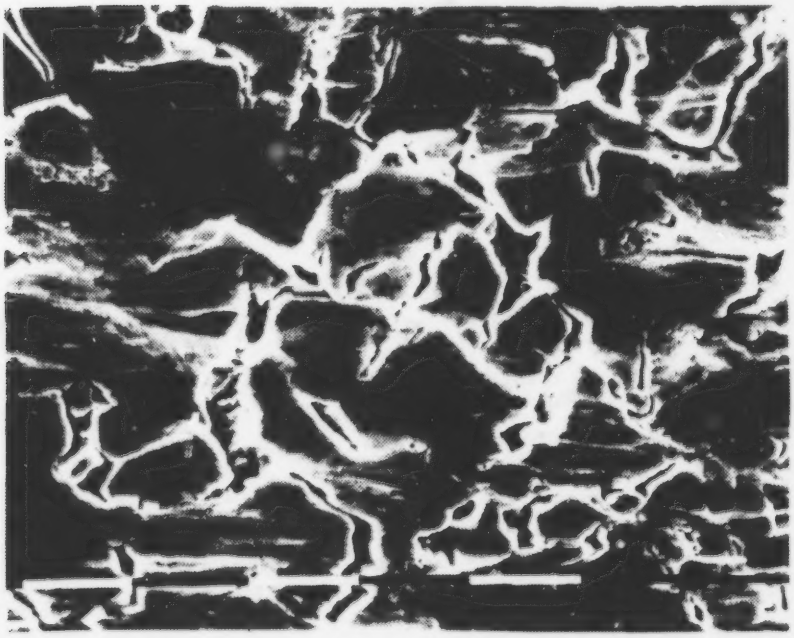

Fig. 18. UC Material at Location 5.
Magnification 1490, Micron Marker = 10 μ.

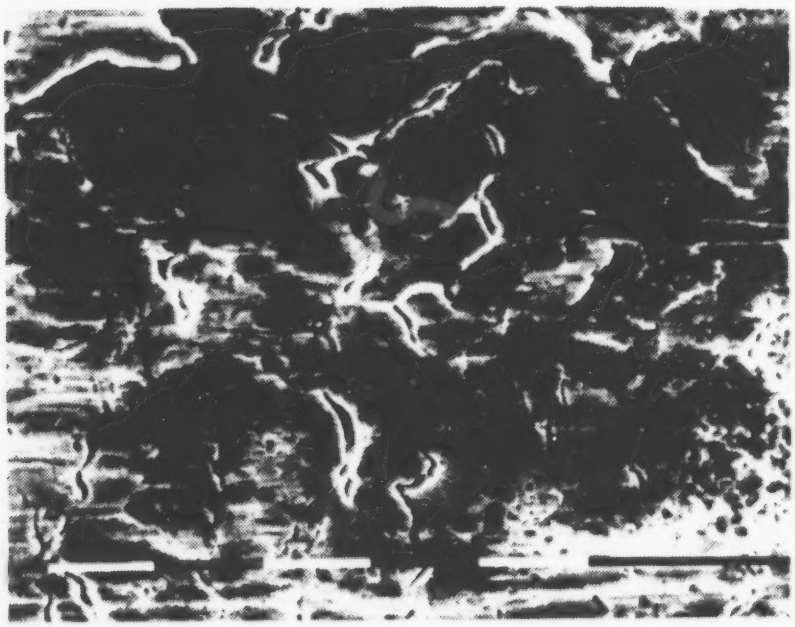

Figure 19 UC Material at Location 3
Magnification 1490, Micron Marker = 10μ.

2. THE DETERMINATION OF THE PLASTIC STRAIN RATIO FOR SOME HOT-DIPPED GALVANIZED STEEL SHEET

2.1 Introduction

In a recent report [1] results of r-value measurements were provided for a number of hot-dipped galvanized steels. The materials included the three sheets discussed in the preceeding Chapter, along with an additional coated steel, designated Alloy Coated (AC).

During the course of the study [1], some preliminary experiments were performed on the RS material (the regular spangle) to assess the influence on the r-value when the coating is removed from the substrate. The experiments indicated that the r-value increased when the zinc coating was removed.

The purpose of the present study was a more detailed investigation into the influence of the zinc coating on the plastic strain ratio. The four hot-dipped steels discussed in Ref. [1] were investigated, these are designated as Regular Spangle (RS), Minimum Spangle (MS), Ultra Coat (UC) and Alloy Coated (AC).

2.2 Experimental Procedure

Tensile specimens were cut in the rolling direction from each of the galvanized sheets in accordance with the ASTM designation - E517 (81).

The zinc coating was removed from the steel substrate by immersing the specimens in a solution of hydrochloric acid. They were removed from the solution once the violent bubbling, due to escaping hydrogen, had ceased. Some specimens were also prepared from the RS material only, with the zinc coating removed from only one side of the test piece. In all cases the width and thickness of the tensile specimens were measured at a number of locations along the gauge length, before and after removal of the zinc.

The test pieces were pulled in a MTS testing machine at a cross-head speed of 1 in/min (25.4 mm/min) with an extensometer of 1 in (25.4 mm) gauge length affixed to the specimen.

The deformation was terminated after an axial engineering strain of 15%, as recorded by the extensometer. The width of each specimen was then measured at a number of positions along the gauge length and an average value recorded. Hence, the average natural width strain was computed. The natural thickness strain was then evaluated, assuming the material to be incompressible. The r-value was determined in the usual manner as the ratio of width to thickness strain.

Each test was repeated a number of times, any extreme values in the calculated r-values were ignored. The recorded r-value was un unweighted average based on the remaining samples.

Table 2.1 lists the calculated r-values for each material with and without the zinc coating. Table 2.2 shows some additional results for the RS material only. Included in Table 2.2 are the r-values for specimens where the zinc had been removed from one side only. The data in Table 2.2 were determined from another batch of tensile specimens, and this accounts for any variation in the r-values between this table and Table 2.1

A series of x-ray diffraction tests were performed on coupons cut from the galvanized sheets, and on similar test pieces when the zinc coating had been removed. It was impossible to detect residual stresses in any of the test pieces with the technique employed.

Finally, and for comparative purposes only, r-values were determined from tensile specimens cut at 0, 45 and 90 degrees to the rolling direction from a sheet of commercial pure zinc. The results are given in Table 2.3.

2.3 Discussion of Results and Conclusions

As is evident from Table 2.1 the presence of the zinc coating generally leads to a diminuation of the r-value compared with that of the steel substrate, i.e. with the zinc coating removed. When the zinc is stripped from one side of a test piece an intermediate value for the plastic strain ratio is observed, as shown in Table 2.2. This latter table was compiled from

tests performed on the RS material only, therefore it is not clear whether this results applies to the other materials.

The similarity in the calculated r-value in Tables 2.1 and 2.2., is an indication of the repeatability of the experimental measures. In fact the r-values given in Table 2.1 for the as-received materials compare favourably with those given in Ref. [1] from some earlier tests on the same materials.

It is not at all clear why the zinc coating is having the effect it has, particularly on the RS and MS materials. Zinc is generally deposited on the steel substrate with the basal planes of the h.c.c. structure lying in the rolling plane. This is not unlike the texture in a commercially pure zinc sheet, which possesses a rather low r-value as indicated in Table 2.3. However, the zinc layer is quite thin (nominally between 20-50 μm for the present materials, see Ref. [2]), compared with the nominal thickness of the galvanized sheets of 0.89 mm. Thus one might anticipate the coating would have a minor effect only, as appears to be the case with the UC and AC materials.

Differences in the r-values between the coated materials and the substrate do not seem attributable to residual stresses, since none were detected by the x-ray diffraction experiments. The bulk of these x-ray experiments were performed on the RS material, which exhibits a variation in r-value between the coated material and the substrate.

Meuleman and his co-workers [3] have also reported a difference in the measured r-value between as-received galvanized steel sheets and when the coating was removed from the substrate. Three different hot-dipped coated materials and one electrogalvanized coated sheet were tested, the authors claim a consistent AKDQ substrate was used throughout.

In agreement with the present work the r-value tended to increase when the coating was removed from the substrate. For three of the materials the increase was marginal, but one of the hot-dipped materials showed a marked increase in the r-value when the coating was stripped from the substrate. This finding is consistent with the present results, where marginal variations in the r-value exists for the UC and AC materials and significant

differences were found for the RS and MS steels. Meuleman et al. [3] were unable to offer an explanation as to why certain coatings appear to exert a strong influence on the r-value while others do not. In Ref. [3] marginal increases in the strain hardening index, n, have been reported upon the removal of the coating from the substrate. In the present work it was not possible to find a systematic variation in the stress-strain behaviour of a coated and uncoated material. Some typical results are shown in Figs. 1 and 2 for the RS and MS materials respectively. These tests were terminated after about 15% axial strain.

While differences in the r and n values were observed in Ref. [3], this seemed to have little effect on a number of formability tests performed by Meuleman and his co-workers, op cit. All the materials performed about the same (with and without the coating) in a number of stretch forming operations e.g. LDH tests, stretch bend tests and plane strain stretch tests. Variations were reported in a deep drawing test as determined by the maximum drawing load. In general this was reduced when the coating was removed. In most cases the differences were small, but did approach 10% for the material which showed the greatest variation in the r-value. However variations as high as 10% were reported between the different substrates i.e. the stripped materials, under identical testing conditions.

Table 2.1 Calculated r-values for the as-received sheets and with the zinc coating removed.

MATERIAL	ZINC COATING	CALCULATED r-VALUE
RS	OFF	1.75
RS	ON	1.57
MS	OFF	1.54
MS	ON	1.16
UC	OFF	1.41
UC	ON	1.27
AC	OFF	0.95
AC	ON	0.93

Table 2.2 Calculated r-value for the RS material, with the coating on, off and removed from one side.

MATERIAL	ZINC COATING	CALCULATED r-VALUE
RS	OFF	1.74
RS	ON	1.52
RS	ONE SIDE	1.62

Table 2.3 Calculated r-values for commercially pure zinc sheet*.

ORIENTATION TO R-D (Degrees)	CALCULATED r-VALUE
0	0.24
45	0.32
90	0.64

* Nominal thickness of sheet 0.89 mm.

REFERENCES

1. Ru Zheng et al., "Normal Plastic Anisotropy in Galvanized and Uncoated Drawing Quality Sheet Steel", Metal Forming Research Report No. 85-003, McMaster University, Sept., 1985.

2. J.D. Embury et al., "Structural Characteristics of Galvanized Coatings", Metal Forming Research Report No. 85-005, McMaster University, August, 1985.

3. D.J. Meuleman, S.G. Denner and F.L. Cheng, "The Effect of Zinc Coatings on the Formability of Automotive Sheet Steels", SAE Paper No. 840370, 1984.

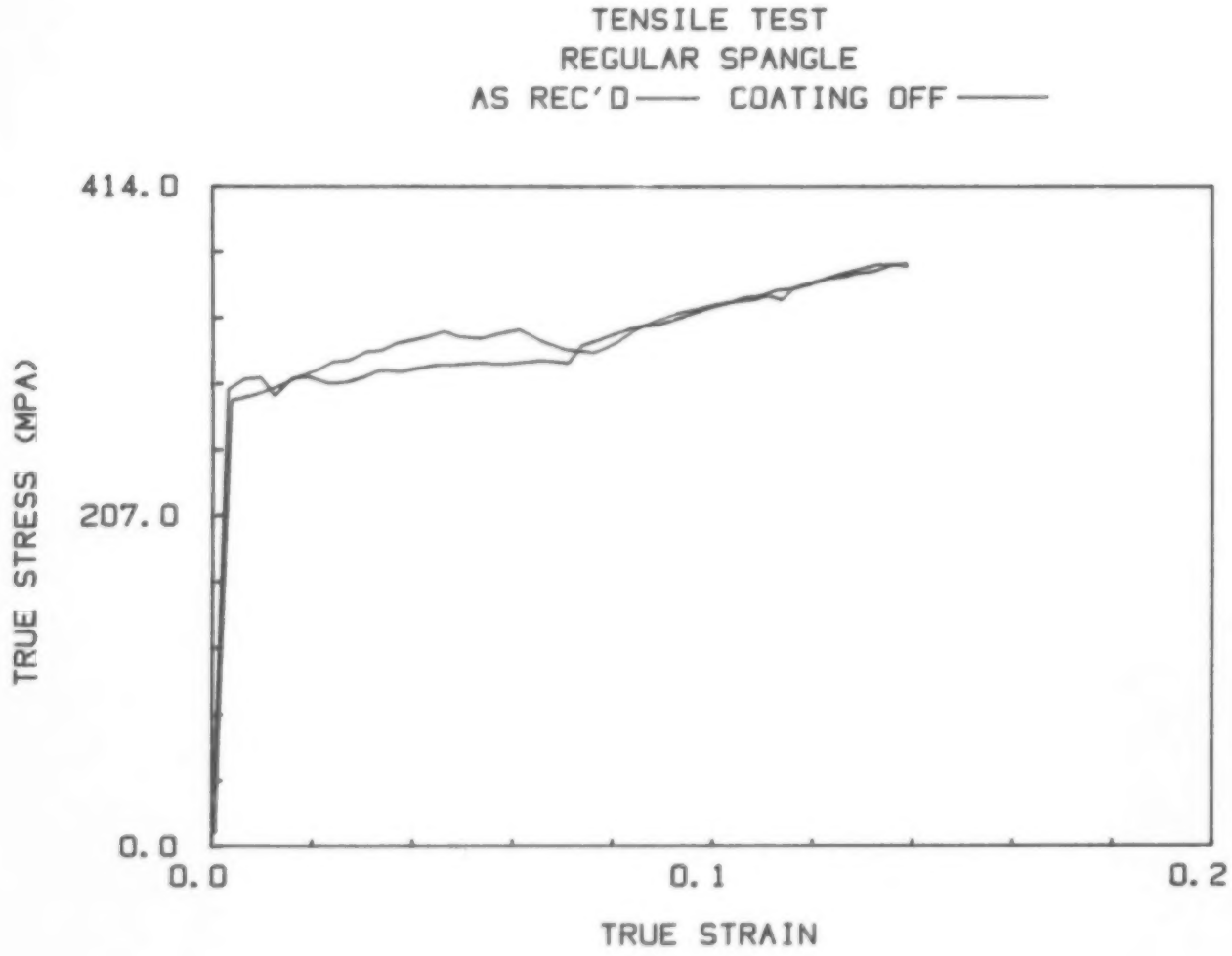

Fig. 1: A Comparison of the Tensile Stress - Strain Curves with and without the Zinc Coating

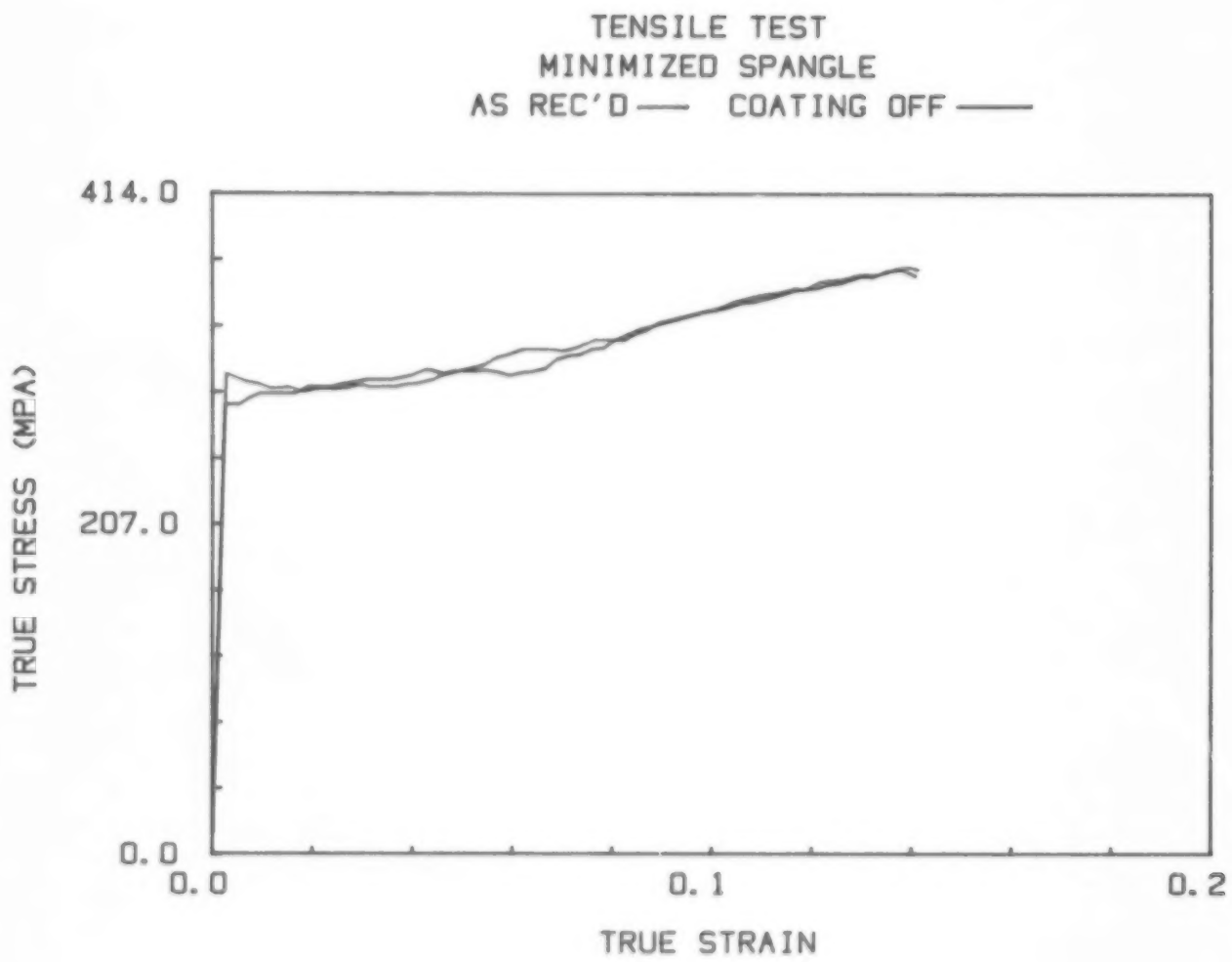

Fig. 2: A Comparison of the Tensile Stress - Strain Curves with and without the Zinc Coating

3. THE CHARACTERIZATION OF THE ZINC COATING FOR A REGULAR SPANGLE HOT-DIPPED GALAVANIZED STEEL SHEET

3.1 Introduction

The preceeding chapter of this report had indicated that the zinc coating can have a marked effect upon the measured r-values for certain hot-dipped galvanized sheet. For two of the materials discussed in the previous chapter, i.e. the Regular Spangle (RS) and Minimum Spangle (MS) materials, the r-value increased when the coating was removed from the substrate. The present chapter provides a more detailed account of the zinc deposit and the nature of the intermetallic layer for the RS material. The coating was examined using an Energy Dispersive X-Ray Spectrometer (EDS) mounted in a Scanning Electron Microscope (SEM).

3.2 Experimental Procedure

A number of coupons were cut from the as-received RS material. The cross-section of the sheets, i.e. in the through thickness direction, were prepared for metallographic examination by grinding, polishing and etching. They were then mounted in the EDS.

Prior to conducting an examination into the nature of the coating, a series of photographs were taken of the prepared cross-sections at different magnifications and viewing angles. An EDS analysis was performed on some of the samples, once the photographs had been taken. A probe was moved over the cross sections and an analysis of the material composition was determined at certain intervals, the incremental steps varied from 0.5 to 2.0 μm. In general the intensity of Fe, Al and Zn was determined in the coating, intermetailic layer and substrate.

3.3 Results and Discussion

Figures 1 to 5 show a normal view of the cross section at different magnifications. At these magnifications, up to 3000, the integrity of the zinc with the substrate appears sound although porosity in the zinc coating itself can be observed. From Fig. 5 it is evident that while the surface of the zinc is relatively flat, the thickness of the deposit is uneven and varies from about 12-25 μm.

The thickness of the intermetallic layer cannot be determined accurately from Figs. 1 to 5. Instead the EDS equipment was used to establish the intensity of Fe, Al and Zn in the coating and substrate. The results of the analysis taken on the surface shown in Fig. 1 is summarized in Table 3.1 and plotted in Fig. 6. The analysis was commenced at about the middle of the Zn coating and terminated when the probe entered the substrate. Unfortunately the readings were not taken at equal intervals and therefore it was not possible to get an accurate measurement for the thickness of the intermetallic layer. As can be seen from Fig. 6 the Zn level decreases and the Fe level increases as the probe moves into the substrate.

A further analysis was conducted on the cross section shown in Fig. 4. In this case the traverse was again started from about the middle of the zinc coating and terminated at about the start of the substrate. Based on the spectrum counts both Fe and Al can be detected throughout the zinc coating. Again there is a rapid increase in the spectrum count of Fe and a corresponding reduction in Zn as the substrate is reached. There is also a peak in the Al count upon reaching the substrate. Figure 7 is a graphical representation of the spectrum counts with location and Table 3.2 lists the experimental data. From this set of data it would appear that the intermetallic layer is about 1.6 μm thick.

Figure 8 is a normal view of the cross-section magnified 10000 times, showing the boundary between the Fe substrate and the zinc coating. Even at this high magnification the adhesion of the coating to the substrate looks good. The boundary region was traversed under the EDS, moving about 5 μm into both the substrate and coating. Table 3.3 is a compilation of

the spectrum counts as a function of the position. The results are plotted in Fig. 9. The intermetallic layer is of the order of 1 μm and again the presence of iron is detected well into the zinc coating.

Figure 10 is another photograph of the Fe substrate and zinc coating at 10000 magnification, but here the specimen has been tilted through an angle of 45 degrees. When viewed at this angle there appears to be a gap between regions of the coating and substrate. This was not an isolated observation since this kind of separation was detected in similar photographs at this magnification.

In the present study we did not attempt to reveal the various compounds which comprise the intermetallic layer. Instead only the presence of Fe, Al and Zn was investigated, and a sense of the relative magnitude of these metals through spectrum counts using the EDS apparatus.

As is well known small amounts of aluminum are added to the galvanizing bath to improve the nature of the coating. The presence of the aluminum leads to the formation of iron-aluminum compounds (Fe_2Al_5 or $FeAl_3$) and these suppress the formation of Fe-Zn compound layers [1]. However the composition of the initial layer which forms, and the subsequent reaction kinetics, are not without dispute [2]. In addition to the Fe-Al compounds a ternary Fe-Al-Zn phase has been reported [3], as well as a combination of all of these phases [4].

It would appear from our work that the intermetallic layer is in the order of 1 μm thick but we did not reveal the nature of its composition. It is difficult to imagine that such a thin layer could influence the r-value to the extent that it does for both the RS and MS materials, as discussed in the preceeding chapter. It was argued in Chapter 2 that the zinc coating would offer some constraint to the deformation of the substrate in certain forming processes, quite apart from the presence of any intermetallic layer. This still seems a plausible supposition, although the gaps between the substrate and coating observed in the present metallographic examination would reduce the constraint. However this still begs the

question as to why the coating exerts a stronger influence on the measured r-values for the RS and MS materials vis a vis the UC and AC materials.

Table 3.1 EDS Analysis, Atomic percent of Fe, Al and Zn

Location	Distance μm	Atomic Percent		
		Fe	Zn	Al
1	0	4.47	84.97	10.56
2	8.0	11.87	81.83	6.30
3	8.8	30.00	59.10	10.89
4	12.0	86.62	13.68	2.70

Table 3.2 Spectrum Counts as a Function of Position

Location*	Counts		
	Fe (K_α 1)	Zn (K_α 1)	Al (K_α 1)
1	33250	18700	14200
2	2650	35900	1000
3	300	36800	
4	1500	36900	
5	1350	38200	900
6	1000	37500	1100
7	750	34600	
8	600	38700	
9	700	36500	
10	400	35400	400

* Increments taken every 1.6 μm.

Table 3.3 Spectrum Counts as a Function of Position

Location*	Counts		
	Fe (K_α 1)	Zn (K_α 1)	Al (K_α 1)
1	49000		
2	48500		
3	48100		
4	48500	470	840
5	44000	1500	2400
6	22400	8100	5050
7	6500	17500	2600
8	2550	21000	800
9	2650	20600	400
10	2200	20800	
11	2000	21100	
12	1700	2100	
13	1600	21500	

* Increments taken every 0.5 μm.

References

1. S.J. Makimattila et al., "The Effect of the Intermetallic Layer on the Adherence of Hot-Dipped Galvanized Coatings", Scripta Met., 1984, Vol. 19, p. 211.

2. N.R. Short and J. Mockowiak, "The Effect of Pressure on the Reactions between Fe-Zn: 1.5% Al at 501°C", Corrosion Sci., 1977, Vol. 17, p. 397.

3. A.R.P. Ghuman and J.I. Goldstein, "Reaction Mechanisms for the Coatings Formed During the Hot-Dipping of Iron in 0-10% Al-Zn Baths at 450° to 700°C", Met. Trans., 1971, Vol. 2, p. 2903.

4. A.R. Borzillo and W.C. Hahn, "Growth of the Inhibiting Aluminum-Rich Alloy Layer on Mild Steel During Galvanizing in Zinc that Contains Aluminum", Trans. Am. Soc. Metals, 1969, Vol. 62, p. 729.

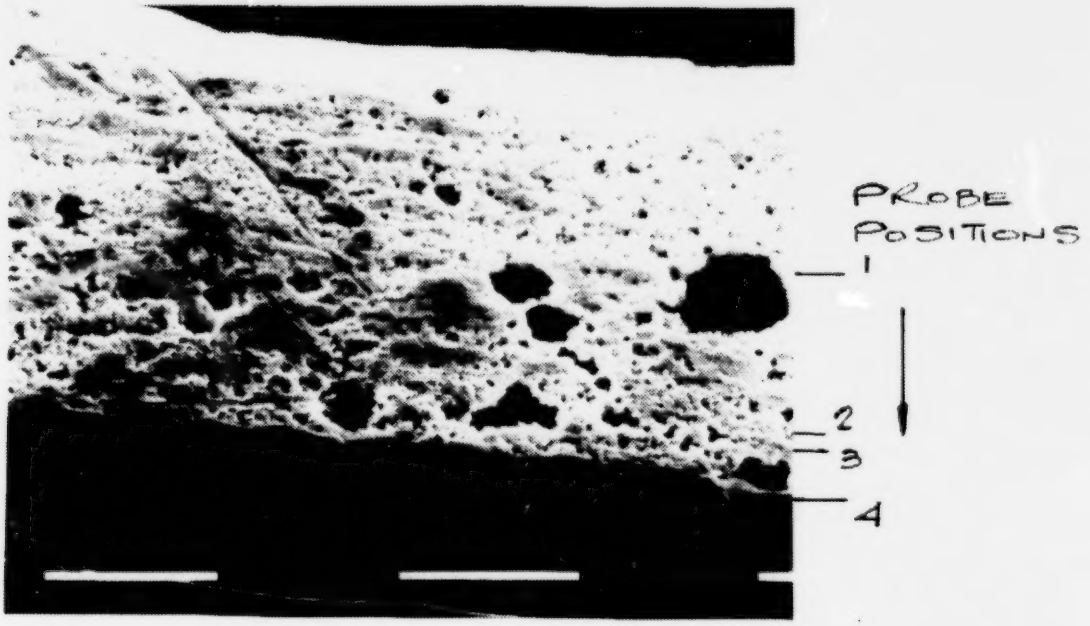

Fig. 1. Zinc Coating RS Material. Magnification 2500, Micron Marker = 10 μ.

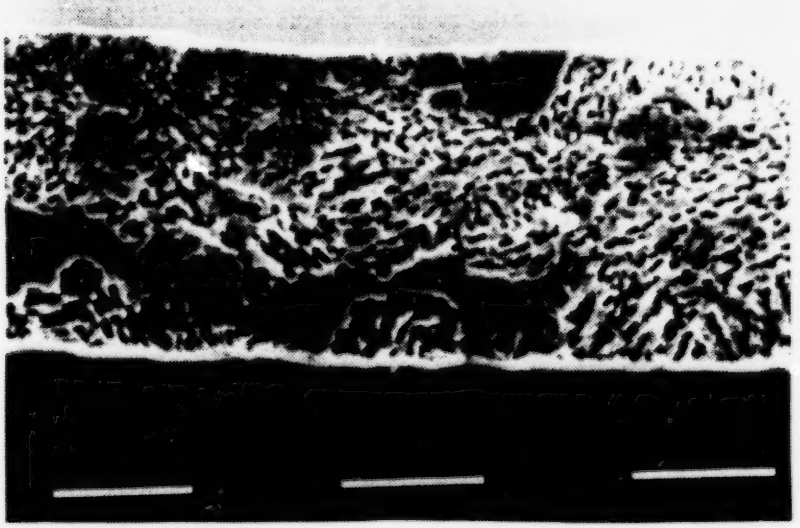

Fig. 2. Zinc Coating RS Material. Magnification 2000, Micron Marker = 10 μ.

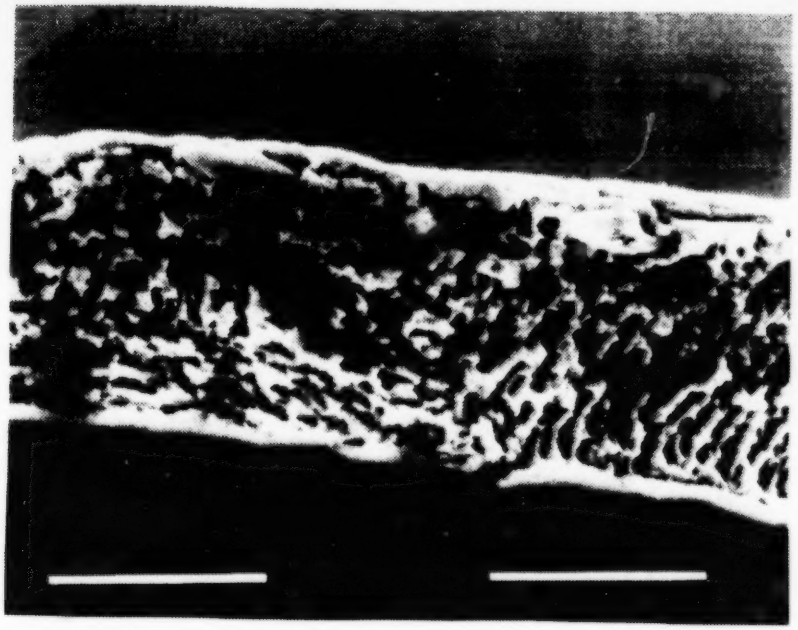

Fig. 3. Zinc Coating RS Material. Magnification 3100. Micron Marker = 10 μ.

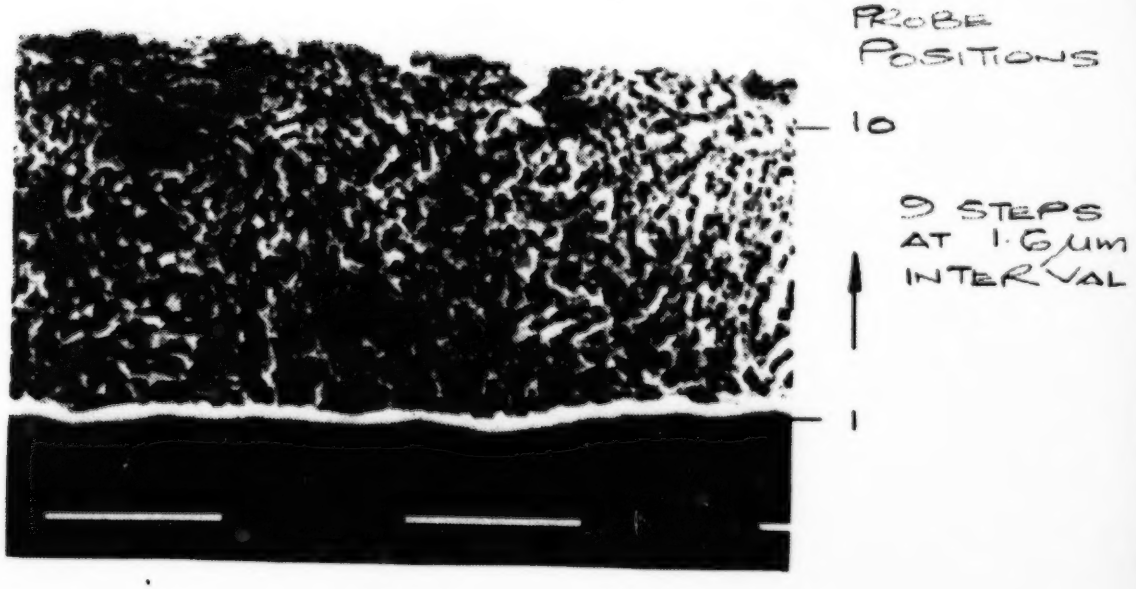

Fig. 4. Zinc Coating RS Material. Magnification 2500, Micron Marker = 10 μ.

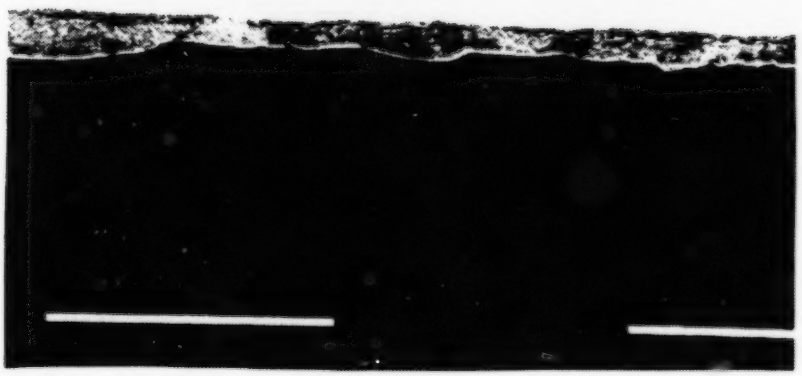

Fig. 5. Zinc Coating RS Material. Magnification 400, Micron Marker = 100 μ.

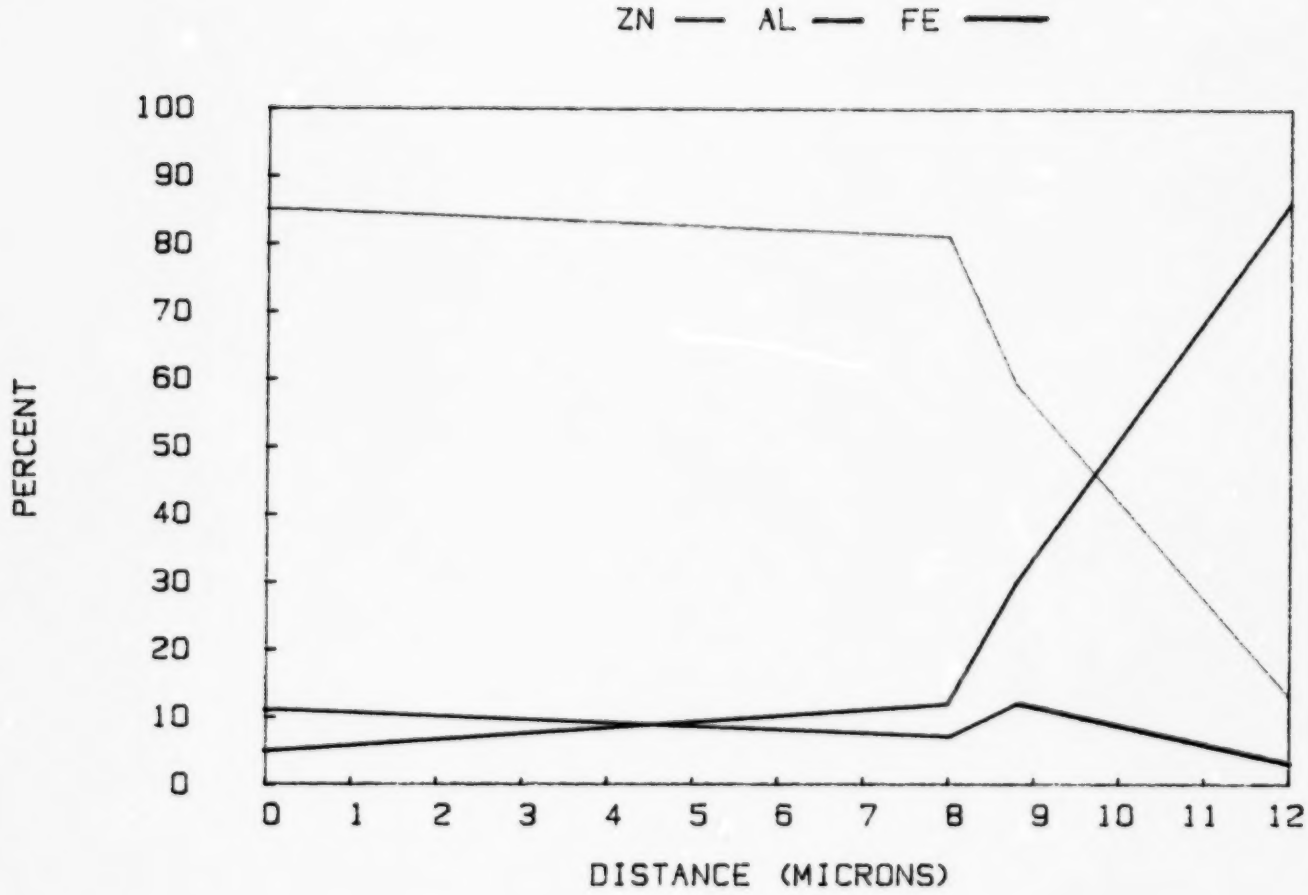

Fig. 6: The Percentage of Fe, Al and Zn as a Function of Position, see Figure 1.

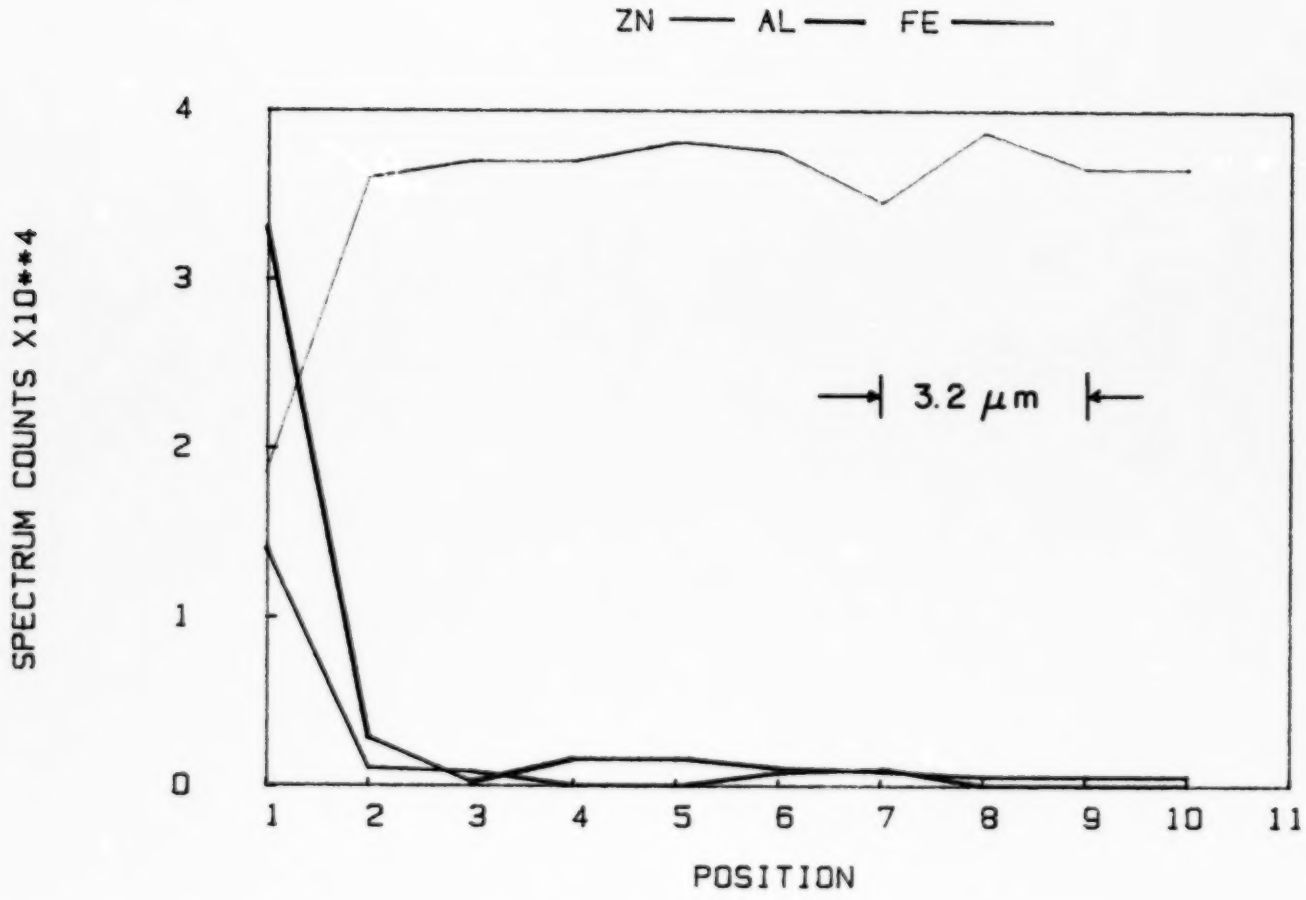

Fig. 7: Spectrum Counts as a Function of Position, see Figure 4.

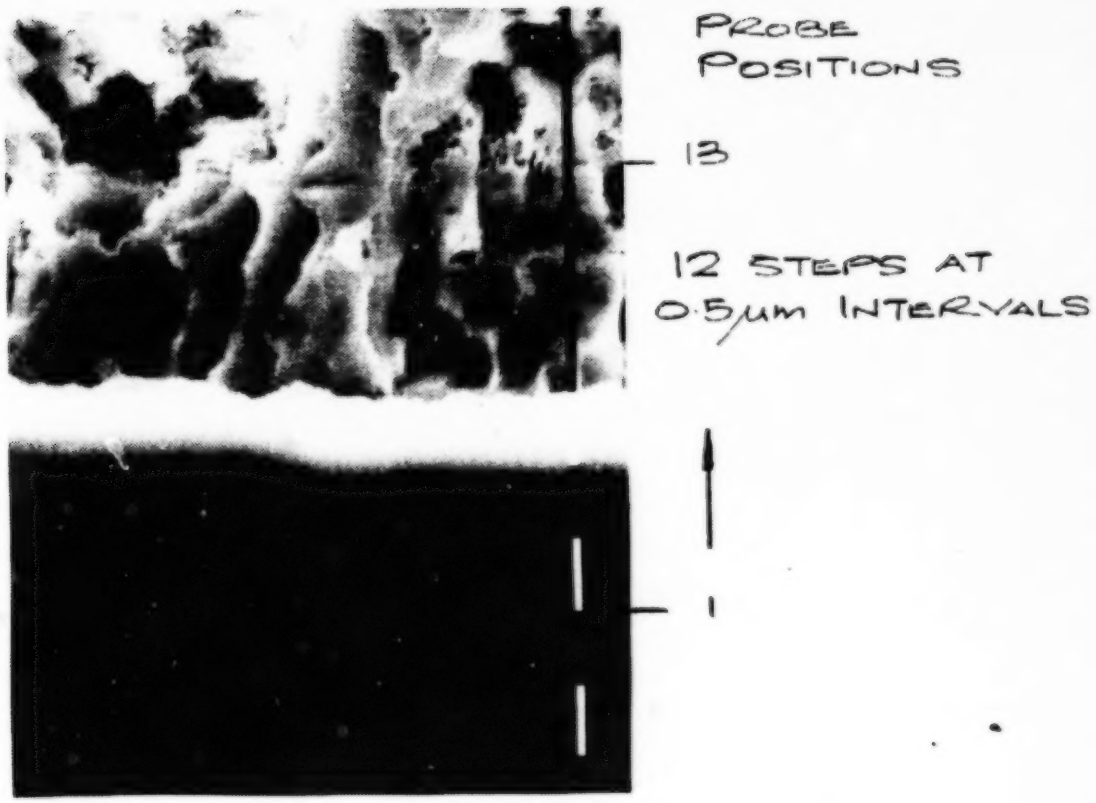

Fig. 8. Zinc Coating and Substrate RS Material.
Magnification 10000, Micron Marker = 1 μ.

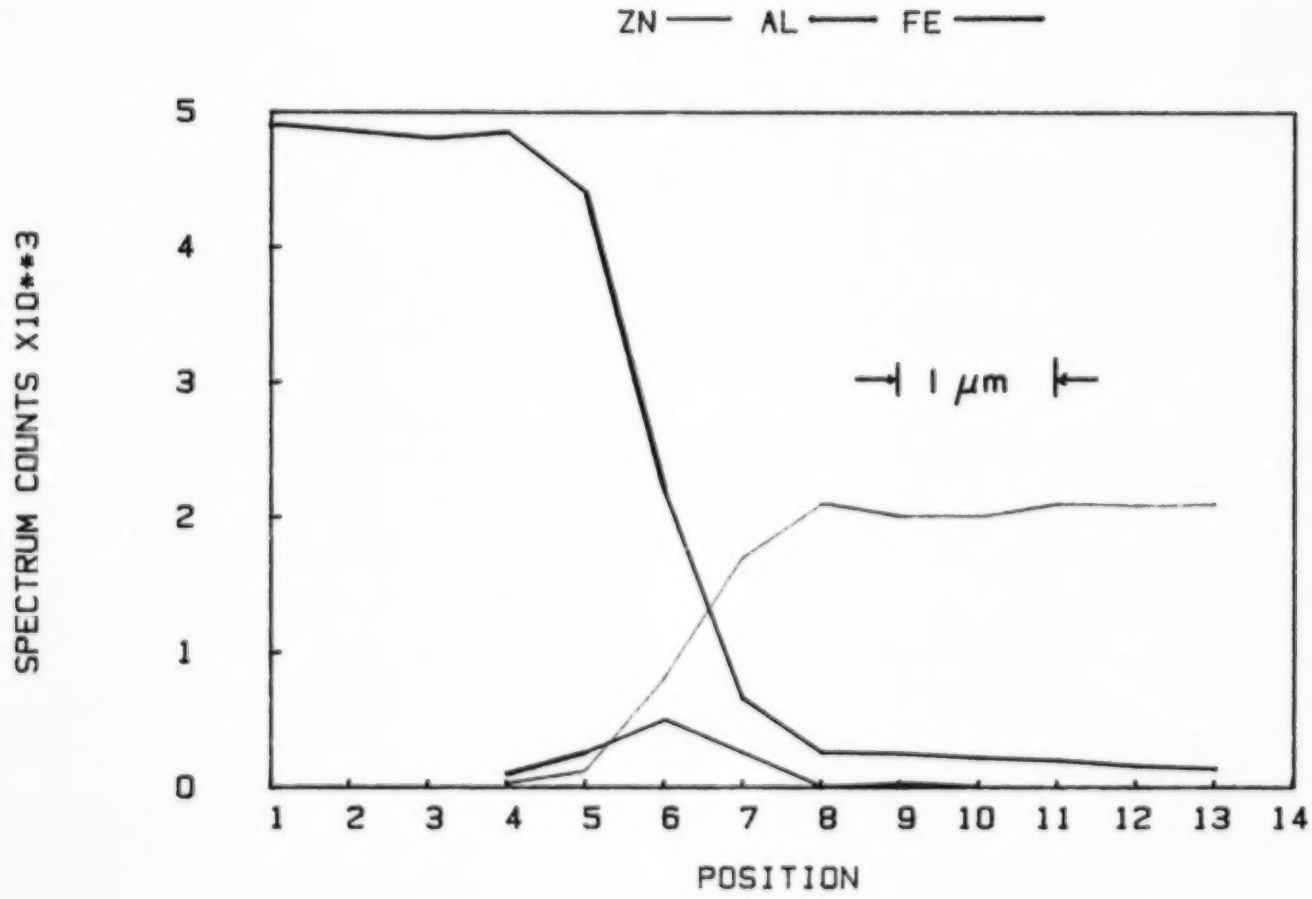

Fig. 9: Spectrum Counts as a Function of Position, see Figure 8.

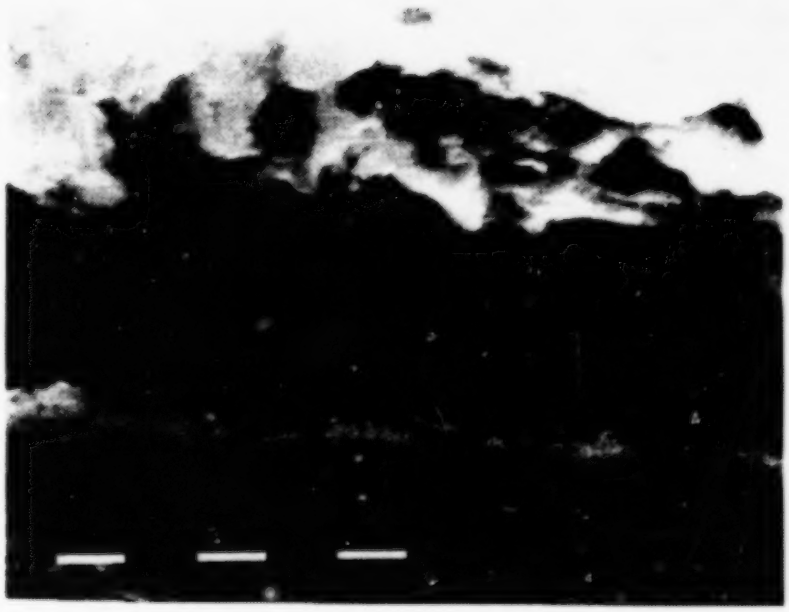

Fig. 10. Zinc Coating and Substrate RS Material. Magnification 10000, Micron Marker = 1μ. Section tilted through 45°.

4. MECHANICAL AND STRIP FRICTION TESTS PERFORMED ON HIGH STRENGTH GALVANIZED STEEL SHEET

4.1 Introduction

Data from tests performed on a high strength, galvanized steel sheet (developed by DOFASCO) are presented in this chapter. Mechanical property data were obtained from tensile and hydraulic bulge tests. The material was also subjected to the strip friction test, discussed in Chapter 1, and the results from the test are discussed herein.

Of interest is the behaviour of the high strength sheet compared with that of the hot-dipped galvanized sheets discussed in the ealier chapters of this report and also in Refs. [1-3].

4.2 Material Classification

The as-received material was measured as being 1.42 mm (0.056 in) thick. The chemical composition of the substrate is given in Table 4.1. The processing route for the present sheet is similar to that of the hot-dipped galvanized sheets with the drawing quality steel substrate.

4.3 Experimental Procedure

4.3.1 Tensile and Hydraulic Bulge Tests

Tensile specimens were blanked from the as-received sheet in the rolling (0 degree orientation) and transverse (90 degree orientation) directions. These tests were performed on a MTS universal testing machine at a cross-head speed of 25.4 mm/min with an extensometer of 25.4 mm gauge length attached to each specimen. True stress-true strain curves for the O° and 90° orientations are shown in Figs 1 and 2 respectively. The results are typical of a number of repeated tests on the material.

It can be seen that the material exhibited a Lüders strain, which is about 4% in magnitude. An upper yield point is barely distinguishable under the selected testing

conditions, but no attempt was made to accentuate the difference between the upper and lower yield point.

An empirical equation of the form

$$\bar{\sigma} = K \bar{\varepsilon}^{n} \tag{4.1}$$

was fitted to the true stress-strain data beyond the end of the Lüders strain. The coefficients K and n, along with other experimentally determined mechanical properties, are listed in Table 4.2.

Subsequent to the completion of the tensile tests a small roller leveller was constructed at McMaster, see Fig. 2 in Chapter 1 of this report. Some additional tensile tests were performed on strips of material (cut from the rolling direction) which had been passed through the leveller a number of times before blanking the tensile specimens. The purpose of the exercise was to ascertain the ease in which the Lüders strain could be eliminated from the as-received material.

Optimum settings for the leveller have not yet been established i.e. the ability to eliminate the Lüders strain in a minimum number of passes without strain-hardening the material. After a number of adjustments to the rolls the results shown in Fig. 3 were obtained. After about 75 passes there has been a marginal reduction in the initial flow stress however, the Lüders strain has been removed without work-hardening the material.

Hydraulic bulge tests were performed in the usual manner on blanks cropped from the as-received sheet. It transpired that the pressure required to fracture the blank was relatively high, the specimens ruptured in a violent manner and there was a danger of damaging the extensometer located at the pole of the deforming specimen. For this reason the majority of the tests were terminated before the blank failed.

A typical true stress-strain curve obtained from the bulge test is shown in Fig. 4. An empirical equation like that of eqn. (4.1) was fitted to the data, the calculated values of K and n are given in Table 4.2.

A comparison of the true stress-strain behaviour of the material in the tensile and hydraulic bulge test is given in Fig. 5.

A number of punch stretch tests were carried out in order to obtain a Forming Limit Curve (F.L.C.) for the material. Rectangular test pieces, of different width, were cropped from the as-received sheet, and an array of grid circles were electrochemically etched on the specimens. The test pieces were then clamped at either end and impressed by a hemispherical punch. In the usual manner grid circles were measured in the region of the fracture site.

The results are shown in Fig. 6. The points coloured green are measurements made on circles close to the fracture site, but failure had not occurred at these locations. The points coloured red are measurements made right in the fractured zone. In some cases the split or tear in the material impinged upon the circle, and in others an obvious localized neck passed through the circle; the measurements were not very precise when this occurred.

4.3.2 Strip Friction Tests

The strip friction test has been described in Chapter 1, and further details are available in Refs. [4,5]. The cross-head speed on the MTS machine was held constant at 2.54 m/min for all the tests conducted.

The original intention was to perform experiments on the as-received material using two pin sizes (12.7 and 25.4 mm diameter) and three lubrication conditions, i.e. dry and with two lubricants - Molyslip and SP-7000 oil. The tests were then to be repeated on specimens from which the Lüders strain had been eliminated. This was achieved by pre-straining strips of material in uniaxial tension, since at the time of performing these experiments the roller leveller had not been constructed. The full complement of experiments was not completed, since part way through the program the 12.7 mm diameter pins on the friction tester were fractured because of the high loads generated with this particular material. The results obtained are summarized in Table 4.3, and these are discussed in the next section.

Typical data from a successful test are illustrated in Fig. 7. This diagram shows the output from the strip friction tester for the as-received material deformed over the 25.4 mm diameter pins with Molyslip as a lubricant. The corresponding, calculated, coefficient of friction as a function of sliding distance (or slip) is given in Fig. 8.

For all the tests performed the width of the specimens was 12.7 mm.

4.4 Discussion of Results

4.4.1 Tensile and Bulge Tests

From the tensile tests it was difficult to distinguish between a lower and upper yield stress and only the yield stress value is quoted in Table 4.2. The yield stress in the rolling direction was measured as 55 ksi (379 MPa) and is somewhat higher in the transverse direction at 59 ksi (406 MPa). The corresponding maximum (true) stresses (at the point of the maximum load) were 79 ksi (545 MPa) and 80 ksi (552 MPa) for the rolling and the transverse directions respectively. Note that the maximum yield stress for the hot-dipped materials, discussed in Chapter 1, was about 42 ksi and this occurred with the RS, MS and AC materials. The corresponding maximum stress was about 55 ksi.

The uniform true strain (up to the point of maximum load) for both the rolling and transverse directions was approximately 0.20. This figure is comparable to the measured values for the hot dipped materials.

The empirical fit to the true stress-strain curve was quite good for the tensile test. Figure 9 is a typical result for the 0° orientation. The fit was not as good for the bulge test data, and the empirical expression could not provide a reasonable match over the complete range of strain. Figure 10 shows a comparison over the initial strain range i.e. up to 30 percent.

The experiments performed using the roller leveller, see Fig. 3, were successful in removing the discontinuous yield behaviour. However, this resulted in only a very minor reduction in the initial flow stress.

Similar experiments performed on the hot-dipped RS material resulted in a considerable reduction in the initial flow stress after roller levelling, see Fig. 3 in Chapter 1.

The behaviour of the high strength material in the bulge test, Figs. 4 and 5, demonstrates the ductility of the material. A true strain of 0.63 was achieved, and it will be recalled that the specimens were not deformed to fracture. This level of strain in the bulge test is comparable with the values obtained from the hot-dipped materials.

As shown in Fig. 5 the true stress-strain curve from the bulge test lies above that from the tensile test. This behaviour is typical of most commercial metals, regardless of the magnitude of the measured r-value.

The yield stress in the bulge test has been quoted in Table 4.2 as 55 ksi (379 MPa). However, the test itself does not lend itself to an accurate determination of yielding. Quite often irregularities in the stress-strain curve are noted in the transition region from elastic to plastic behaviour. This is because the extensometer does not provide very accurate measurements when the specimen is almost flat.

4.4.2 Strip Friction Tests

When the test was performed without lubrication it was found impossible to stretch the horizontal portion of the specimen. With increasing load the vertical portions of the strip continued to elongate, but the material did not slide around the pins. Fracture eventually took place in one of the vertical legs of the strip. This type of behaviour was rarely observed with the hot-dipped materials, since sliding of the material around the pins usually occurred under unlubricated conditions. These results suggests that difficulties may arise with the high strength material in certain stamping operations, particularly the forming of shallow panels. If the lubrication is squeezed out at the interface between the workpiece and the tools, relative sliding of the material could cease in such regions and therefore stretching would no longer occur at other parts of the panel.

Under lubricated conditions the calculated coefficients of friction were in the range, $0.03 < \mu < 0.06$. These are relatively low values but quite typical of values reported in the literature for both sheet and bulk forming operations. It would appear that the SP-7000 oil is a more effective lubricant than Molyslip under the present operating conditions. Furthermore, the coefficient of friction tends to decrease as the pin diameter increases, this latter observation is consistent with the results reported in Ref. [5].

References

1. Ru Zheng et al., "Normal Plastic Anistropy in Galvanized and Uncoated Drawing Quality Steel", Metal Forming Research Report No. 85-003, McMaster University, Sept., 1985.

2. J.D. Embury et al., "Structural Characteristics of Galvanized Coatings", Metal Forming Research Report No., 85-005, McMaster University, August, 1985.

3. Ru Zheng and D. Overby, "Formability Characteristics of Galvanized Steel Sheet", Metal Forming Research Report No. 85-008, McMaster University, Nov., 1985.

4. X.J. Wang, J.L. Duncan and M.L. Devenpeck, "Punch Friction Tests for Sheet Metal Forming", Jnl. Applied Metalworking, 1983, Vol. 3, p. 3.

5. Ru Zheng and D. Overby, "Strip Friction Tests for Electrogalvanized Steel Sheet", Metal Forming Research Report No. 85-002, McMaster University, Sept., 1985.

Table 4.1 Composition of Material by Weight %

C	M_n	P	S	S_i	C_u	N_i	C_r	T_i	Al	Z_r	M_o	N_b	O	N
0.06	0.66	0.011	0.010	0.39	0.03	0.03	0.03	0.003	0.062	0.120	<0.02	0.011	0.006	0.006

Table 4.2 Mechanical Property Data

TENSILE TEST	YIELD STRESS* ksi (MPa)	MAX. STRESS ksi (MPa)	UNIFORM STRAIN	r-VALUE	$\sigma = K\varepsilon^n$	
					K (MPa)	n
0°	55 (379)	79 (545)	0.200	0.90	746	0.189
90°	59 (406)	80 (552	0.190	1.21	733	0.174
BULGE TEST	55 (379)				827	0.218

* Cannot distinguish between upper and lower yield stress in the tensile test.

Table 4.3 Calculated Values of the Coefficient of Friction

PIN DIA. (mm)	LUBRICANT	PRESTRAIN	COEFFICIENT OF FRICTION
12.7	MOLYSLIP	NONE	0.060
25.4	MOLYSLIP	NONE	0.046
25.4	SP. 7000	NONE	0.036
25.4	SP. 7000	4%	0.031

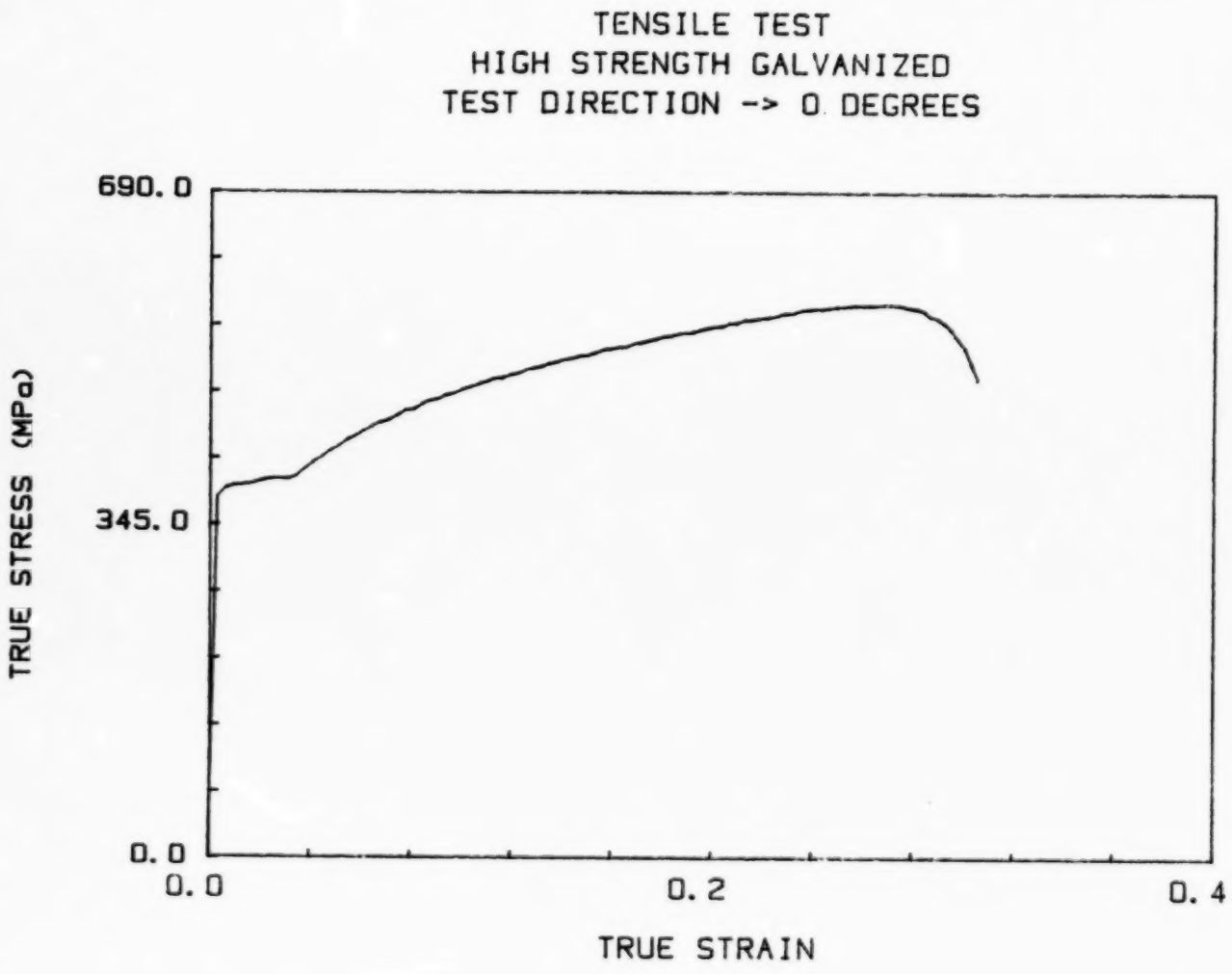

Figure 1: True Stress – Strain Curve for Tensile Test at 0 Degree Orientation

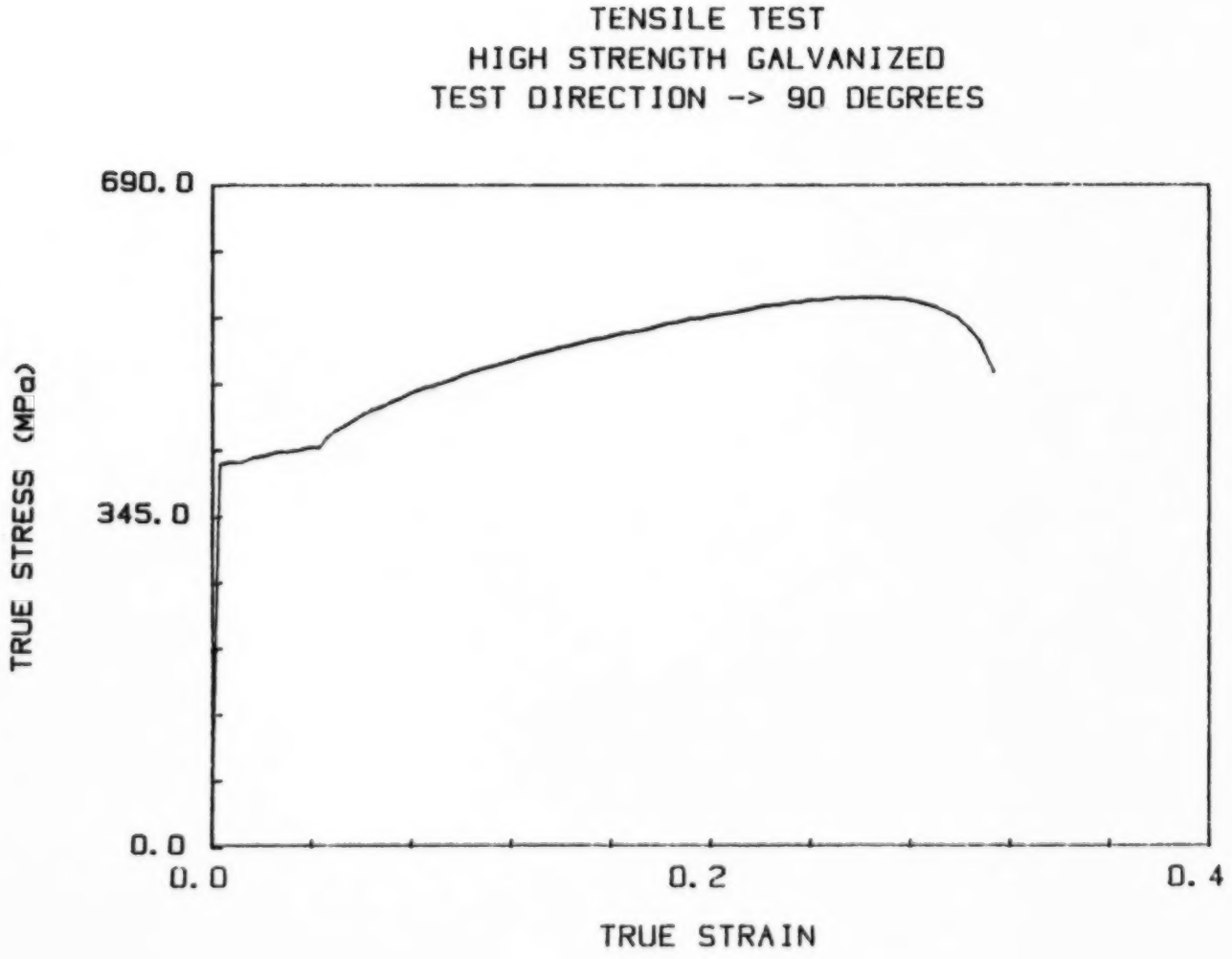

Figure 2: True Stress – Strain Curve for Tensile Test at 90 Degree Orientation

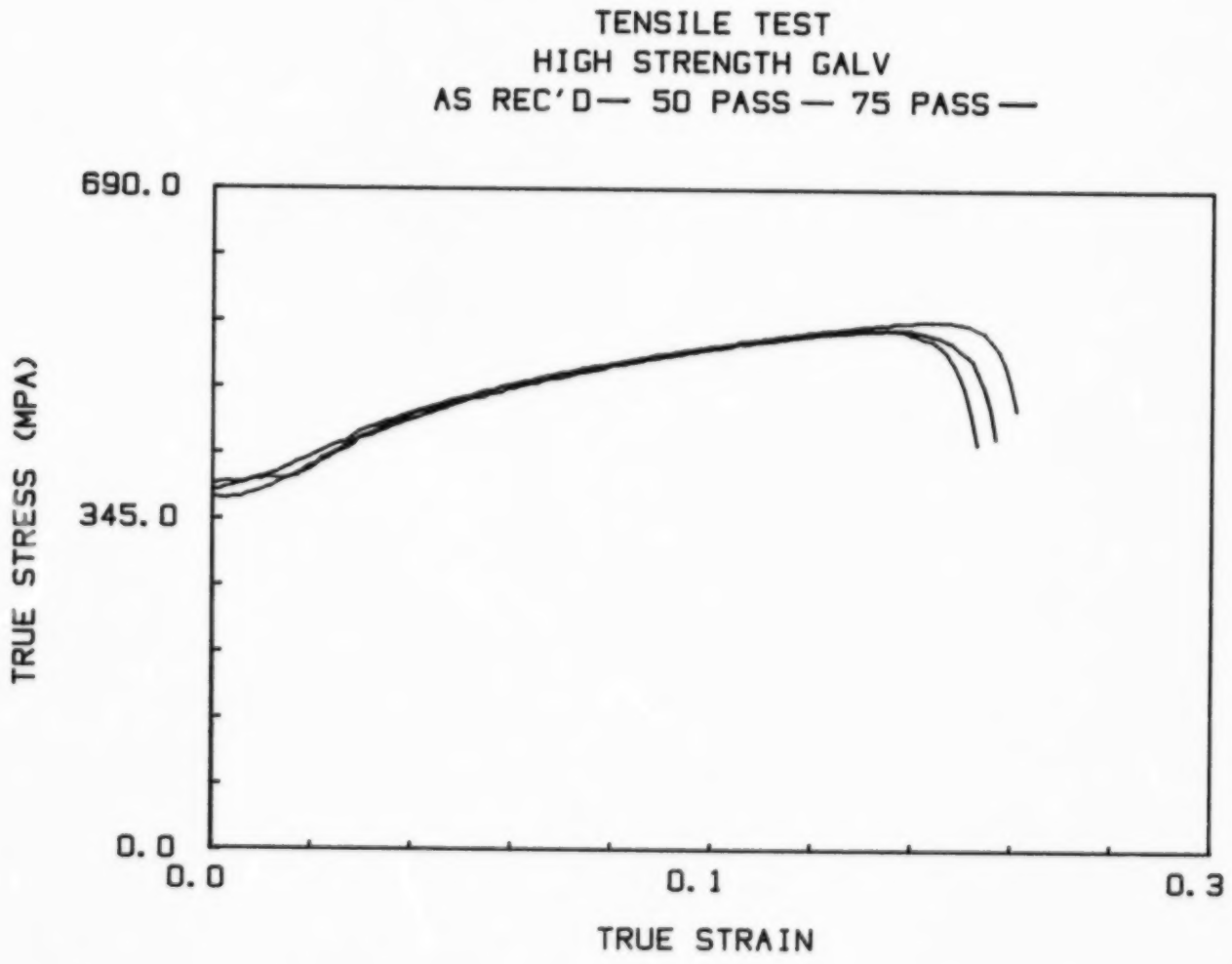

Figure 3: The Effect of Roller Levelling on the True Stress-Strain Curve with Specimens Cut at 0 Degree Orientation

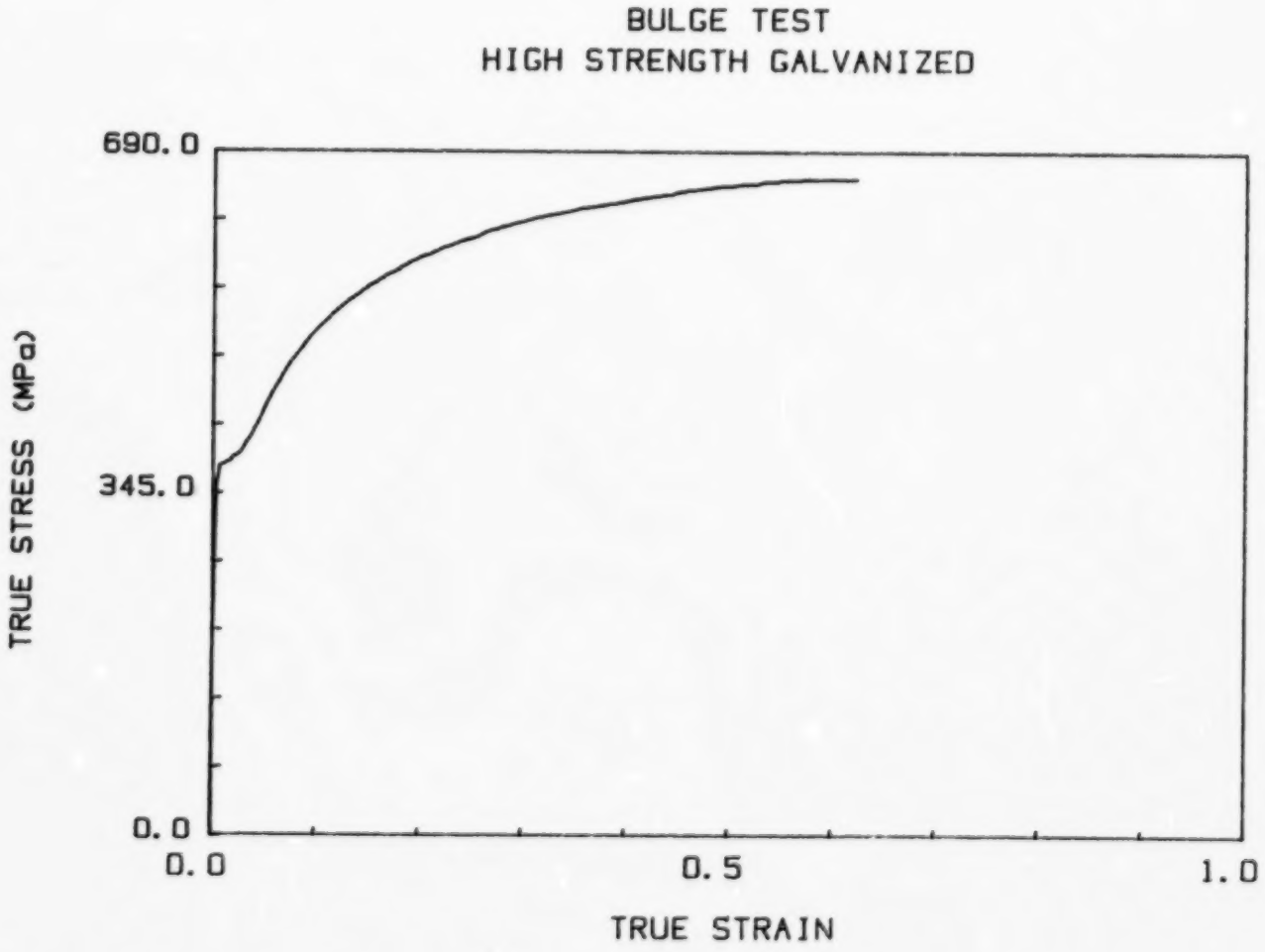

Figure 4: True Stress – Strain Curve from the Bulge Test

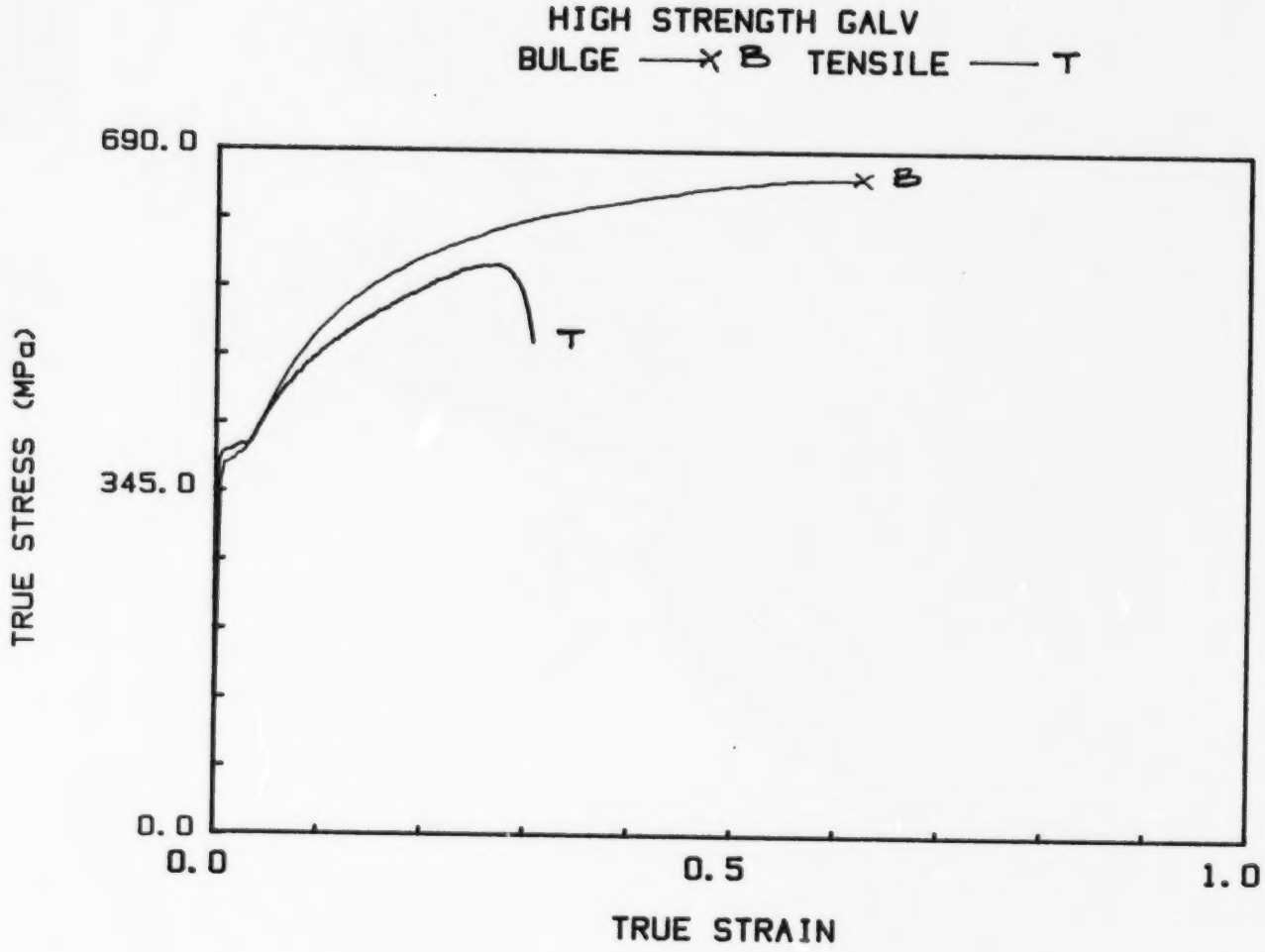

Figure 5: A Comparison of the Bulge and Tensile (0 Degree Orientation) Stress – Strain Curves

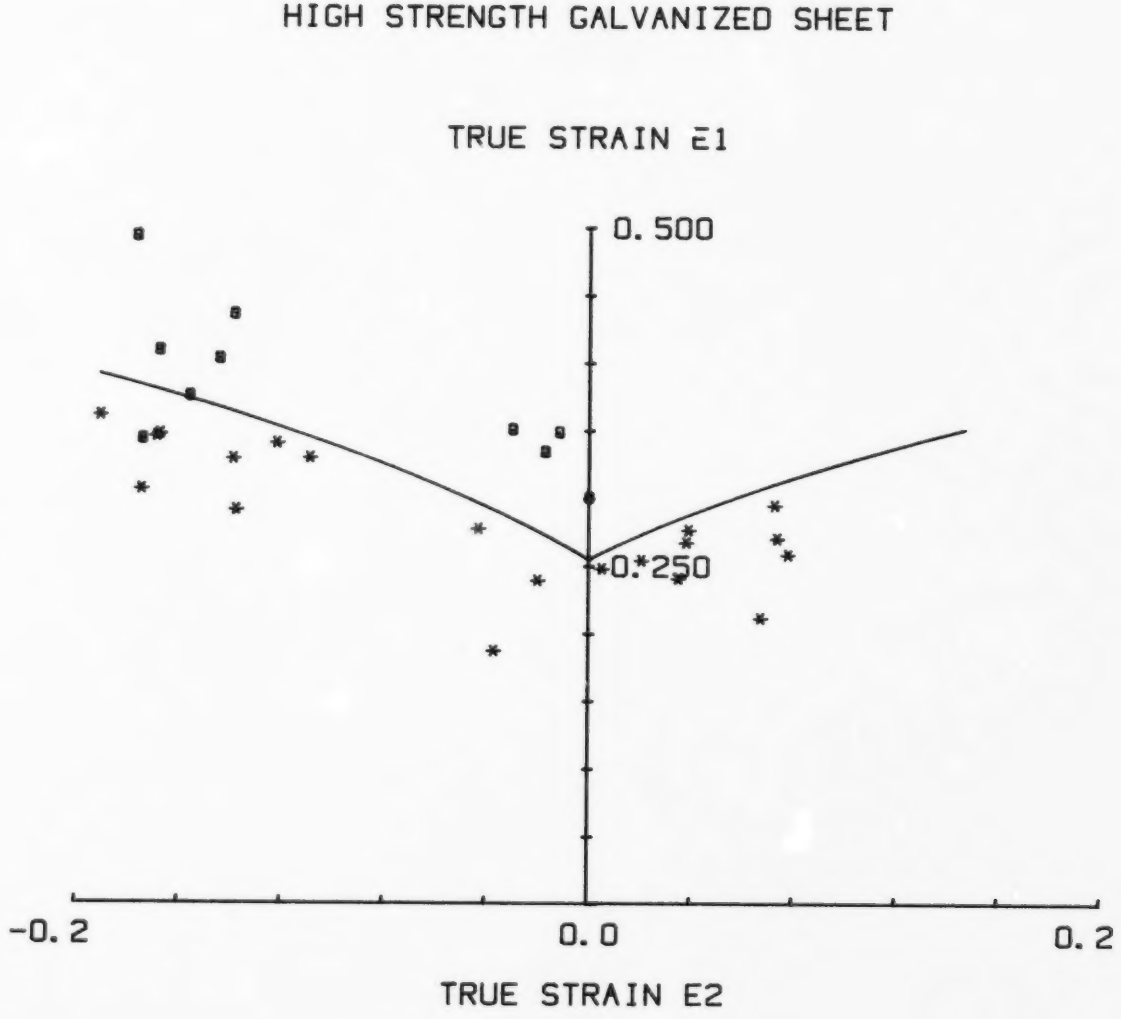

Figure 6: A FLC for the material

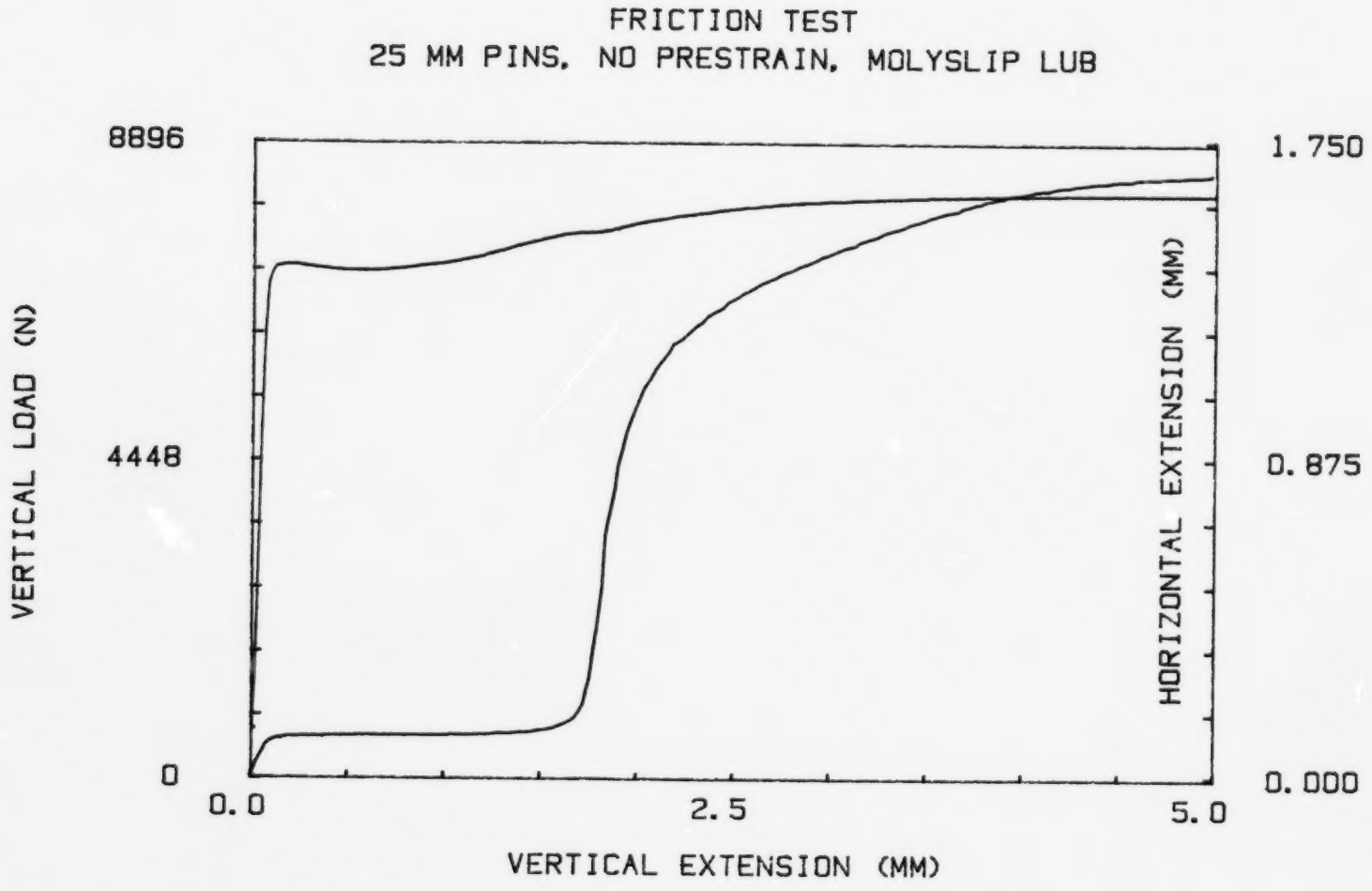

Figure 7: Output from the Strip Friction Tester

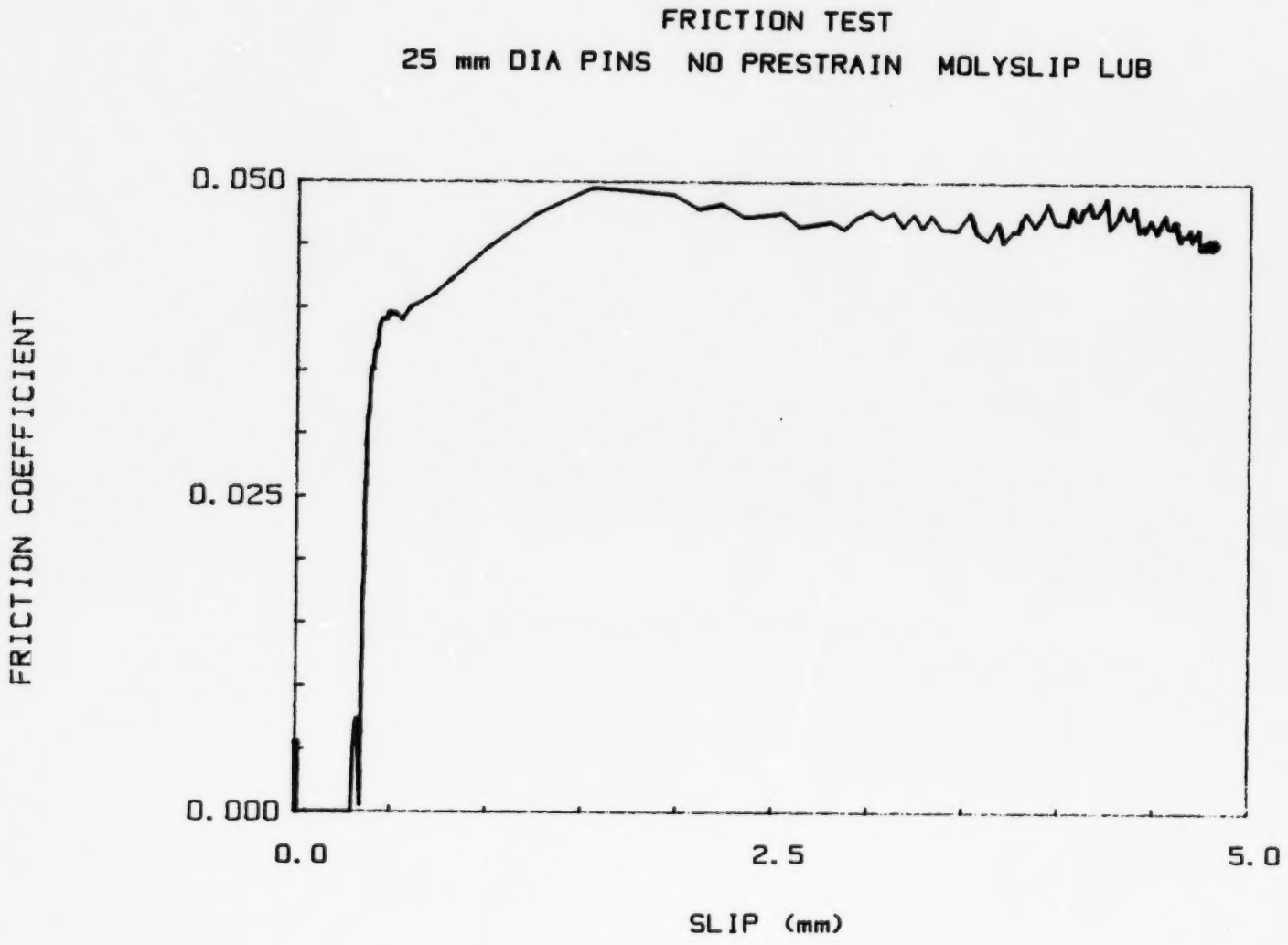

Figure 8: Calculated Coefficient of Friction against Sliding Distance for the Data given in Figure 7

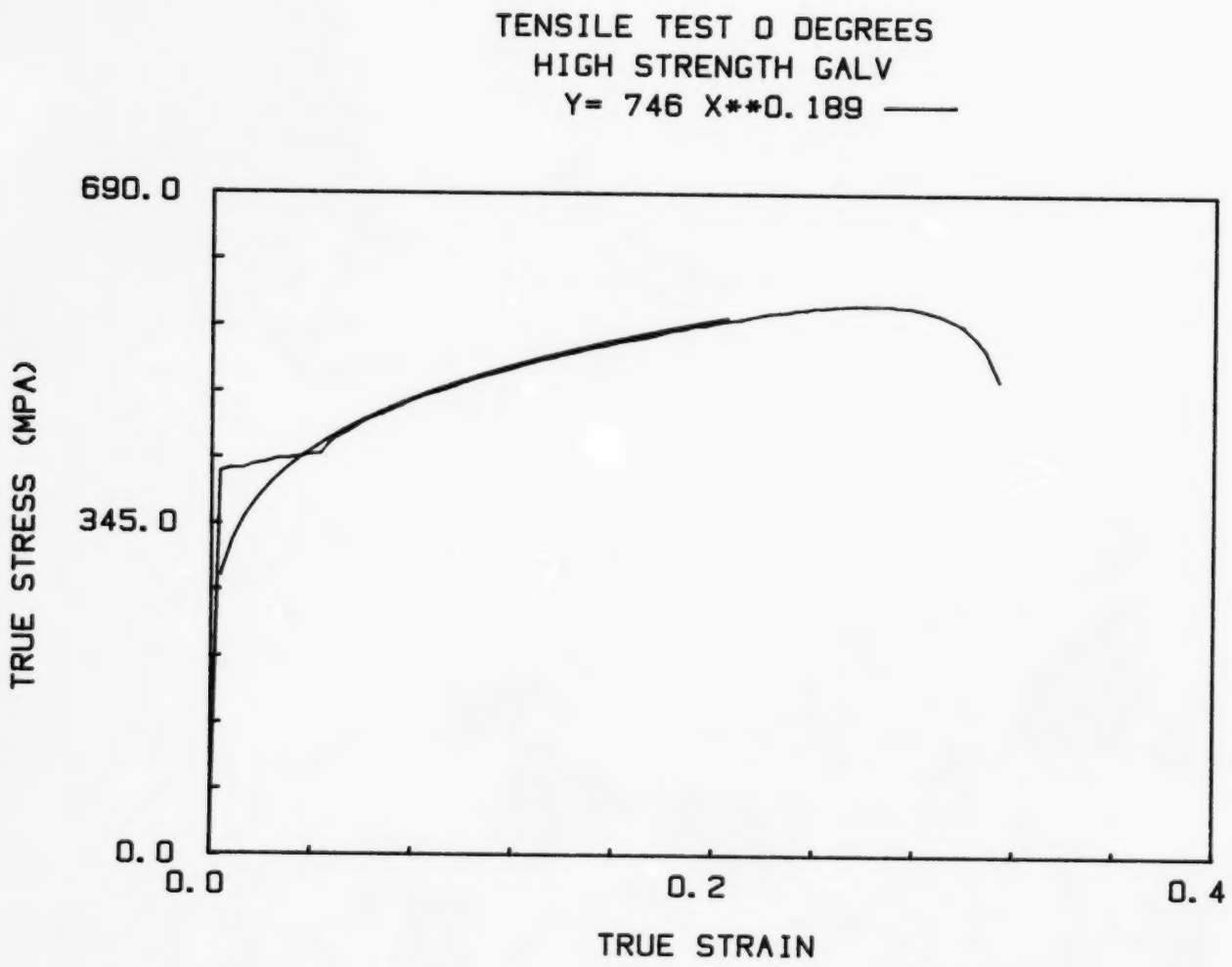

Figure 9: A Comparison of the Actual and Fitted Stress - Strain Data for the Tensile Test 0 Degree Orientation

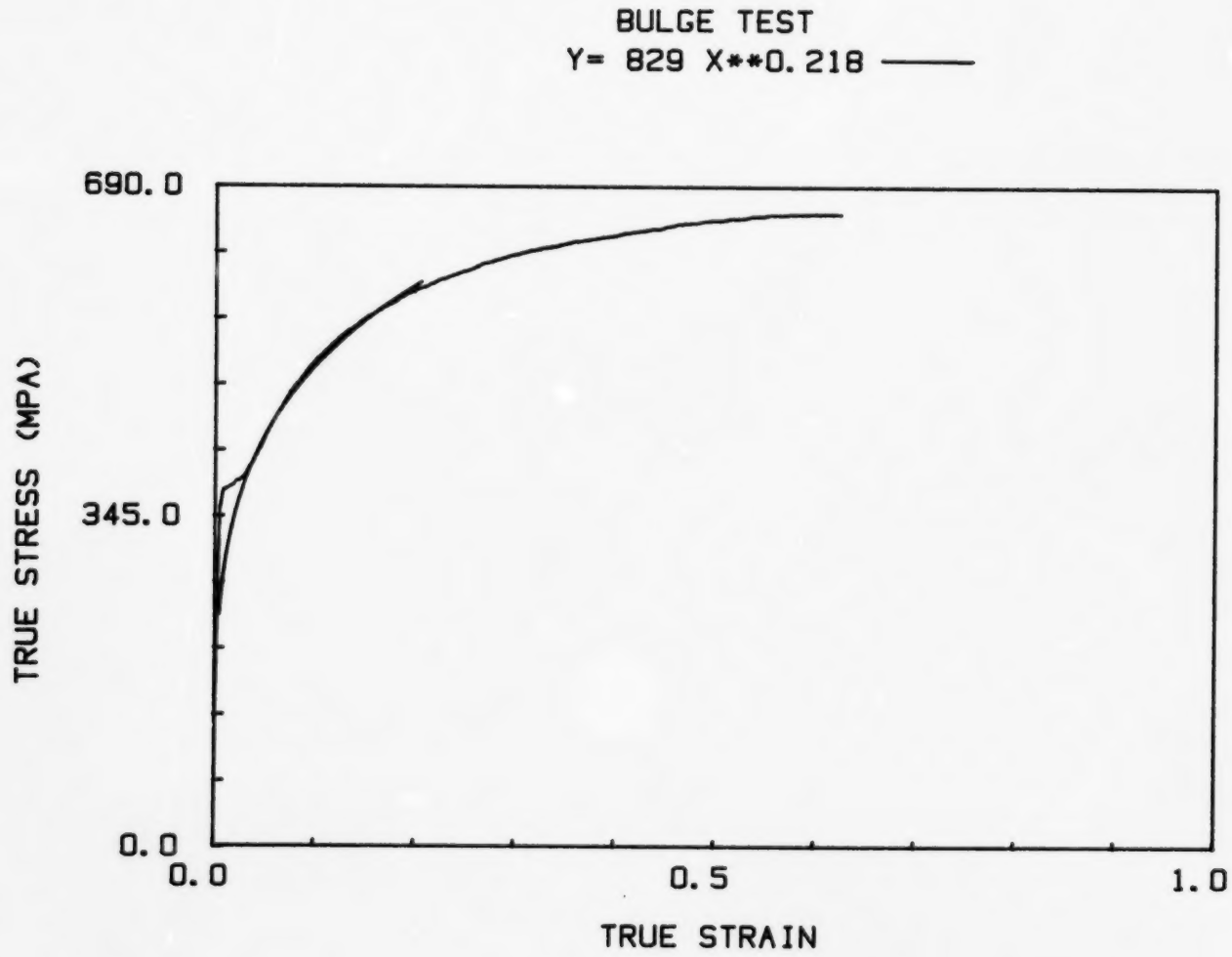

Figure 10: A Comparison of the Actual and Fitted Stress - Strain Data for the Bulge Test

5. BIAXIAL DEFORMATION OF REGULAR SPANGLE SHEET

5.1 Introduction

In a previous report [1], the deformation characteristics of the zinc coating on four hot-dipped steel sheets were investigated. The materials were subjected to metallographic examination following balanced biaxial stretching. In Chapter 1 of this report, a similar but more detailed study was performed on the same four materials after deformation in the strip friction test.

In this chapter, the results of a preliminary study concerned with the deformation of the RS material only, are presented. Specimens of the material were subjected to different biaxial straining modes, and the nature of the surface examined after deformation.

5.2 Experimental Procedure

Strips of different width were cut from the rolling direction of the as-received material. On one side of each test piece, an array of grid circles, approximately 5 mm in diameter, was electrochemically etched.

The test pieces were clamped at each end and impressed by a hemispherical punch 100 mm in diameter. By altering the width of the test pieces, it was ensured that the strain path to failure of each specimen was different. The experimental technique is identical to that employed when obtaining a forming limit curve (F.L.C.). Measurement of the grid circles in the vicinity of the fracture site provided an estimate of the limit strains.

After fracture, coupons were cut from each test piece close to the failure site, and prepared for metallographical examination in a scanning electron microscope. In all cases, the exterior surface of the test piece, i.e. the side away from the punch, was examined.

5.3 Results and Discussion

Table 5.1 summarizes the limit strains for the different test piece geometries. It should be noted that in the punch stretch tests, the straining path to failure is monotonic but not strictly linear. To achieve balanced biaxial tension, a hydraulic bulge test was performed on a number of test pieces. The figures quoted in Table 5.1 are principal engineering strains and represent the average of at least three tests. The different test piece geometries have been classified as A, B, C, etc., in Table 5.1, and for convenience, this nomenclature will be retained in the remaining discussion.

Figure 1 shows a micrograph of the surface for geometry A. At this magnification (80×), the surface looks uneven, and there appears to be a network of widely spaced slip markings running diagonally across the photograph. Two cracks are clearly visible and their orientation is aligned (approximately) with the diagonally downward (left to right) deformation markings. The cracks look like gouges in the material, and it is proposed here that they originated as cleavage cracks (possibly between the basal planes), and have grown to the shape shown through continuing deformation. In fact, all the observed surface cracks for all the test pieces had this appearance.

Figure 2 is a view of the surface of the B-geometry test pieces, and it is similar in appearance to Fig. 1. This might be anticipated since the two straining modes are not very different. However, the photograph shown in Fig. 3 was taken in the same region as that of Fig. 2, but the surface is covered with coarse deformation markings which run in two well defined directions. The orientation between the two sets of markings is approximately 70°. The markings are deformation twins and a few cracks can be observed in Fig. 3, whose orientation bisects the angle between the twin bands.

The deformation path to failure for specimens of geometry C was almost plane strain, and Fig. 4 is a view of the deformed surface. A grain boundary crack is visible along with a criss-cross pattern of slip (deformation twin) markings; the angle between the slip markings is approximately 80°. Superimposed on the slip/twin markings are the surface cracks, and

they possess the same orientation in individual grains. In the present case, the cracks appear to bisect the angle between the slip/twin markings, also the cracks seem to be more numerous vis à vis geometries A and B. Another view of the surface in this region is provided by Fig. 5. The deformation bands look rather like a string net that has been laid on the surface.

Figure 6 shows the surface for specimens with geometry D. Since this deformation mode is close to plane strain, the appearance of the surface is similar to that shown in Fig. 4. Again, a crisscross pattern of deformation bands is present, and surface cracks bisect the angle between them.

Figures 7-9 show the surface of specimens deformed in the hydraulic circular bulge test. The photographs were taken in the region of the pole of the specimens. Balanced biaxial tension appears to give rise to the largest number of surface cracks, and this is consistent with the hypothesis that the cracks form by cleavage. Within each individual grain, the cracks have a particular orientation. However, in certain grains two sets of cracks are visible at right angles to each other.

The deformation twins are not very pronounced in Figs. 7-9, but they can be observed in Fig. 8. This latter figure again illustrates that the surface cracks bisect the deformation markings.

In the RS materials, the zinc coating exhibits a strong texture with the basal planes lying parallel to the surface of the substrate. Furthermore, the principal deformation modes in zinc are: a) Basal Slip, b) Pyramidal Slip, and c) Deformation Twinning. Bell and Cahn [2] have discussed the various twinning and cleavage modes in zinc. Some of the present experimental results agree with the observations made in [2].

It is evident that large cleavage cracks can only impair the corrosion resistance of the coatings. In addition, the surface of the deformed test pieces is rough, with unsightly deformation markings. Such factors will dictate how well paint will adhere to the surface and the number of applications required to cover the surface.

References

1. J.D. Embury, et al., "Structural Characteristics of Galvanized Coatings", Metal Forming Research Report No. 85-005, McMaster University, August 1985.

2. R.L. Bell and R.W. Cahn, "The Initiation of Cleavage Fracture at the Intersection of Deformation Twins in Zinc Single Crystals", J. Inst. Metals, 1975, Vol. 86, p. 433.

Table 5.1 Biaxial Straining of Galvanized Steel Strips

SPECIMEN GEOMETRY	LIMIT STRAIN		BLANK SIZE (mm) Length × Width
	e_1%	e_2%	
A	69	−24	175 × 25
B	51	−17	175 × 50
C	44	1	175 × 75
D	43	9	175 × 100
BULGE TEST	45	45	

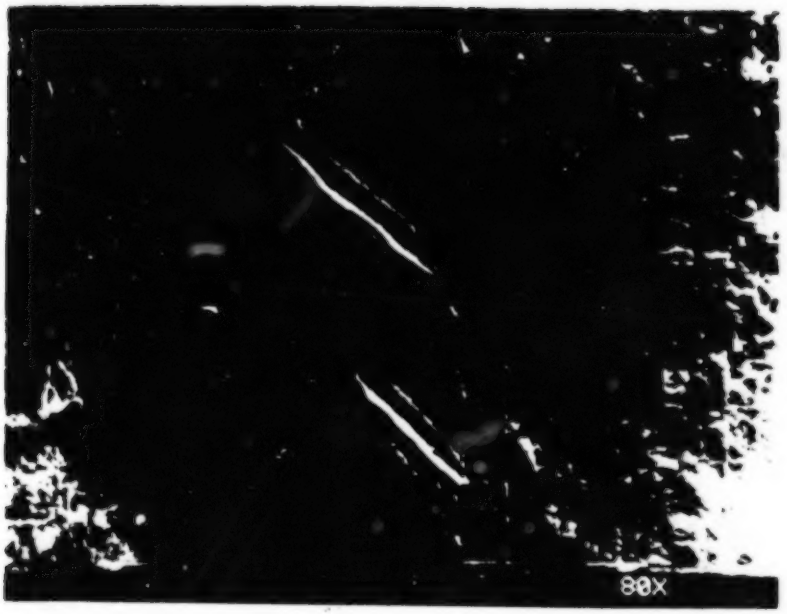

Figure 1. Surface Characteristics for Specimen Geometry A, Magnification 80x.

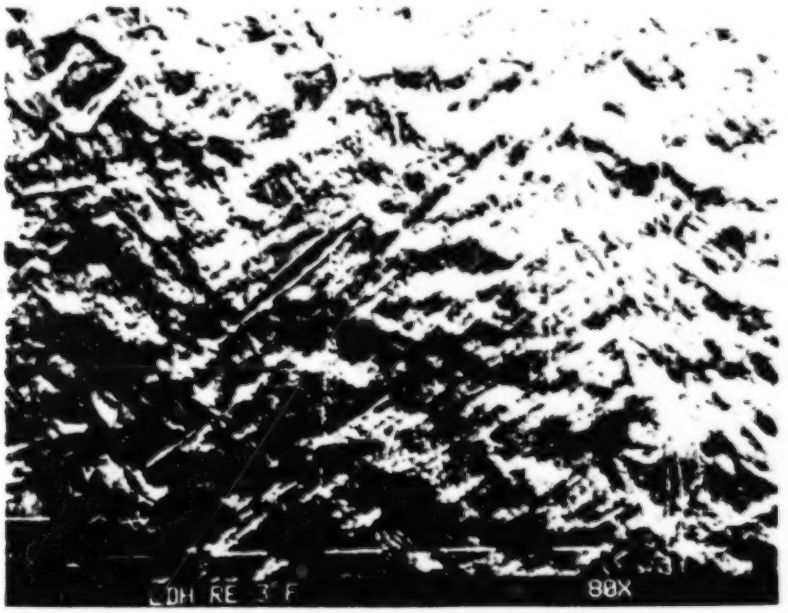

Figure 2. Surface Characteristics for Specimen Geometry B, Magnification 80x.

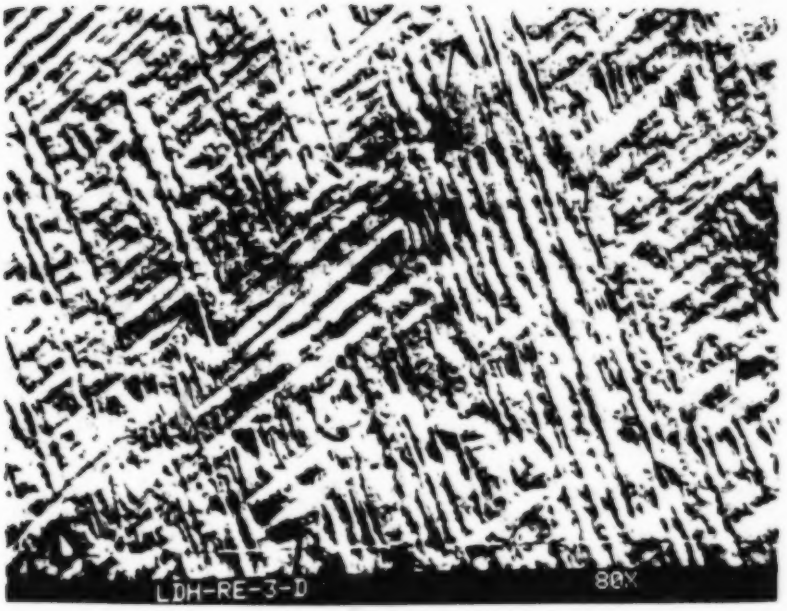

Figure 3. Surface Characteristics for Specimen Geometry B, Magnification 80x.

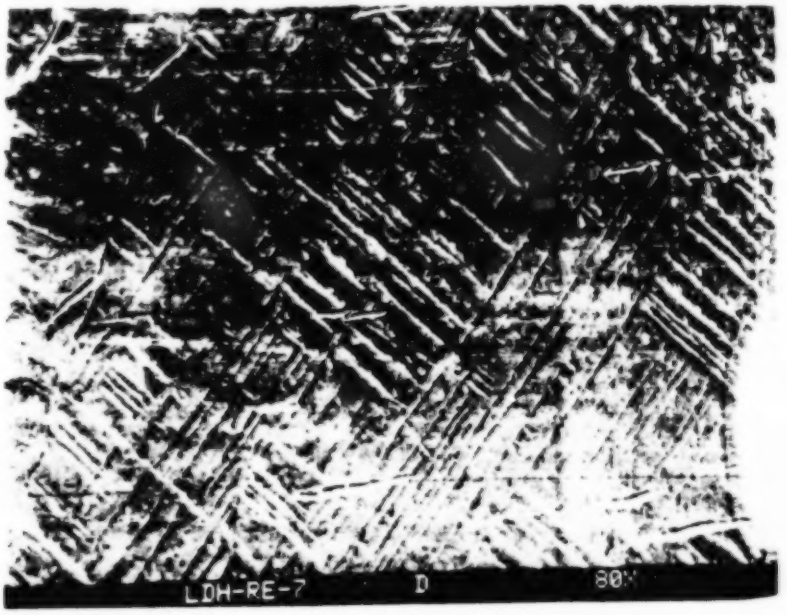

Figure 4. Surface Characteristics for Specimen Geometry C, Magnification 80x.

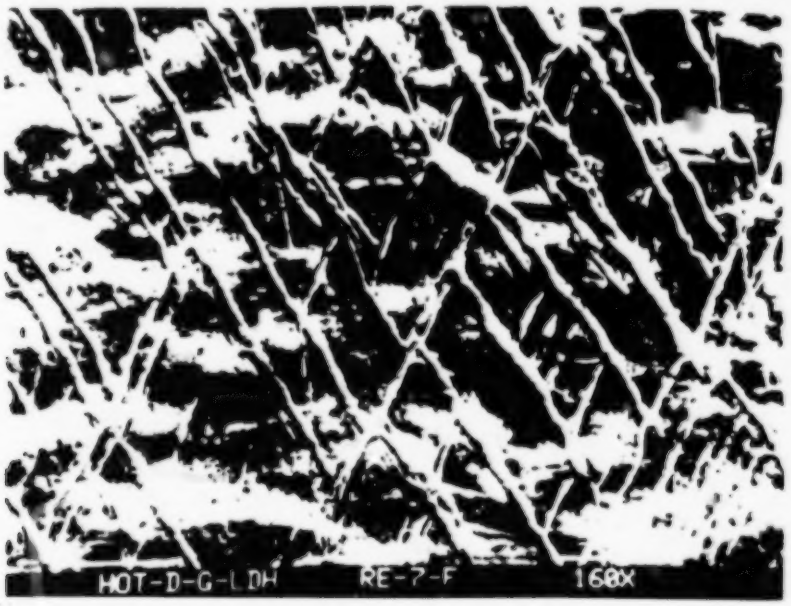

Figure 5. Surface Characteristics for Specimen Geometry C, Magnification 160.

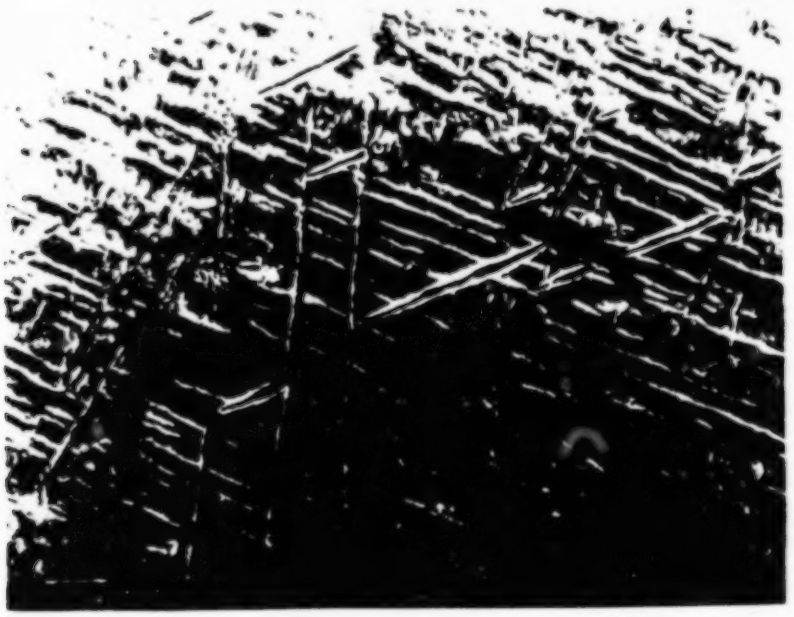

Figure 6. Surface Characteristics for Specimen Geometry D, Magnification 80x.

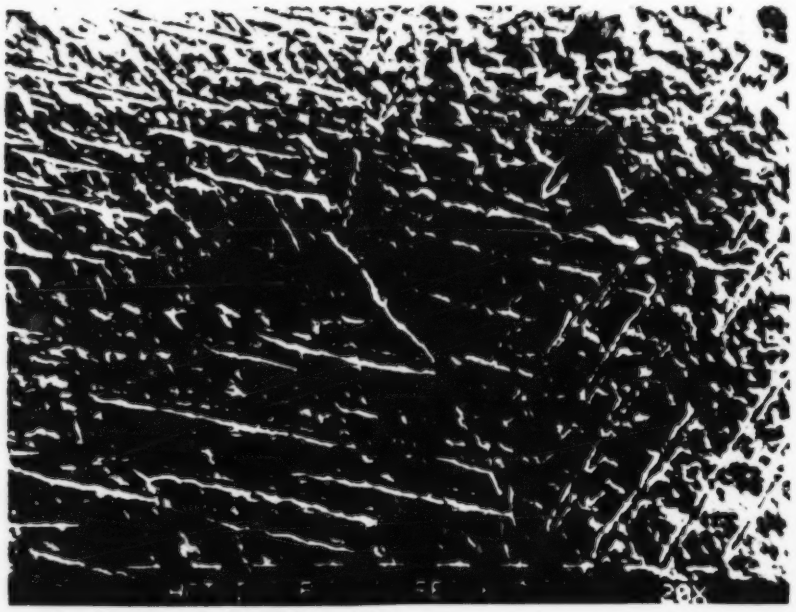

Figure 7. Deformed Surface in the Bulge Test, Magnification 20x.

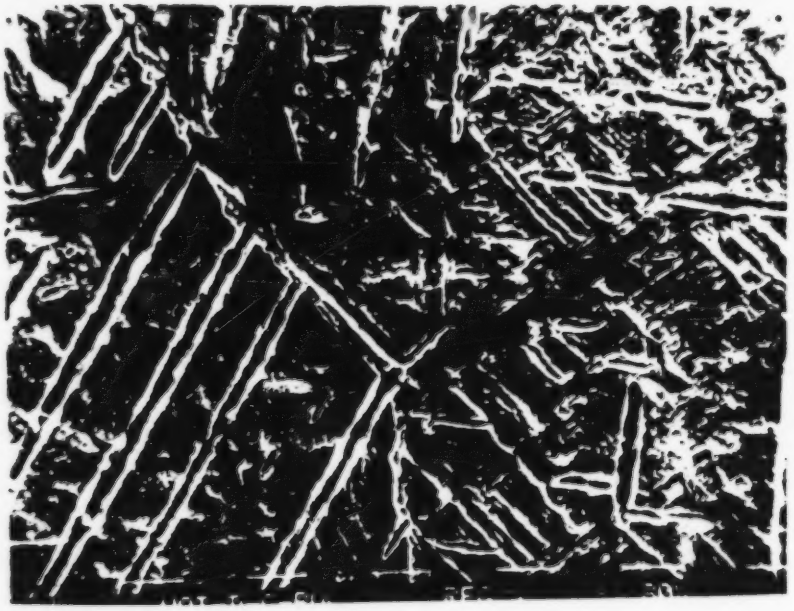

Figure 8. Deformed Surface in the Bulge Test, Magnification 80x.

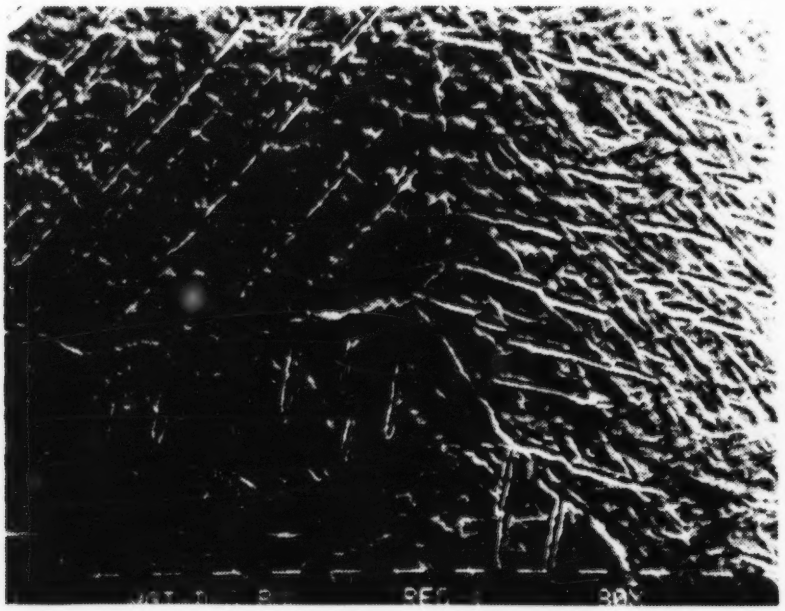

Figure 9. Deformed Surface in the Bulge Test, Magnification 80x.